The University of Sheffield

Department of Materials Science and Engineering
& Department of Civil and Structural Engineering

Microstructural Characterisation of Structural Bolt Assemblies in Fire

By Lucy Johnson

A thesis submitted for the degree of Doctor of Philosophy

September 2014

Summary

In structural fire engineering, the importance of bolt assemblies is often overlooked. Connection design uses the temperature-dependent bolt strength-reduction factors prescribed in Eurocode 3, despite the existence of two distinct failure modes under tension; bolt breakage, and thread-stripping. This thesis investigates the factors which influence failure modes at ambient and elevated temperatures and a range of strain-rates through microstructural characterisation, tensile testing and finite element modelling.

Microstructural characterisation carried out on M20 galvanised bolt assemblies consisting of Grade 8.8 bolts and Property Class 10 nuts from a range of manufacturers has highlighted that, despite a specified tempered-martensite microstructure, microstructural variations existed between different manufacturers and within a single batch. These microstructural variations not only affected the flow behaviour of the bolt material but determined the failure modes of bolt assemblies at ambient temperatures. Tensile testing of turned-down bolts allowed the temperature and strain-rate dependent flow behaviour of bolt material to be investigated, eliminating the effect of thread deformation. The flow curves obtained were input to a finite element model to represent true bolt material behaviour, which was validated against force-displacement curves obtained from uniaxial tensile testing of bolt assemblies from the same batch.

Both experimental and finite element modelling work have highlighted the importance of using a tight thread tolerance class combination and a suitably tall nut to ensure ductile bolt breakage failures and avoid thread-stripping.

Page Intentionally Left Blank

Contents

List of Figures

List of Tables

Symbols

$f_{y,\theta}$	the effective yield strength of steel at elevated temperature θ_a
$f_{p,\theta}$	the proportional limit for steel at elevated temperature θ_a
$\varepsilon_{y,\theta}$	yield strain
$\varepsilon_{p,\theta}$	strain at the proportional limit
$\varepsilon_{t,\theta}$	limiting strain for yield strength
$\varepsilon_{u,\theta}$	ultimate strain
$k_{y,\theta}$	reduction factor for effective yield strength
$k_{p,\theta}$	reduction factor for proportional limit
$k_{E,\theta}$	the reduction factor for the slope of the linear elastic range
$k_{b,\theta}$	the reduction factor determined for the appropriate bolt temperature
L_0	original gauge length
k	coefficient of proportionality
S_0	original cross-sectional area of parallel length
d_0	original diameter of parallel length
L_c	parallel length

Acknowledgements

This research was funded by the Engineering and Physical Sciences Research Council (EPSRC) through the Advanced Metallic Systems Centre for Doctoral Training (CDT).

Thanks firstly to my four supervisors Dr Eric Palmiere, Dr Richard Thackray, Prof Ian Burgess and Prof Buick Davison for their support and for agreeing to collaborate in this joint interdisciplinary project. Thanks also to the firm which provided the bolt assemblies used in this research and to Bill Eccles from Bolt Science, and Brian Kirby from Pyro Fire for taking an interest in my research and for answering numerous questions about bolting standards and literature.

Special thanks also go to Dr Krzysztof Muszka who tutored me in the use of Abaqus and proof-read the finite element modelling chapter, and to Chris Todd for setting up Labview and the automatic trigger system for DIC.

Thanks to the Fire Research Group for being so friendly and welcoming, to Tinsley Bridge Group for being so understanding while I juggled full time work with writing up and to my University colleagues in D1 for regular banter and tea breaks.

A final thank you must go to family and friends, especially Adi, who I promise I will now make more time for.

Declaration

Except where specific reference has been made to the work of others, this thesis is the result of my own work. No part of it has been submitted to any University for a degree, diploma, or other qualification.

Lucy Johnson

1 Introduction

Two distinct failure modes occur in bolt assemblies under pure tension; thread-stripping and necking of the bolt shank. Thread-stripping is often considered to be a brittle failure mode, due to the rapid reduction in load capacity at the onset of failure. This failure mode involves the heavy deformation of one or both thread sets, with the nut eventually pulling off the end of the bolt shank. This failure mode has been observed in a number of published tensile tests [1-5] and was evident in a study carried out by the Fire Research Group at Sheffield [6], the purpose of which was to test two types of connection to failure; however, thread-stripping failure occurred prior to connection failure at 550˚C. Subsequent tests were carried out with two nuts per bolt, to avoid premature failure. At ambient temperature, ductility is less important than strength in standard applications, due to the very small beam deflections which are permissible. Despite the nature of thread-stripping failure, it is therefore an acceptable failure mode according to EN 15048-2 [7] as long as it satisfies the minimum specified tensile resistance. At elevated temperatures, however, ductility becomes far more critical in connections (including bolt assemblies) which must continue to transfer loads effectively from beams to columns during thermal expansion and subsequent sagging of beams during the growth of a fire.

A table containing strength reduction factors specific to bolts and welds is provided in Annex D of Eurocode 3 [8]. The values in this table came directly from the results of testing carried out during the 1990s on bolt assemblies manufactured in the UK [1, 2], and are independent of failure mode. At the time at which this research was carried out, 'structural' bolting assemblies did not exist. All nuts and bolts could be purchased individually and interchangeably. Quality assurance testing, therefore, did not include the mechanical testing of the assembly as a whole, as it does now. Many other differences exist between modern bolt assemblies and those used at the time of Kirby's study [1]; all bolt assemblies are currently imported from overseas, while those tested by Kirby were manufactured in the UK, and tighter geometrical tolerances and galvanised surface coatings are commonly specified.

Due to the many changes between modern assemblies and those tested by Kirby, it was decided that a single batch of galvanised M20 "structural" bolting assemblies, compliant with BS EN 15048 [9], would be studied, as they are commonly used in UK construction. The bolts were Grade 8.8, while the pairing nuts were of Property Class 10. In galvanised assemblies the nut has its threads tapped over-size to accommodate the zinc layer thickness on the bolt threads. Therefore, a higher property class nut has been used than the pairing bolt and nuts tested by Kirby. The bolt assemblies were donated by a UK distributor; which had imported the components, carried out quality assurance testing and applied its own manufacturer's mark. This is common practice in the UK, where all structural bolts are currently imported, due to the high cost of raw materials [10]. According to ISO 898-1 "A distributor who distributes fasteners that are marked with his (or her) own identification mark shall be considered to be the manufacturer" [11], which makes the original overseas manufacturer untraceable.

The research in this thesis has examined the steady-state tensile behaviour of bolt material, in the form of turned-down bolts, and bolt assemblies, at a range of temperatures and strain-rates. Reducing the cross-sectional area of the turned-down bolt specimens allowed the material properties of the bolts to be investigated by removing thread deformation effects. The results of these tests has provided material properties which were input into a finite element model allowing true strain-rate and temperature dependent material properties to be included. Such a finite element model has allowed the influence of effects which cannot be investigated through mechanical testing to be investigated. These include the number of threads in contact, relative thread strengths and thread tolerance. The finite element model was validated by tensile tests carried out at the same temperature and strain-rate combinations on bolt assemblies from the same batch, previously published test data, and the strength reduction factors prescribed in Eurocode 3.

In order to determine whether this finite element model and the results of bolt-assembly testing, are typical of all M20, Grade 8.8 bolts, microstructural characterisation was also carried out on bolt assemblies from other batches and manufacturers. This study involved six bolts, including one from the same batch as those used for turned-down bolt and bolt-assembly testing, and consisted of chemical composition analysis, micro-hardness testing, optical and scanning electron microscopy, prior-austenite grain size measurement, CCT curve calculation, and the uniaxial-tensile testing of turned down bolts. The purpose of this research was therefore two-fold; firstly to characterise the microstructures of a range of M20, Grade 8.8 bolts and comment on the consistency of quality, and secondly to investigate the impact of a range of variables on failure-mode in an assembly commonly used in UK construction. These variables include temperature

and strain-rate dependence, thread tolerance, relative thread strength and nut height. Their effects will be investigated through finite element modelling and uniaxial tensile testing.

2 Background

2.1 History of Bolts

The first screws are thought to have been used in printing presses in the 15th Century, and were made by hand. A system for the mass production of screw threads patented by J and W. Wyatt in 1760, around the same time as the start of the industrial revolution, led to a large increase in production [12]. In the mid-late 19th Century many countries worked to develop an international standard of thread pitch angles and screw diameters, eventually agreeing on flat crests, rounded roots and a 60° angle between the straight edges connecting the crest and root. This allowed nuts and bolts made by manufacturers around the globe to be used interchangeably. The British Standards Institution requested in 1965 that all future designs should include the ISO metric thread which is still in use today and can be identified by the letter 'M' followed by the diameter in mm on each component. Metric property classes and ISO standards now describe strength and test methods in detail.

According to the Metals Handbook [13], the purpose of bolting specifications is to ensure both the dimensional and functional interchangeability of fasteners. Until recently, all nuts and bolts were specified in this way; each component could be purchased separately and quality testing therefore did not include mechanical

testing of the assembly as a whole. In this case, the tensile strength of the bolt and proof (yield) strength of the nut are determined through tensile testing of each component on a hard, threaded mandrel. It is known that thread-stripping strength is dependent on the relative strengths of nut and bolt threads. Threads of similar strength are more likely to strip because one set of threads is not sufficiently strong to prevent deformation of the other. The method of testing individual components on a hardened mandrel therefore gives an unrealistically high value of thread-stripping strength. Recently published work in EN 15048-1 [9], addresses this issue, and specifies that structural bolting assemblies must be purchased as a complete unit from a single manufacturer who will also apply any surface coatings to all components. This is the only difference between structural and general-purpose bolting assemblies, but it is an important one, as the stripping of threads in a structural connection could lead to loss of life.

2.2 Structural Behaviour in Fire

Two hot-rolled structural steel grades, S275 (0.25 wt%C, 1.6 wt%Mn, 0.5 wt%Si) and S355 (0.23 wt%C, 1.6 wt%Mn, 0.5 wt%Si, 0.003-0.1 wt%Nb and V) [14] make up a high proportion of the steel used in beams and columns in UK construction. Numerous tests were carried out under transient and steady-state conditions to determine elevated temperature properties [15] which contributed to the inclusion of temperature-dependent strength reduction factors in BS 5950-8 [16] which has since been superseded by Eurocode 3 [8]. The behaviour of structural steel during and after fire has been well documented and a number of publications verify the accuracy of the temperature-dependent strength reduction factors prescribed for structural steelwork in EN 1993-1-2 (Eurocode 3) [8]. A paper summarising the high-temperature properties of steel [17] references much of this research which also extends to hot-rolled steel grade S460 (0.12 wt%C, 1.6 wt%Mn, 0.5 wt%Si,

0.015 wt%Al, 0.2 wt%V), designed for use in harsh environments such as off-shore applications [18, 19].

In the past, a single table of temperature-dependent strength reduction values was given for 0.5, 1.5 and 2% strain, and steel of grades 43 to 50 [16], equivalent to S275 and S355. Based on the large amount of research carried out in this area, Eurocode 3 now gives separate strength reduction factors for the linear elastic region, yield strength and proportional limit (ultimate tensile strength), it also gives calculations of stress for given ranges of strain, so that a stress-strain curve can be approximated based on Young's Modulus, nominal tensile strength and nominal yield strength alone (Figure 2.2-1).

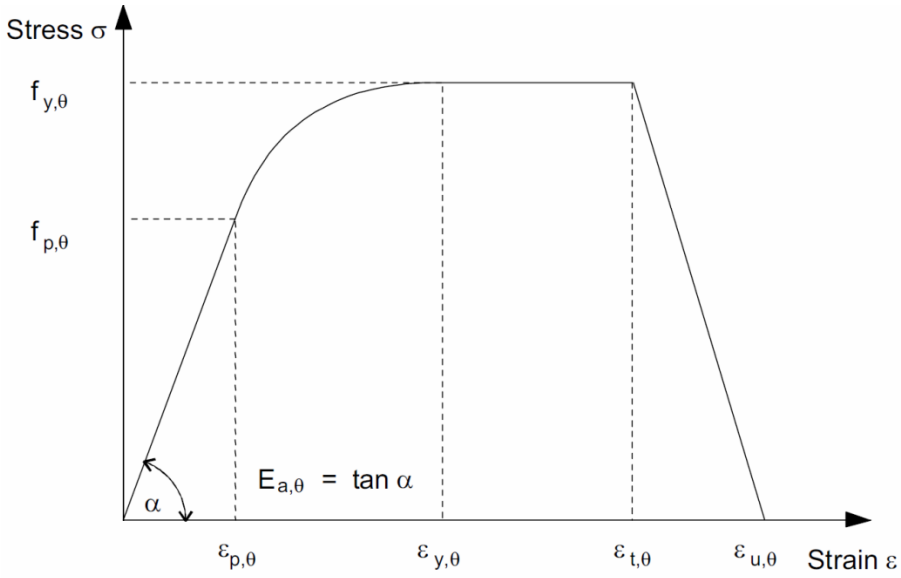

Figure 2.2-1 Stress-strain relationship for carbon steel at elevated temperatures (Figure 3.1 copied from EN1993-1-2 [8])

2.2.1 Structural Response to Fire

Assuming that structural steel members such as beams and columns are the weakest points in a structure during fires, structural behaviour can be predicted based on these reduction factors with relative confidence, although further refinements including the inclusion of creep models are currently being developed

[20]. In structural fire engineering, a structure is deemed to have failed only at the point of collapse. The purpose of fire safety engineering is to ensure the safety of occupants and fire service personnel, and not to avoid structural damage. The prescriptive approach to fire engineering is to specify minimum fire resistance periods, within which the structure must satisfy structural resistance, compartment integrity and insulation criteria during fire; these are typically 30, 60, 90 and 120 minutes [21]. These fire resistance times are usually obtained by using passive protection such as intumescent paint, cementitious sprays or fire-resistant boards. An alternative approach to fire engineering is performance-based design, which uses calculation methods based on full-scale fire tests, component testing and investigating buildings previously damaged by fire. Many of these are based on time-temperature curves which approximate the temperature during the heating, flash-over, and cooling phases of a fire. Time-temperature curves include the "standard" and "parametric" fire curves which are available in EN 1991-1-2 [22] (Figure 2.2-2). More recently, research at The University of Edinburgh has also considered the travel of fires (and therefore time-and-location-varying temperatures) across compartments [23].

Research in this field accelerated after a European, joint-research programme [24] carried out a number of full-scale fire tests on a purpose-built 8-storey office block, complete with office furniture, in 1995-96. Sand bags simulated applied loading during the tests, and heating methods ranged from gas fired furnaces heating individual elements, to a realistic fire load consisting of 20% plastics, 11% paper and 69 % wood fuelling a full scale 'office' fire (Figure 2.2-3). To date this is the only project to have been carried out at this scale, and it provided considerable information, including; the magnitudes of vertical deflection observed in beams and the temperatures experienced by them.

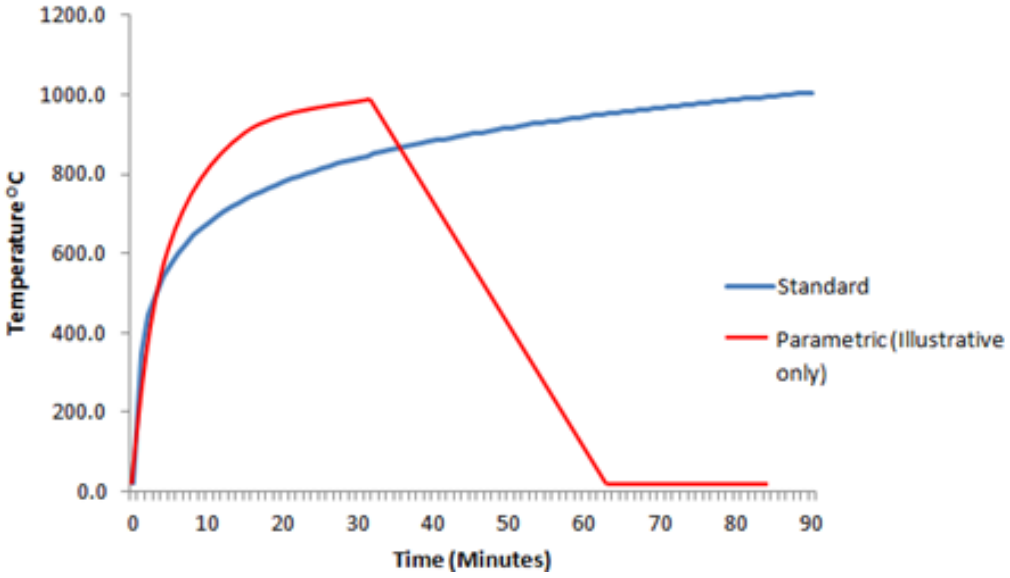

Figure 2.2-2 Standard and typical parametric fire curves. (copied from [25])

The idea of compartmentation, or treating isolated areas independently, allows the temperatures likely to be obtained in a fire to be calculated using parametric fire curves based on the volume of the compartment, the fuel within it, and the number and sizes of potential openings. It also allows predictions of the behaviour of the structure within that compartment to be made. One discovery during the Cardington fire tests was that a composite floor (metal deck and concrete slab) can behave as a tensile membrane under the right conditions with a ring of compression around fire protected periphery beams and the central portion of the slab sagging in tension [26, 27]. In some instances, the structure may be less likely to collapse if the internal beams are not fire protected to allow membrane action to occur.

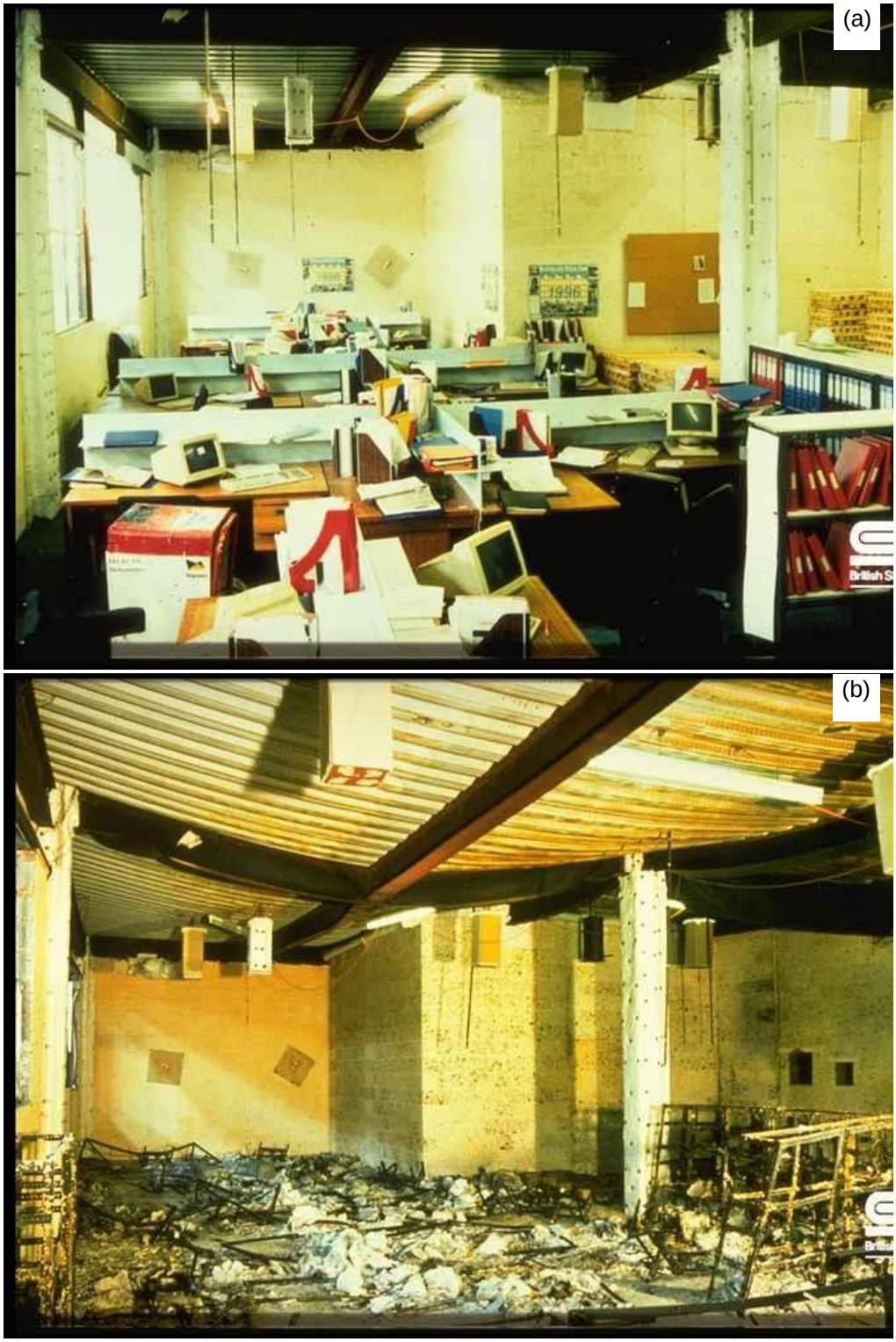

Figure 2.2-3 Internal view of office compartment (a) prior to and (b) following the Cardington fire test (Figures 6.41 and 6.45 copied from [24]).

One of the most significant findings to come out of the Cardington tests was that very high steel temperatures were achieved without causing failure of the structure. Failures are observed at significantly lower temperatures in individual member tests. This highlights the importance of understanding the behaviour of a structure as a whole during fire; something which is much more complicated to predict than the behaviour of the individual parts in isolation.

2.2.2 Connection Behaviour

Advances in the prediction of connections behaviour were further stimulated by the well-documented collapse of World Trade Centre 7, late in the day of 11 September 2001, which was subsequently rationalised [28] as having been caused by the shearing of bolts and consequent connection failure. This 47 storey office block was ignited by debris following the collapse of WTC 1, one of the 'Twin Towers' impacted by aircraft. The collapse of this building could have been prevented if the sprinkler system was operational. However, the excessive thermal expansion of long floor beams and connections which had not been properly designed to accommodate thermally induced lateral loads led to the building's collapse.

One method of modelling the behaviour of connections in fire is using component models, which use a series of non-linear springs to represent the behaviour of different zones (e.g. compression and tension zones) of the connection. This method is now widely accepted, and ambient-temperature component models are now included in EN 1993-1-8 [29] for 'semi-rigid design' of frames. Applying elevated-temperature material properties to the ambient-temperature models yielded elevated-temperature component models [30]. This was found to give conservative results, and a new empirical model was adapted by Spyrou [31, 32]

based on experimental work carried out on individual components, such as the column web in compression and end-plate in tension. These tests were carried out in a large electric furnace with full-scale components and the relevant tensile/ compression force applied using a hydraulic jack. The component models were developed further by Block [33], and can now be included in the overall component-based connection representation.

A large study has since been carried out at The University of Sheffield using the furnace originally used by Spyrou [31, 32], to test full-scale fin-plate [34] and end-plate [35] connections to steel column sections. This work was later extended to end-plate and innovative reverse-channel connections [6] to composite columns under fire conditions (Figure 2.2-4). The test-setup for both of these programmes allowed large rotational and axial forces, typical of those experienced during fires, to be applied to the connections.

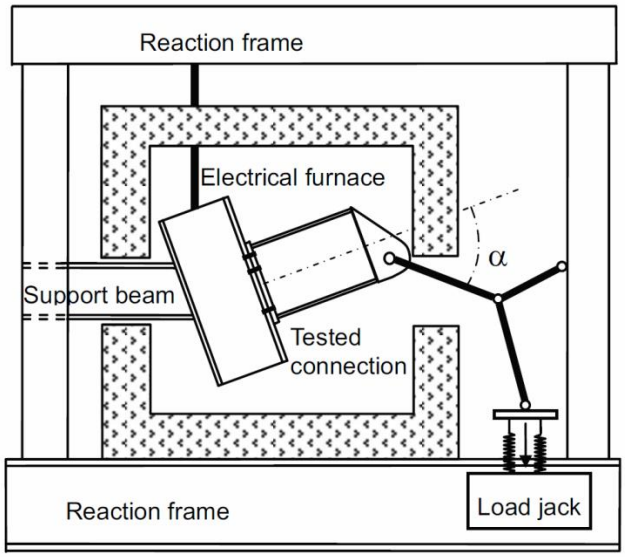

Figure 2.2-4 Test set-up for the full-scale connection test of end plate connections at elevated temperature (Copied from Figure 1 [35])

The research, particularly that carried out on composite column connections, identified thread-stripping failure of the bolt assemblies, prior to failure of the

connections being tested. Since the aim of the project was to test connections to failure, two nuts were used per bolt, in order to avoid premature thread-stripping failures [6]. Although this issue was not explicitly stated in [35], it is clear from images within the paper that two nuts were also used in this research. When bolt assemblies fail at an early stage, especially in a 'brittle' mode such as thread-stripping, the robustness of the connections will be impaired.

2.2.3 Bolts

Within this part of the literature review the results of some of the more significant studies carried out on the behaviour of nuts and bolts will be discussed. The section is separated into four themes; temperature, strain-rate, load distribution and failure mode. A large number of variables control the prediction of strengths and failure modes of bolt assemblies, and these can be difficult to quantify.

Temperature

While 'nominal fire' curves describe continuously increasing temperature with time, both heating and cooling phases are present during a real fire. Both phases were considered within the international research project COSSFIRE (Connections of Steel and Composite Structures under Natural Fire Conditions) on connections under natural fire conditions [36, 37]. This project included a study of the behaviour of M12 bolts of Grade 8.8 in accordance with the German standard, DIN 931 [37]. This research focused on 'natural fire conditions', including both the heating and cooling phases during fires. Strength reduction factors normalised against ambient-temperature steady-state test results were plotted on the same charts for heating and cooling, in order to show the extent of recovery of material properties after being cooled from 400, 600 and 800°C. Strength reduction factors obtained from tensile tests are given in Figure 2.2-5.

For the steady state-tests the bolts were heated without load, at a rate of 10-30˚C/min, until the desired temperature was reached, and were then held there for 15 minutes prior to testing. In the “natural” fire test, the temperature was stabilised at the desired “upper” temperature T_u for 15 minutes before cooling at a rate of 10-30˚C/min, to the desired test temperature T_f , when the specimen was loaded immediately. A test velocity of 0.01mm/s was used.

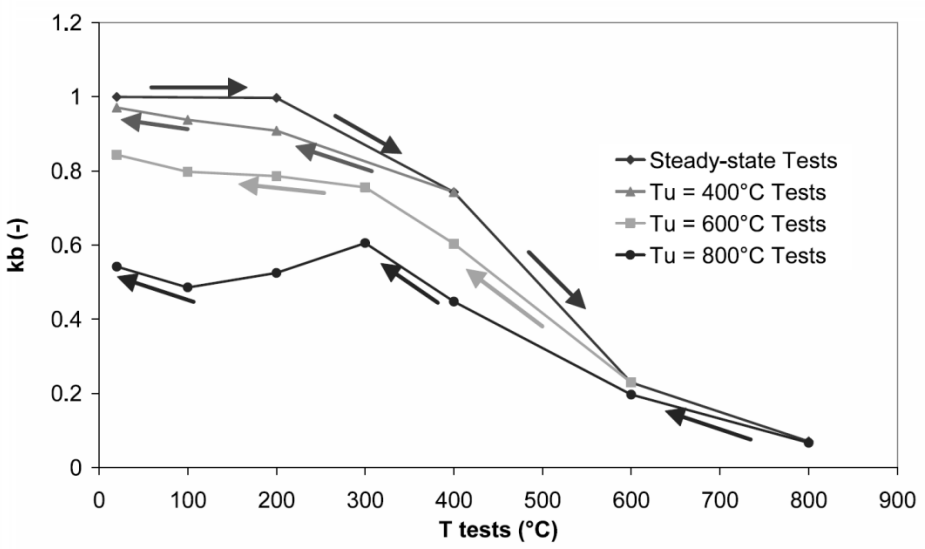

Figure 2.2-5 Tensile strength reduction factors (Figure 10 copied from [37])

No stripping failures were observed in this series of tests. Rockwell hardness measurements were performed at the surface, centre, and close to the surface for two specimens prior to testing, and a uniform hardness was measured with readings of 64 or 65 HRA (equivalent to approximately 290 HV [38]) at all locations. An analytical model was proposed for the strengths obtained during the cooling phase based on an analytical model first proposed by Riaux [39] which fitted the experimental data well.

The results of steady state tests, in which the bolts were heated to the desired test temperature and held for 15 minutes prior to testing, showed reduced strength and increased ductility with increasing temperature (Figure 2.2-6). There was one

exception, at 200˚C, which showed a slight increase in strength compared to ambient-temperature behaviour, which may be attributable to secondary tempering, precipitation of carbides and associated precipitate strengthening.

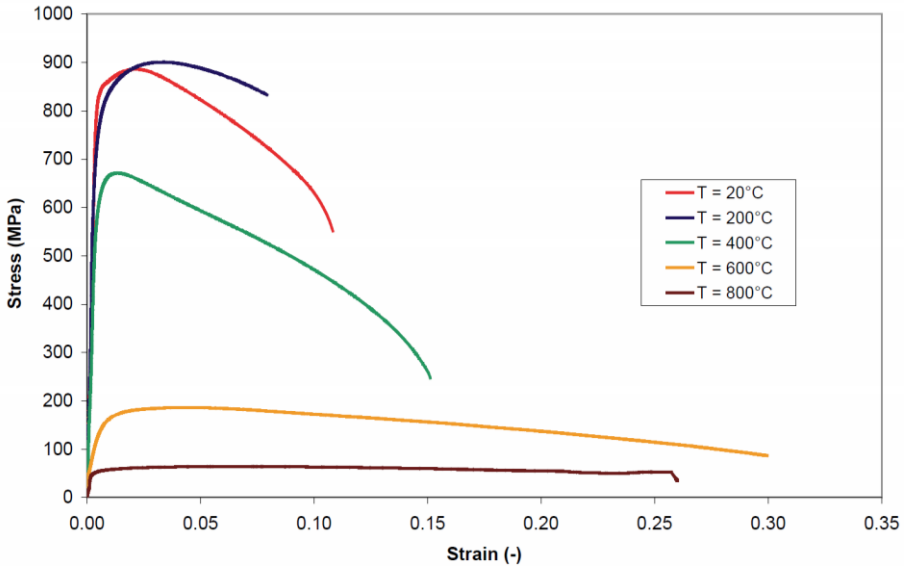

Figure 2.2-6 Stress strain curves obtained from steady state tests (Copied from figure A-9 [36])

The results obtained following a heating stage up to 800˚C gave interesting results (Figure 2.2-7). Not only was there an increase in strength with increase in temperature from 100 to 200˚C, but the testing at 300˚C showed significantly higher strength than at any other temperature. In addition to these observations, the shapes of the stress-strain curves obtained at 20°C and 100°C are very different from those at other test temperatures, exhibiting the upper and lower yield points characteristic of a pearlite microstructure.

Plotting ultimate tensile strength against temperature for the results of tests carried out at 200˚C and above (which did not exhibit upper and lower yield strengths) indicates an increase in strength at 300˚C due to strain aging and maximum work hardening (Figure 2.2-8).

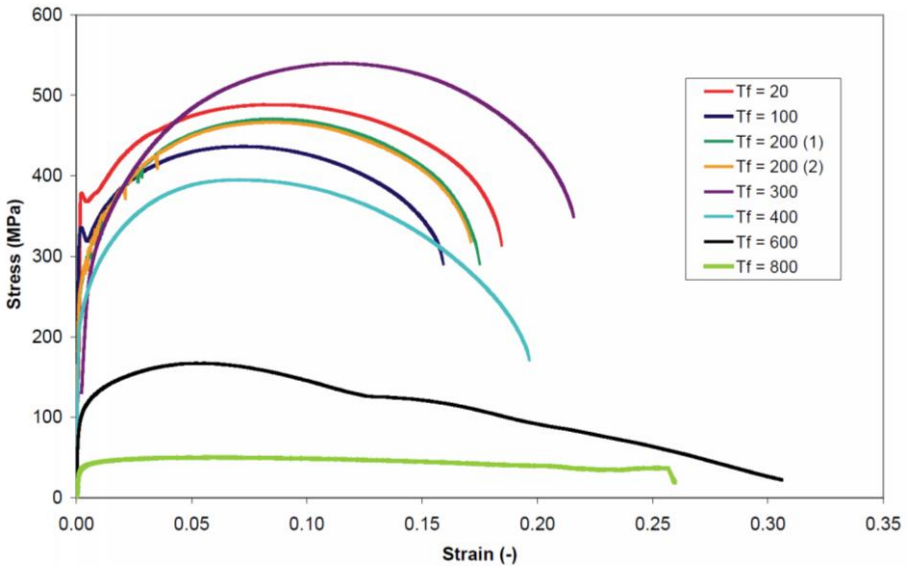

Figure 2.2-7 Stress strain curves obtain from "natural fire" tests after being heated to T_u = 800˚C (Copied from Figure A-10 [36])

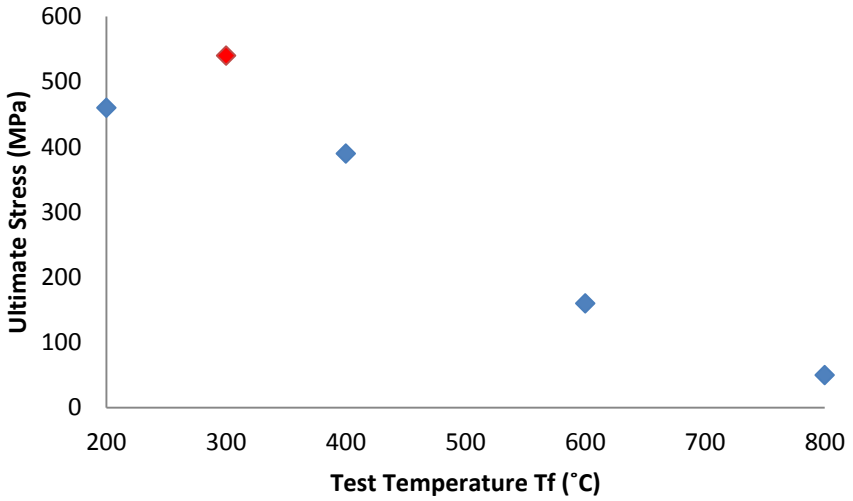

Figure 2.2-8 Ultimate stress vs test temperature of "natural fire" tests after being heated to Tu = 800˚C

In order to explain the upper and lower yield points present in the results at 20°C and 100°C, the time-temperature history of the bolts should be considered (Figure 2.2-9). Grade 8.8 bolts such as those used in this study are quenched and tempered during manufacture. During this process the steel is heated above the A3 line (Figure 2.2-10) and held for a sufficient time to allow all carbon atoms to form a

solid solution in single-phase austenite. The austenite is then quenched rapidly to form martensite, and subsequently tempered at approximately 420°C to improve its ductility; more detail will be provided about the heat treatment process within the discussion later.

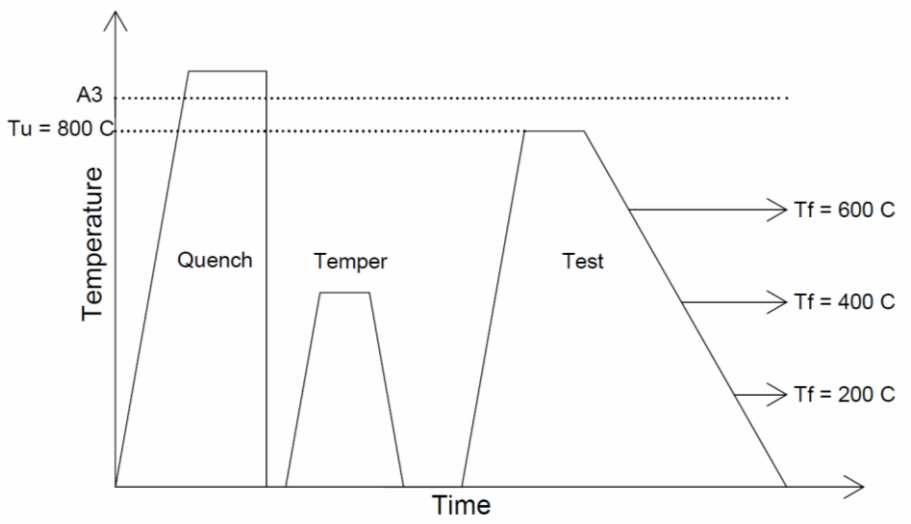

Figure 2.2-9 A schematic of the time-temperature history of bolts tested after being heated to Tu = 800˚C [36]

During the “natural fire” tests carried out in this research, the bolts were re-heated to an “upper” temperature. In the case of Figure 2.2-7 this temperature was 800°C. At 800°C steel containing a carbon content of 0.25-0.55wt%, as specified in ISO 898-1 [11], will be fully, or at least partially austenitic, and a slow cool will transform austenite to pro-eutectoid ferrite and pearlite, effectively annealing the microstructure. The upper and lower yield behaviour experienced by steel subsequently cooled to 20°C and 100°C is characteristic of well-annealed steel containing a low dislocation density. Upon loading at these temperatures the dislocation density is increased, and interstitial atoms such as C and N cluster around these defects, locking the dislocations in place [40]. The upper and lower yield observed are caused by the sudden breaking away of dislocations from these interstitial clusters. For temperatures greater than 100˚C it is likely that the

dislocation density has not been reduced sufficiently to cause this behaviour, and therefore there is a smooth transition between elastic and plastic behaviour.

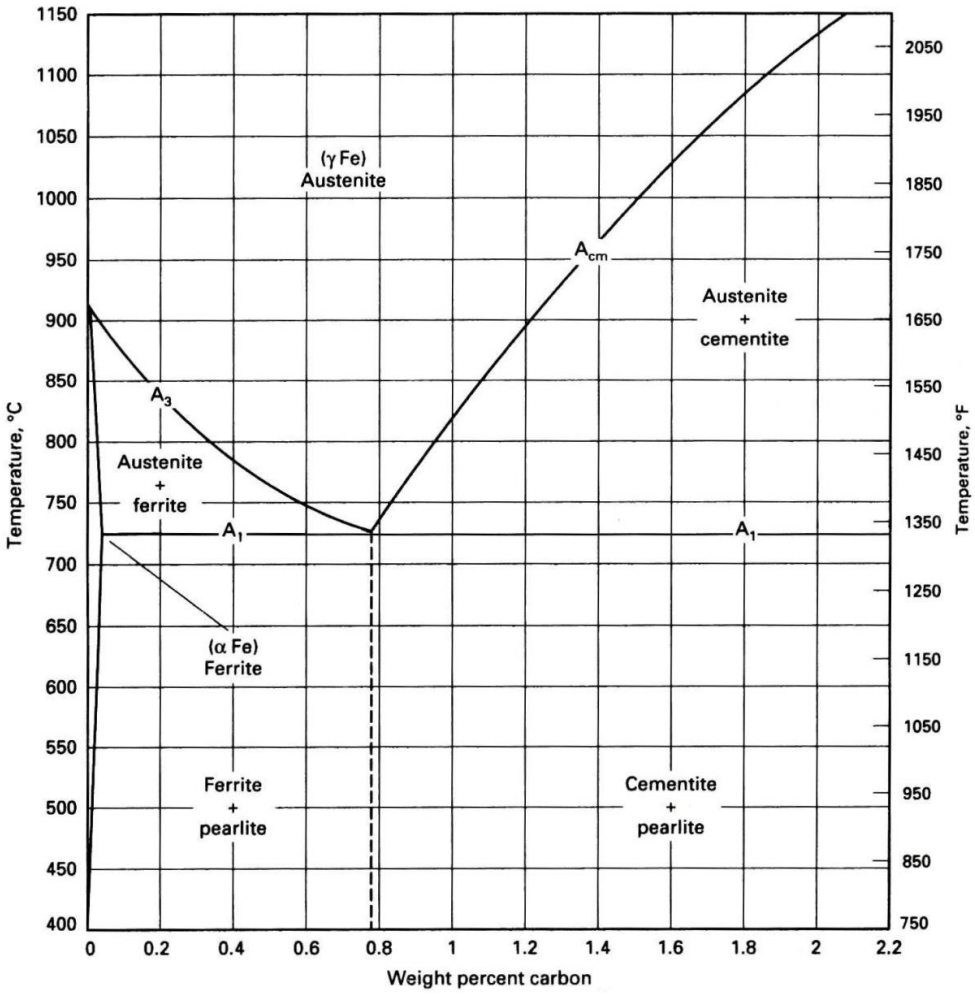

Figure 2.2-10 Iron-carbon binary phase diagram. (Copied from Figure 2, ASM Handbook, Vol. 4 [41])

Another piece of evidence to support a full or partial phase change to austenite at higher temperatures, and annealing of the steel during cooling, is shown in Figure 2.2-11. The stress-strain curves contained in this figure were obtained at test temperatures of 20°C and 400°C after being heated to, and cooled from, a range of high temperatures. Bolts which had been heated to 800°C and 900°C have been heated to a sufficiently high temperature to transform, partly or fully, to austenite.

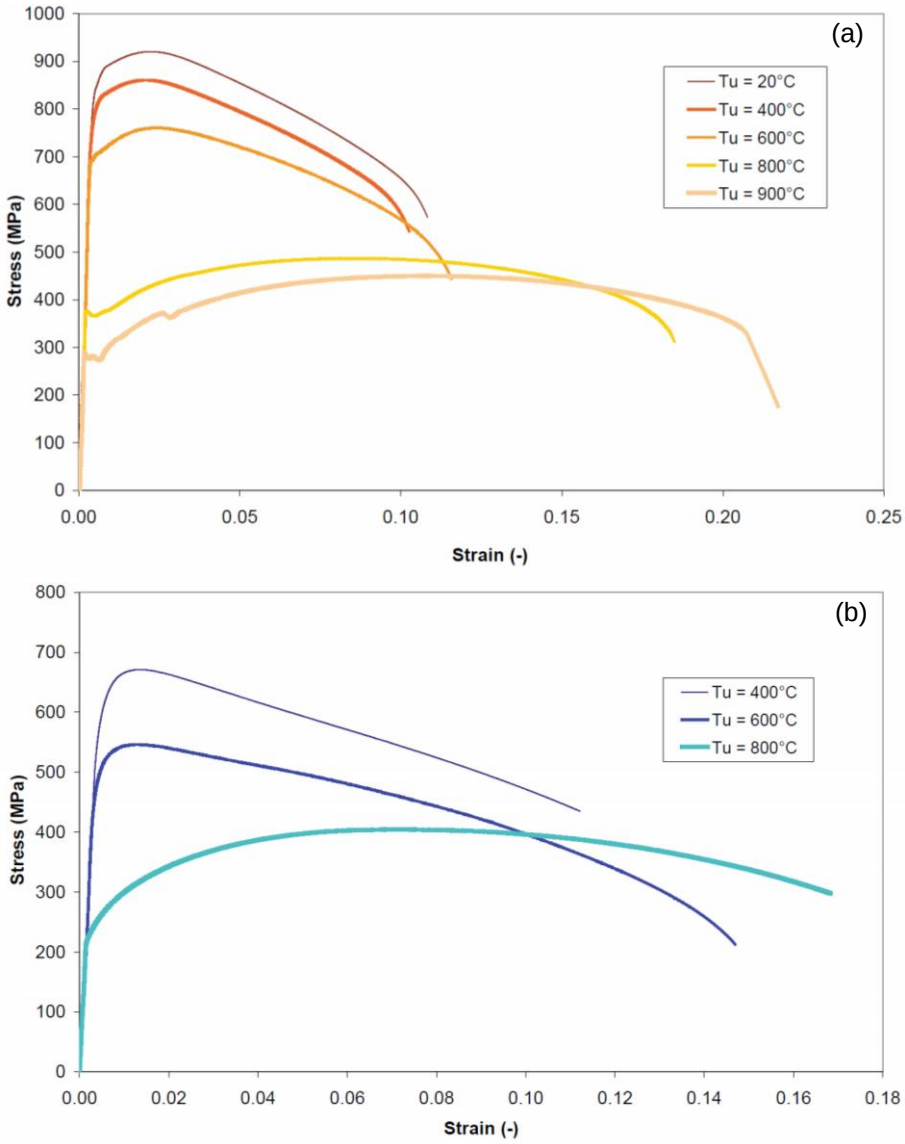

Figure 2.2-11 Stress-strain diagrams obtained from "natural fire" tests carried out at a test temperature of (a) 20°C and (b) 400°C following heating to a range of "up" temperatures as specified in the key. (Copied from Figure A-11 [36])

After cooling slowly to 20°C from these temperatures, both curves exhibit upper and lower yield points; again indicating a well-annealed microstructure at 20°C (Figure 2.2-11 (a)). However, when a bolt was cooled from 800°C and tested at 400°C a smooth curve was produced, again suggesting insufficient annealing to reduce the dislocation density to levels where an upper and lower yield point are produced (Figure 2.2-11(b)). It is interesting to see the change in stress-strain

behaviour once the upper temperature moves from the ferrite and pearlite to austenite and ferrite region of the phase diagram. At 20-600°C (Figure 2.2-11 (a)), the steel is undergoing a second temper; however, at 800-900°C the steel has undergone a phase transformation to ferrite and austenite or pure austenite.

Strain Rate

The strain-rate dependence of structural bolts, including uncoated Grades 8.8 and 10.9, galvanised Grade 8.8, and stainless steel Grades A470 and A480 with diameters of 12 and 16 mm, has been investigated under dynamic loading rates of 100kN/ 5, 15 and 30s [42]. While self-coloured bolts failed through thread-stripping, stainless steel performed much better, with higher strength and ductility and no thread-stripping failures. The failure mode of the carbon steel bolts was changed to necking from thread-stripping if two or more nuts were used on each bolt, and doing this increased the ductility by 3.5–4.5%. At these high rates of loading, both strength and ductility were observed to decrease. Stainless steel bolts had very good strength and ductility, and always failed through necking, even with a single nut.

Another study was carried out by Fransplass [43] on 4.7mm threaded rod and turned-down rod of Grade 4.6 in order to make modifications to a detailed mathematical model which exists for ambient-temperature failure-mode prediction [44]. The existing model omits strain-rate (and temperature) dependence, and calculates bolt breakage and nut- and bolt-stripping loads for a given thread combination, based on the material strength and tensile stress area of each component, and a number of factors which take into account nut dilation and thread bending. The lowest of these three calculated strengths determines the mode of failure [44]. In Fransplass's research [43] the rod was tested within internally threaded tool-steel fixtures of significantly higher strength than the rod

threads. This would have reduced the likelihood of thread-stripping because the stiffness and strength of the tool-steel threads prevents deformation of the bolt threads. It also gave an inaccurate representation of a real nut-bolt assembly, in that the internally threaded fixtures would exhibit different dilation behaviour from that of nuts, a factor which has been suggested to affect the likelihood of thread-stripping [44]. The modification made to Alexander's model [44] was to include strain-rate-dependent values of tensile strength in the bolt fracture and nut and bolt stripping force calculations, rather than including a strain-rate-dependency parameter in the equation. This modification therefore requires strain-rate-dependent values of strength to be known by the user. The calculated failure loads fitted the test data well, but the study should have been extended to include complete nut-to-bolt assemblies, and materials of different steel grades, for further validation. The results were compared with those from a similar study which had been carried out by Mouritz [45] at similar rates of strain using the same steel grade with similar Vickers hardness values. The test procedures used by the two authors varied, however, with Mouritz using tensile testing ($\approx 2.5 \times 10^{-5} s^{-1}$), drop tower impact testing ($\approx 1\text{-}10 s^{-1}$) and underwater explosion shock testing ($\approx 10^{2} s^{-1}$) and Fransplass using a servo-hydraulic testing machine, and a split-Hopkinson tension bar for measurement at high strain-rates. The results from Fransplass showed a trend that, with increasing strain-rate, there was an increase in ductility and strength, which was claimed to be in disagreement with previously published results of Mouritz. What Mouritz had discovered, however, was that the ratio between thread-stripping strength and necking strength decreased with increasing strain-rate (rather than the material strength itself). At $2.5 \times 10^{-5} s^{-1}$ thread-stripping strength was 29-52% of necking strength, 38% at $1\text{-}10 s^{-1}$, and decreasing to just 8-15% at $10^{2} s^{-1}$. Both of these studies focused on grade 4.6 bolts with a microstructure consisting mostly of ferrite with small amounts of pearlite, and

average Vickers hardness values of 212 [43] and 218 HV [45]. These results, therefore, cannot be used to predict the strain-rate dependence of Grade 8.8 bolts which contain a tempered martensite microstructure.

The literature suggests that all threads are not subjected to evenly distributed loading, with threads more heavily loaded at the bearing (loaded) face of the nut [46, 47], with little load applied to threads near to its free face (closest to the end of the bolt shank) . This is not reflected by a micrograph presented by Mouritz [45], showing equal amounts of thread deformation on each thread, which indicates an even load distribution over the entire nut height. The reasoning given for this is that stress distributions may become more even beyond the yield strength.

Load Distribution

One of the first studies into the distribution of force in threads was performed in 1948 by Sopwith [46]. This produced a detailed mathematical model for the calculation of load concentration at certain distances from the loaded face of the nut, and proposed a number of methods for producing a more uniform force distribution. One proposal was to use a smaller pitch (spacing) in the bolt threads than in the nut threads, with the bolt thread pitch decreasing from the unloaded towards the loaded face of the nut, the reason being the surmise that prior to loading only the threads at the unloaded face of the nut would be in contact. Upon loading, the engagement length would increase until the whole nut was in contact. Another proposal was to reduce the elastic modulus of the nut, reducing its stiffness by using Duralumin ® rather than steel, was found to reduce the load concentration factor by 25%. Reducing the nut stiffness by reducing its external dimensions had the opposite effect, however, because the axial strain was increased while the stiffness's of individual threads were unaffected. Following this publication, a number of finite element models [48-51] were developed and

validated against Sopwith's mathematical model. Until 1985, the force distribution in threads had not been obtained experimentally. Kenny and Patterson [47] were able to do this by machining a 30mm diameter bolt assembly from solid blocks of Araldite ®, (a clear structural, epoxy resin adhesive) and loading it in a stress-freezing cycle to 1.2% strain in the unthreaded section of the bolt. Once stressed, the nut was cemented in place and 1.5mm thick slices were cut. The photo-elastic fringe pattern was then observed using a fringe-multiplying polariscope (Figure 2.2-12). This method used double-refraction birefringence of polarized light to identify stress bands in the Araldite bolt assembly. The locations and fringe orders of each band were extrapolated to provide load and position data which correlated well with Sopwith's theoretical model.

Figure 2.2-12 The x3 multiplied fringe pattern for a thread half a pitch from the loaded face of the nut x26 (copied from [52])

A method for studying three dimensional force distributions using a virtual contact loading method (VCLM) was applied to a bolt assembly in 1994 [53], providing a theoretical method for calculating force distribution of three-dimensional threads. The frictionless model agreed well with Sopwith's model and previously published

FE data [48-50]. One of the finite element models mentioned above [48] investigated the influence of root radius on the bolt threads and found that, within the range of root radii (0.3-0.43mm) specified in the standards, there was little increase in stress concentration factor. Below the minimum root radius, however, the stress concentration factor decreased rapidly with decreasing root radius.

Failure Modes

Bolt necking and thread-stripping are two common failure modes of bolt assemblies under tension. Whilst necking failures involve localised necking in the bolt shank, thread-stripping involves heavy deformation of one or both thread sets, with the nut eventually pulling off the end of the bolt shank. Thread-stripping is often considered to be a “brittle” failure mode, due to its rapid reduction in load capacity at the onset of failure. Clearly thread-stripping should be avoided in order to prevent sudden failure of bolted connections. It is a failure mode which may occur in an end-plate connection, such as that shown in Figure 2.2-13, where bolt rows are under a uniform fastening tension at ambient temperature and varying tensions, some of which may be very high, at elevated temperatures once beams have begun to sag.

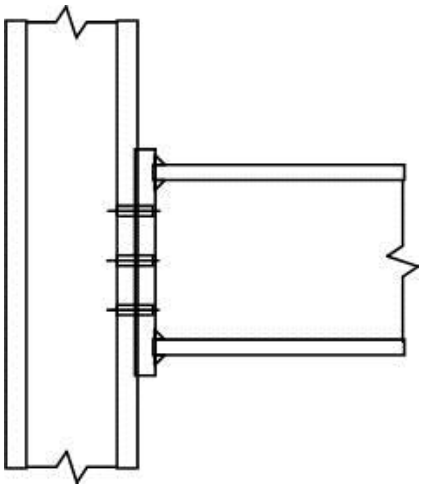

Figure 2.2-13 End-plate connection

Strength reduction factors, prescribed by Eurocode 3 Part 1-2 [8] are currently applied to fasteners in structural fire design, despite the possibility of either bolt breakage (shank necking) or thread-stripping as the failure mode in tension. A simplistic assumption is that the failure mode depends on the thread engagement length and the relative strength of the mating threads. When the thread engagement length is long and the mating thread strengths are comparable, bolt breakage is most likely. When the strength of one thread set is greater than the other and the length of thread engagement is short, thread-stripping is likely to occur in the weaker thread set. A detailed mathematical model [44] based on this assumption allows for failure mode prediction of bolt assemblies at ambient-temperature. Modifications to this model [43] have recently been made for elevated rates of strain, but no attempt has yet been made to include temperature and low strain-rate dependency on failure mode prediction.

A number of bolt assembly tests [1, 3-5] have been carried out at elevated temperatures to evaluate and compare the performance of various bolt assemblies in fire. As yet, no direct comparison has been made between the results of these tests. Comparisons can easily be made on the basis of failure mode and ultimate load capacity; however, it is difficult to draw conclusions about the effects of different parameters on the failure mode, due to the number of variables present in the bolt assemblies investigated, and in their test methods. Tests have involved assemblies of different geometrical tolerances, diameters, steel grades, forming methods (hot and cold) and finishes, as detailed in Table 2.2-1.

Only González has explicitly stated that they had considered ‘structural’ bolting assemblies in accordance with EN 15048 [9]. However, no research has yet been carried out into galvanised structural bolting assemblies consisting of Grade 8.8 bolts and property Class 10 nuts. While González [4, 5] researched galvanised bolt

assemblies, these were high-strength assemblies suitable for pre-loading [54] and consisted of Grade 10.9 bolts and property Class 10 nuts.

Table 2.2-1 Summary of the processing and geometrical tolerances of bolt assemblies tested at elevated temperatures in previously published work [1, 3-5]

Author	Assembly			Bolt				Nut			
	Ref	d (mm)	Tol.	Code	Grade	Formed*	Finish	Code	P. Class	Formed*	Finish
Kirby	1	20	8g7H	4190	8.8	CF	SC	4190	8	HF	SC
	2	20	8g7H	4190	8.8	CF	SC	4190	8	CF	G
	3	20	8g7H	4190	8.8	CF	SC	4190	8	HF	SC
	4	20	8g7H	4190	8.8	CF	SC	4190	8	CF	G
	5	20	8g7H	4190	8.8	HF	SC	4190	8	HF	SC
González	6	16	6g6AZ	14399-4	10.9	CF	G	14399-4	10	-	G
	7	16	6g6AZ	14399-4	10.9	CF	G	14399-4	10	-	G
Hu	8	20	-	4190	8.8	-	-	-	10	-	-
	9	20	-	ISO 4014	8.8	-	-	-	10	-	-

*Where CF = cold formed, HF = hot formed, SC = self-colour and G = hot dip galvanised

The chemical compositions of bolts 1-5 tested by Kirby are given in Table 2.2-2, and show a significant range in wt%C. At the time that his research was published, the detailed chemical compositions in ISO 898-1 (and the standard itself) did not exist. Those compositions which fall outside the current limits are highlighted in red and, despite the wide range of compositions present in the bolts he tested, most of these comply with the current standard.

The steady-state test methods (constant temperature and strain-rate) employed by the different authors, and their resulting ultimate tensile capacities and failure modes, are shown in Table 2.2-3. While some assemblies failed in a single failure mode, others failed in a combination of modes. Kirby [1] tested at a constant strain-rate of 0.001-0.003 min^{-1} until ultimate capacity was exceeded. González [5], however, tested at 0.001min^{-1} up to the 2% proof stress, and then at 0.025min^{-1} to rupture, this means that ultimate load capacities obtained may be

disproportionately high if the strain-rate was increased before the ultimate load capacity was reached. Test methods and strain-rates were not specified by Hu [3], and therefore his strain-rate was estimated assuming a gauge length of 30mm, based on the specified test velocity of 0.003mm/min.

Table 2.2-2 Chemical compositions (wt%) of the bolts and nuts tested by Kirby [1]

	Composition (weight %)							
	C	Si	Mn	P	S	Cr	Mo	Ni
Bolt A	0.19	0.21	1.16	0.02	0.017	0.19	0.027	0.14
Bolt B	0.21	0.25	1.02	0.009	0.009	0.23	0.021	0.10
Bolt C	0.41	0.16	1.61	0.021	0.021	0.13	0.130	0.12
Nut A	0.25	0.21	0.77	0.010	0.010	0.06	0.018	0.08
Nut B	0.18	0.02	0.45	0.024	0.024	0.03	0.005	0.04

	Composition (weight %)						
	Cu	Al	B	N	Nb	Ti	V
Bolt A	0.22	0.029	0.005	0.008	-	0.036	0.006
Bolt B	0.14	0.029	0.002	0.012	-	0.042	-
Bolt C	0.23	0.018	-	0.013	-	-	-
Nut A	0.16	0.017	-	0.012	-	-	-
Nut B	0.04	0.037	-	0.006	-	-	-

Table 2.2-3 Summary of the ultimate load capacities and failure modes obtained from steady-state tensile tests at a range of temperatures in previously published work **[1, 3-5]**

Ref.	Strain rate (min-1)	Heating rate (˚C/min)	Hold time (min)	Fu (kN) at Temperature (˚C)										Failure Mode**
				20	100	150	200	300	400	500	550	600	700	
1	0.001-0.003	5-10	15	226	216	-	215	217	178	126	94	59	24	N
2				198	191	-	177	190	168	118	86	54	23	S
3				206	201	-	206	203	168	122	96	62	27	N
4				189	180	-	168	176	158	112	85	54	25	S
5				232	217	-	215	206	183	144	116	80	28	C
6	0.001-0.005	-	30	266	-	-	254	252	210	123	78	47	19	C
7				264	-	-	256	245	203	121	76	50	18	C
8	0.0001*	2-2.5	15	202	-	198	-	187	140	75	-	39	-	N
9				239	-	232	-	225	168	115	-	48	-	N

* Assuming a 30mm gauge length

** Where N = necking, S = thread-stripping and C = combination

The general trend observed for Grade 8.8 bolts was for assemblies which failed by necking to fail at higher ultimate tensile strengths than those which failed by stripping. Assembly 5 failed in combinations of necking and thread-stripping at all temperatures, with both modes occurring at similar ultimate load capacities. Grade 10.9 bolts from Assemblies 6 and 7 exhibited temperature-dependent failure-modes, with a combination of necking and thread-stripping up to 420°C, "liquid metal embrittlement" caused by melting of the zinc coating from 420-650°C, and pure stripping above 650°C.

Using the published tabular or graphical data given in Table 2.2-3 the ultimate load capacities at elevated temperature have been normalised with respect to ambient temperature in Table 2.2-4, and compared to the strength reduction factors prescribed by Eurocode 3 (Figure 2.2-14).

Table 2.2-4 Strength reduction factors calculated from published data [1, 3-5]

Ref.	Reduction Factor									
	20	100	150	200	300	400	500	550	600	700
1	1.00	0.95	-	0.95	0.96	0.79	0.56	0.42	0.26	0.11
2	1.00	0.97	-	0.90	0.96	0.85	0.60	0.44	0.27	0.11
3	1.00	0.97	-	1.00	0.99	0.81	0.59	0.46	0.30	0.13
4	1.00	0.95	-	0.89	0.93	0.84	0.59	0.45	0.28	0.13
5	1.00	0.94	-	0.93	0.89	0.79	0.62	0.50	0.35	0.12
6	1.00	-	-	0.96	0.95	0.79	0.46	0.29	0.18	0.07
7	1.00	-	-	0.97	0.93	0.77	0.46	0.29	0.19	0.07
8	1.00	-	0.98	-	0.92	0.69	0.37	-	0.19	-
9	1.00	-	0.97	-	0.94	0.70	0.48	-	0.20	-
EN1993-1-2	1.00	0.97	0.95	0.94	0.90	0.78	0.55	-	0.22	0.10

The strength reduction factors given in Eurocode 3 fit the experimental data well up to 300°C, beyond which the experimental data from Kirby's research continues to fit the prescribed curve well. However, the results of Hu [3] and González produce significantly lower strength reduction factors, most significantly at 500°C. Despite having a significantly higher strength at ambient temperature, those assemblies

containing Grade 10.9 bolts exhibited comparable strength to Grade 8.8 bolts at 500°C and lower strengths at temperatures 550°C and higher.

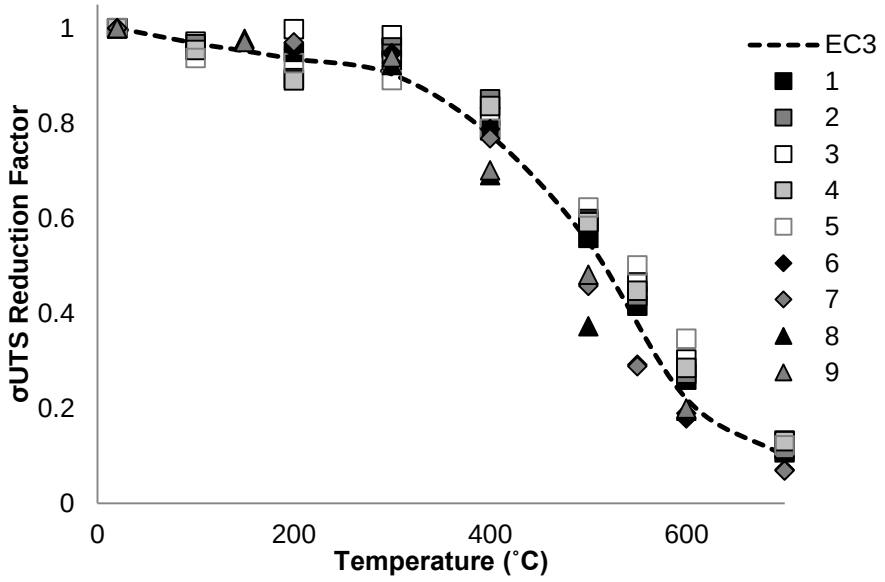

Figure 2.2-14 Ultimate tensile strength reduction factors normalised with respect to ambient temperature strength for assemblies 1-9 and compared to EN 1993-1-2 (Table 2.2-3)

Turned-down Bolts

González also carried out both steady-state and transient tests on turned-down bolts with a cross-sectional diameter of 6mm and gauge length of 30mm [5]. The transient tests were stressed at constant load and constant heating rate of 10°C/min, while steady-state tests were heated at an unspecified rate to the test temperature and then held for 30 minutes, before being tested at constant temperature at a strain-rate of 0.001/min, up to the 2% proof stress and then at 0.025/min to rupture. The results of the transient tests are not given in tabular or graphical form, however it is stated that the static test results gave significantly lower ultimate strengths than the comparable transient test results. The strength reduction factors calculated from the steady-state turned-down bolt test results correlated well with those prescribed in EN 1993-1-2, despite bolt assemblies from

the same batch showing a significant loss of strength in comparison to the Eurocode values at temperatures above 450°C.

Kirby also carried out tensile tests on turned-down bolts. These were steady-state tests performed at a constant temperature and strain-rate of 0.002/min up to the 5% proof stress before being raised to 0.1/min until rupture. Comparing the temperature-stress curves obtained at the 5% proof stress for the material of bolt set A with the temperature-force curves obtained for bolt A with nut set A (which failed by necking) and nut set B (which failed through stripping) it is clear that the values obtained with nut set A show behaviour very similar to the bolt material. However, the assembly which failed through thread-stripping failed at a significantly lower capacity. Comparing the results of bolt set C with those obtained for bolt set C and nut set A (which failed in a combination of necking and stripping at all temperatures) it is clear that the shapes of the curves are not identical. Calculating the equivalent load capacity for the maximum stress of 910N/mm^2, obtained at 250°C for the material of bolt C and a stress area of 245mm^2 for an M20 bolt, gives 223 kN, which corresponds to the peak observed at approximately 250°C for bolt set C.

All of Kirby's tensile results obtained for both bolts and bolt-material show reductions in strength with temperature, with the exception of a peak in strength observed at around 300˚C (Figure 2.2-15). This behaviour was also observed in nuts and bolts studied under steady-state conditions as part of the COSSFIRE research programme [36] (Figure 2.2-6) at 200°C, and suggests either an incomplete temper during heat treatment, or a secondary tempering effect when the steel is re-heated to around 300˚C.

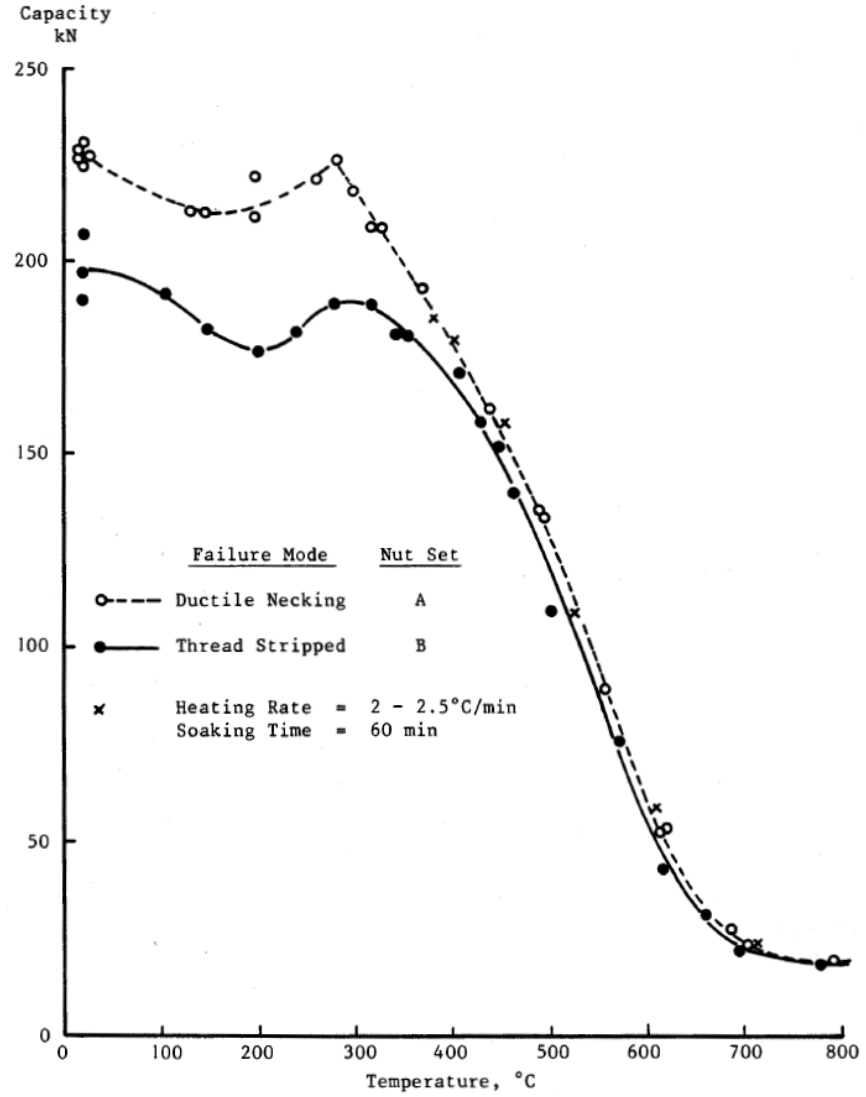

Figure 2.2-15 An example of the peak in strength observed at approximately 300°C for bolts and bolt material tested by Kirby (the results shown are from bolt set A). Copied from [55]

Typically the precipitation of carbides including epsilon carbides (in high C steels) at up to 200°C, and rod-shaped carbides at between 200-320°C, lead to a significant drop in hardness [56]. Carbide-forming alloy elements including B, Mo, Ti, V and W, however, can lead to hardening and are present in small quantities in the steels used to make bolts. The precipitation of these carbides impedes the dislocation motion, as dislocations must either climb around precipitate particles or cut through them. This becomes increasingly difficult as the precipitates coarsen

with increasing temperature, until they become so large that it becomes energetically favourable for dislocations to loop around an obstacle in a process called Orowan looping [57]. Beyond this point, the hardness again begins to drop with increasing temperature.

Finite Element Modelling

Finite element models have been proposed on the basis of bolt assemblies [4, 58] and a bolt installed in a tapped part [59] in order to investigate thread-stripping failures. Martínez-Martínez [58] was specifically investigating the effect of thread engagement length on thread-stripping strength using M10, Grade 12.9 bolt and copper and AU4G nuts. The model was validated by steady-state tensile tests carried out on assemblies using nuts of varying height. It is not specified whether the nuts were purpose-made at different heights for the investigation, or whether nuts were partially-threaded onto the end of the bolt shank so that only the desired number of threads were engaged, however, a linear relationship between maximum load and engagement length was observed when thread-stripping failures were observed. The experimental and finite element results correlated well, but failure loads were significantly lower than the mathematical model proposed by Alexander [44], particularly in the case of AU4G nuts for which the results calculated using Alexander's model gave a failure load 62% higher than that obtained in tensile testing. Martínez-Martínez also determined an empirical model for the prediction of the failure mode of a bolt installed in a tapped part [59], which is common in mechanical applications. The purpose was to determine the minimum thread engagement required to avoid thread-stripping. When thread-stripping failures were observed, there was again a linear relationship between ultimate load capacity and thread engagement length, up to the critical thread engagement length. Above this value, where necking failures occurred, a constant ultimate load

capacity was observed. Simulation results, in terms of nominal bolt diameter and ultimate resistance of the bolt against failure load for the model determined, were again lower than those calculated using Alexander's model [44].

An axisymmetric FE model was developed by Gonzaléz [4] as part of his PhD thesis. However, the results from the FE model have not been published. The model was created using realistic material data determined by uniaxial tensile testing of turned-down bolts. The results correlated well with the steady-state tests carried out on nuts and bolts in terms of failure load and temperature. Failure modes, however, could not be accurately modelled due to liquid metal embrittlement failures occurring between 420-650˚C; a failure criterion does not exist for this mode of failure. At temperatures greater than 650˚C, necking and thread-stripping failures were in good agreement with test data.

2.3 Bolting Standards

European standards are identified by the prefix "EN", an abbreviation of "Euronorm", and are available nationally in English (BS EN), German (DIN EN) or French (NF EN). The content of these national standards is identical; they have simply been translated into the appropriate languages. International Standards, identified by the prefix "ISO", an abbreviation of "International Organisation for Standardization", are internationally recognised. Many of these are adopted as National or European Standards, the British versions of which are identified by the prefix BS ISO or BS EN ISO respectively. National British Standards, identified by BS, are gradually being phased out and conflicting national standards are being withdrawn without replacement. Standards will be referred to as "EN" or "EN ISO" throughout this document. The prefix "BS" has been removed unless a national British standard is being referred to, in which case it is only preceded by the prefix "BS".

2.3.1 Property Class Designation

The strength of standard ISO metric nuts and bolts can be identified from the markings on each component. The grade of a bolt describes its nominal yield strength and nominal ultimate tensile strength. The first number is one hundredth of the nominal ultimate tensile strength (MPa) and the second number is ten times the ratio between nominal yield strength and nominal ultimate tensile strength [60]. For example, a Property Class 8.8 bolt has a nominal ultimate tensile strength = 100 x 8 = 800 MPa and nominal yield strength = 0.8 x 800 = 640 MPa. Nuts are marked with a single number, which is usually equal to the first number marked on the pairing bolt. In this case, the proof load stress can be calculated by multiplying the number by 100, so that a Property Class 8 nut will have a proof stress of 8 x 100 = 800 MPa.

For structural applications, the most commonly used bolt is a galvanised M20 non-preloaded bolt of Property Class 8.8 as recommended by the Steel Construction Institute and British Constructional Steelwork Association [61]. While uncoated Grade 8.8 bolts are typically paired with Property Class 8 nuts, galvanised nuts are tapped over-size to accommodate the additional thickness of the zinc coating layer on bolt threads in accordance with section 5.6 of ISO 10684 [62]. Therefore a higher strength property Class 10 nut should be used to achieve full assembly strength [62].

Structural bolts are marked with their property class (8.8) and ‘SB’ which notifies the contractor that the bolt is a structural bolt, ‘M’ to indicate that the bolt is ISO metric; the bolt diameter and length (M20x80), and the identification mark of the manufacturer. Self-coloured nuts are marked with their Property Class (8) and ‘SB’ as well as the marking of the manufacturer. Galvanised nuts tapped over-size to tolerance 6AZ should be marked with their Property Class (10) followed by ‘Z’ [62].

Due to the high cost of raw materials in the UK, the majority of structural bolt assemblies are currently imported [63], largely from China and India. A UK distributor, such as the one that donated the assemblies for this research, will commonly import the components, carry out quality assurance checks and stamp their own identification mark on the surfaces. According to ISO 898-1 [11] a distributor which distributes fasteners marked with its own identification mark is considered to be the manufacturer, which makes the original overseas manufacturer untraceable unless the UK distributor is willing to share that information.

2.3.2 Mechanical Properties

A large number of standards exist for nuts and bolts, which can largely be split into two categories: (1) those which specify general mechanical properties, and (2) those which specify thread tolerance (the tightness of fit between threads). The ISO standards describe the strengths and test methods for the individual components and assemblies as a whole, as outlined in Table 2.3-1.

Table 2.3-1 Testing of mechanical characteristics of components [9]

Component	Mechanical Characteristic	Test	Reference Standard for test procedure
Bolt	Elongation after fracture	Tensile test	ISO 898-1 [11]
	Minimum tensile strength	Tensile test	ISO 898-1 [11]
	Lower yield stress at 0.2 % non-proportional elongation	Tensile test	ISO 898-1 [11]
	Stress under proof load	Proof load test	ISO 898-1 [11]
	Strength under wedge loading	Wedge loading test	ISO 898-1 [11]
	Hardness	Hardness test	ISO 898-1 [11]
	Impact strength	Impact test	EN 10045-1 [64]
Nut	Stress under proof load	Proof load test	ISO 898-2 [65]
	Hardness	Hardness test	ISO 898-2 [65]
Washer	Hardness	Hardness test	ISO 6507-1 [66]
Assembly	Tensile resistance	Tensile test of assembly	EN 15048-2 [7]

In addition to complying with these, mechanical characteristics after hot-dip galvanising must also comply with Annex F of ISO 10684 [62].

2.3.3 Thread Tolerance

Thread tolerance class defines the geometry of bolt (external) and nut (internal) threads, and is identified by a number-and-letter system. Since the tightness of fit between nut and bolt threads is thought to affect the likelihood of thread-stripping, with stripping more likely for loose fitting threads, it is important to understand thread tolerance classes and their associated thread geometries when trying to predict failure modes. Tolerance determines how far from the theoretical (basic) thread profile the actual thread profiles will lie, while deviations are also specified to provide allowable maximum and minimum diameters at a number of key points on the thread profile, including the minor (D1, d1), major (D, d) and pitch (D2, d2) diameters of the internal and external threads respectively. Here major diameter refers to the distance between external thread crests (d) or internal thread roots (D), while minor diameter refers to the distance between external thread roots (d1) or internal thread crests (D1). Pitch diameter refers to the theoretical diameter of the unthreaded shank prior to rolling of the external threads. The basic thread profile is a theoretical profile which assumes that the geometries of internal and external threads are identical. British Standard BS 3643-1 [67] contains all information about basic profile geometry, tolerances and deviations, and calculated geometries for galvanised threads, while BS 3643-2 [68] contains the calculated geometries for uncoated threads. European Standards split this information so that ISO 68-1 [69] contains basic profile geometry while tolerances and deviations for uncoated and galvanised threads are specified in ISO 965-1 [70] and ISO 965-5 [71] respectively. All dimensions are identical in the British and European Standards.

The basic profile is based on thread pitch (the distance measured parallel to the bolt length between corresponding points on adjacent threads), which is 2.5 mm for 20 mm diameter coarse pitch components such as those considered in this study. The profile and dimensions are illustrated in Figure 2.3-1, and given in Table 2.3-2 for pitch (P) = 2.5 mm and fundamental triangle height (H) = $\sqrt{3}/2$ P.

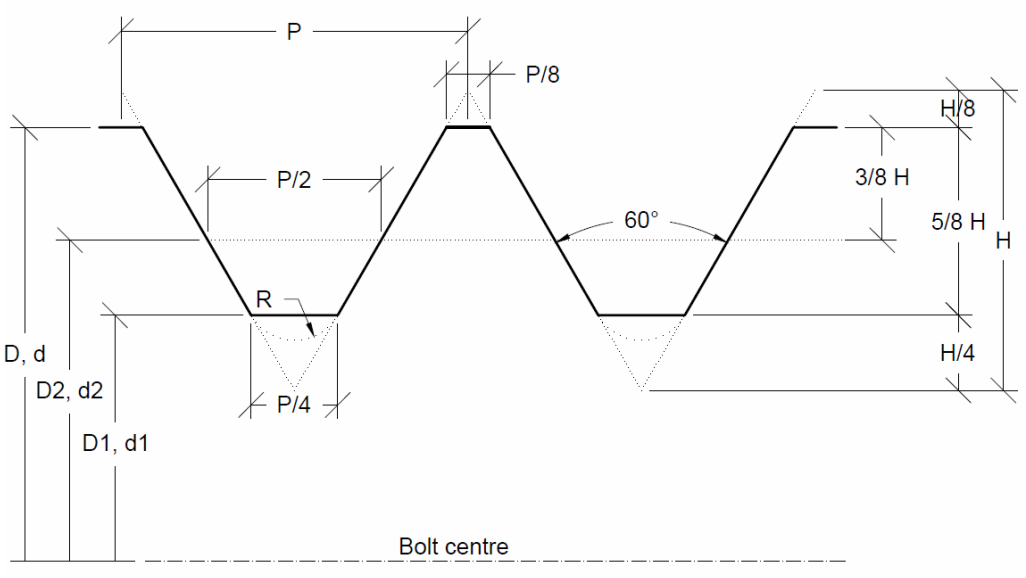

Figure 2.3-1 Basic thread geometry [67, 69]

Table 2.3-2 Basic profile dimensions for P = 2.5 mm [67, 69] (all dimensions in mm)

D,d	D1,d1	D2,d2	H	P	Rmin	Rnom*
20	17.294	18.376	2.165	2.5	0.313	0.361

*Where Rnom = H/6, Rmin = 0.125P [67]

In reality, to avoid thread overlap, external thread diameters must be less than or equal to the basic profile, and internal thread diameters must be greater than or equal to the basic profile. The difference between the basic and real thread profiles is the tolerance, which is determined by tolerance class. The tighter thread tolerance classes (Product grades A and B) are 6g for fully threaded bolts and 6H for nuts, and are specified to product standards ISO 4017 [72] and ISO 4032 [73] respectively. The looser thread tolerance classes (Product grade C) are 8g for fully

threaded bolts and 7H for nuts, and these are specified to product standards ISO 4018 [74] and ISO 4034 [75] respectively.

In the case of galvanised threads, for which nut threads are tapped over-size, the external thread is produced to tolerance class 6g prior to hot-dip galvanising, and the nut is galvanised as an unthreaded blank, and the internal threads are then tapped over-size to thread tolerance class 6AZ in accordance with ISO 965-5 [71]. The dimensions of threads of tolerance class 6AZ and 6H are almost identical, except that 6AZ threads are offset to accommodate the zinc thickness on the external bolt threads. A minimum clearance of 392 µm and a maximum coating thickness of 98 µm for tolerance class combination 6AZ6g is specified in ISO 10684 [62].

Thread tolerances and deviations are shown in Table 2.3-3, where tolerance (T) is followed by the relevant minor (D1, d1), major (D, d) and pitch (D2, d2) diameters of the internal and external threads respectively. The lower deviation (EI) is the minimum distance between the internal thread and basic thread profiles, and the lower deviation (es) is the minimum distance between external thread and basic profiles. These are specified to ensure that there is no overlap between internal and external threads.

Table 2.3-3 Thread tolerances and deviations for bolts of tolerance class 6g and nuts of tolerance class 6H and 6AZ for P = 2.5 mm. All dimensions in mm.

6g		6H		6AZ	
Td	0.335	TD	0.000	TD	0.000
Td1	0.000	TD1	0.450	TD1	0.450
Td2	0.170	TD2	0.224	TD2	0.224
es	0.042	EI	0.000	EI	0.350

Geometries specific to thread tolerance class 6AZ are given in BS 3643-1 and 6g and 6H in BS 3643-2, however, ISO 965-1 only contains thread tolerances and deviations. Thread geometries and their calculations are contained in Table 2.3-4

for tolerance class 6g, and Table 2.3-5 for tolerance classes 6H and 6AZ, assuming a pitch of 2.5 mm and diameter of 20 mm. Thread geometries can be calculated in the same way, using the relevant tolerances and deviations for the looser fitting tolerance classes 7g and 8H.

Table 2.3-4 Thread geometry calculation and values for bolt thread tolerance class 6g

	6g		
	d (crest)	d2 (pitch)	d3 (root)
Max	d-es	d2-es	d1-es
Max (mm)	19.958	18.334	17.252
Min	d-es-Td	d2-es-Td2	d1-es-2y
Min (mm)	19.623	18.164	16.990

Where $y = R_{min}\{1 - \cos[\pi/3 - \cos^{-1}(1 - T_{d2}/4R_{\min})]\}$

Table 2.3-5 Thread geometry calculation and values for nut thread tolerance classes 6H and 6AZ

	6H			6AZ		
	D (root)	D2 (pitch)	D1 (crest)	D (root)	D2 (pitch)	D1 (crest)
Max	NA	D2+EI+TD2	D1+EI+TD1	NA	D2+EI+TD2	D1+EI+TD1
Max(mm)	NA	18.6	17.744	NA	18.95	18.094
Min	D+EI	D2+EI	D1+EI	D+EI	D2+EI	D1+EI
Min(mm)	20	18.376	17.294	20.35	18.726	17.644

In order to visualise these values, Figure 2.3-2 highlights the permissible thread profile geometries of the nut and bolt for two tight-fitting tolerance class combinations; uncoated 6H6g and galvanised 6AZ6g. The ranges of permissible deviation are highlighted in blue for internal threads and red for external threads for tolerance class 6H6g and 6AZ6g in Figure 2.3-2(a) and Figure 2.3-2(b) respectively, with the black dotted line representing the basic profile. In these figures flank angles (The angle between thread face and perpendicular to the thread axis measured in the axial plane) are not equal to 30˚ for the profiles associated with maximum possible deviations. Maximum and minimum permissible thread profiles of the nut also intersect one another. This highlights the fact that

tolerances are provided purely as a method of inspection, and not as recommended thread profile geometries.

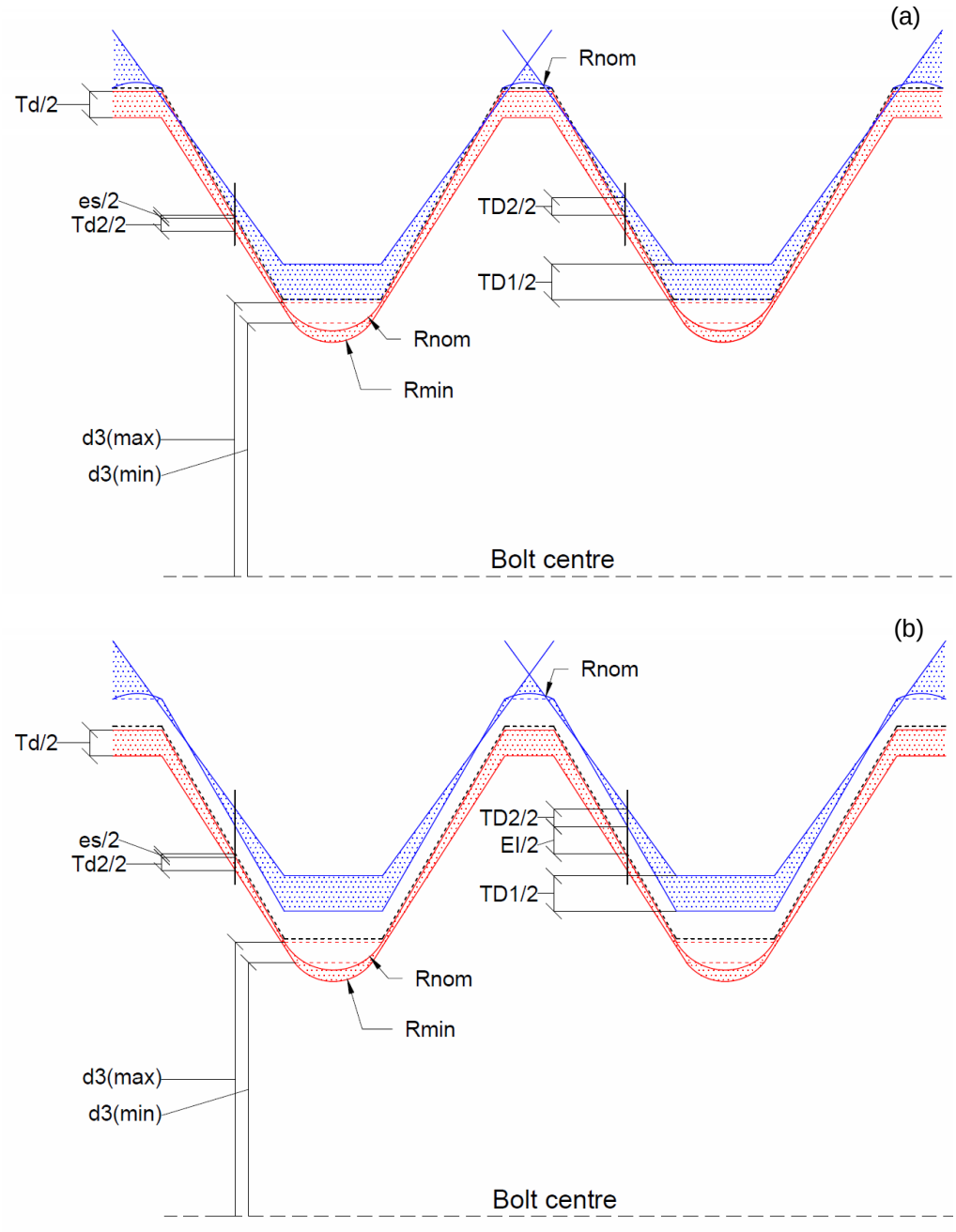

Figure 2.3-2 Permissible geometries for tolerance class combination (a) 6H6g and (b) 6AZ6g where the blue and red hatched areas represent permissible profile geometries of the nut and bolt respectively and the black dotted line represents the basic thread profile.

Methods of inspection in industry are not designed to measure the exact thread profiles. They include GO and NO-GO screw gauges to check pitch and minor diameter, using a micrometer to measure the major diameter, a floating carriage diameter-measuring machine for minor and pitch diameters of the external thread, and a sliding pair of wedges to measure the minor diameter of the internal screw thread [76].

2.3.4 External Geometry

Bolt head and external nut geometries are included within the relevant product standard, which is again related to the specified thread tolerance class. The tighter thread tolerance classes of 6g for fully threaded bolts and 6H for nuts are related to ISO 4017 [72] and ISO 4032 [73] respectively. For the looser thread tolerance class 8g for fully-threaded bolts and 7H for nuts, the relevant product standards are ISO 4018 [74] and ISO 4034 [75] respectively. A detailed description of the geometry of nuts and bolt heads exists; however, the most significant dimensions are the widths across the flats (e) and corners (s) (Figure 2.3-3) and nut and bolt heights (m and k respectively). Values associated with 20 mm diameter components are given in (Table 2.3-6).

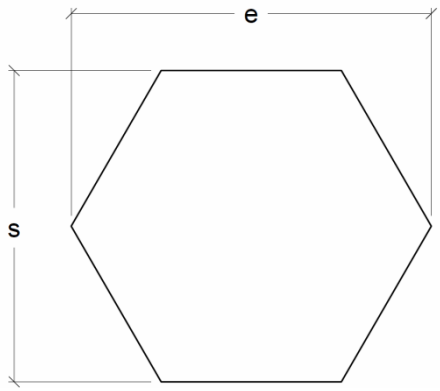

Figure 2.3-3 Symbols and descriptions of external nut and bolt head dimensions

Table 2.3-6 External nut and bolt head dimensions for tolerance classes 7H, 6H, 8g and 6g for 20 mm diameter (all dimensions in mm)

Part	Product Grade	Tolerance Class	s		e	m (nut) or k (bolt)		
			Max.	Min.	Min.	Max.	Nom.	Min.
Nut	C [75]	(7H)	30.00	29.16	32.95	19.00	19.00	16.90
Nut	A and B [73]	(6H)	30.00	29.16	32.95	18.00	18.00	16.90
Bolt	C [74]	(8g)	30.00	29.16	32.95	13.40	12.50	11.60
Bolt	A [72]	(6g)	30.00	29.67	33.53	12.72	12.50	12.29
Bolt	B [72]	(6g)	30.00	29.16	32.95	12.85	12.50	12.15

According to ISO 4017 [72], product Grade A applies to threads M1,6 to M24 and to nominal lengths up to and including 10d or 150 mm, whichever is the shorter, and product Grade B for threads over M24 or nominal lengths over 10d or 150 mm, whichever is the shorter. The bolts considered in this research are M20 and 90 mm long, and therefore product grade A should be assumed.

2.4 Manufacture

Galvanised bolt assemblies such as that being considered in this research consist of a standard geometry bolt and a nut with threads tapped over-size to accommodate the thickness of the coating layer on the bolt threads. Galvanised bolts are manufactured in the same way as uncoated bolts, using cold heading and thread-rolling techniques followed by a quench-and-temper heat treatment before a final galvanising step (Figure 2.4-1).

Uncoated nuts, however, are typically hot-forged and punched, which is a very different process from that used for galvanised nuts. These are cold-forged and punched, quenched and tempered, and then galvanised before threads are tapped over-size to accommodate the zinc layer on the bolt threads.

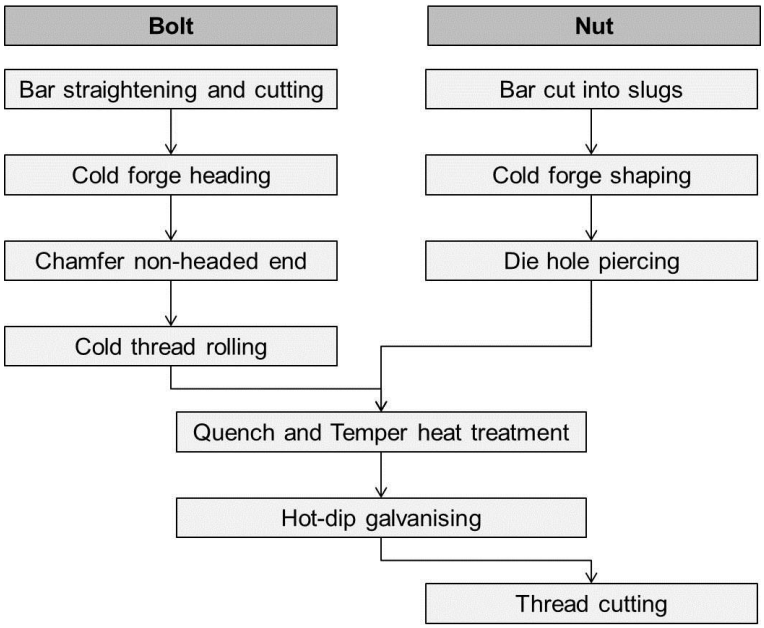

Figure 2.4-1 Processing steps during the manufacture of galvanised nuts and bolts

2.5 Chemical Composition and Heat Treatment

Nuts and bolts can be made from any material meeting the chemical composition requirements specified in Table 2 of ISO 898-1 [11] and Table 3 of ISO 898-2 [65]. Exact processing parameters, such as temperature and holding time prior to quenching, quench media, tempering temperature and holding time, are chosen at the discretion of the manufacturer and are dependent on chemical composition. A minimum tempering temperature of 425˚C is specified for bolts [77]; however, no limit is specified for nuts [65]. Detailed testing methods of bolts and nuts for room temperature applications are specified by ISO 898-1 [11] and ISO 898-2 [65] respectively, to verify whether an adequate heat treatment has been carried out to transform to at least 90% martensite at the bolt centre and provide adequate mechanical properties. Chemical composition limits (Table 2.5-1) allow a range of 0.3 percent carbon by weight (wt%C), a range which will have a significant effect on the steel hardenability, maximum hardness obtainable and the temperature at which austenite will transform to martensite (martensite start temperature (Ms)).

Table 2.5-1 Chemical composition limits of quench and tempered carbon steel property class 8.8 bolts and 10 nuts

Component	Chemical Composition Limits (wt%)*					
	C (min)	C (max)	Mn (min)	P (max)	S (max)	B (max)
Property Class 8.8 bolt [11]	0.25	0.55	-	0.025	0.025	0.003
Property Class 10 nut [65]	-	0.58	0.30	0.048	0.058	-

* All elements abbreviated using standard IUPAC nomenclature

Steel is an extremely versatile material. Its mechanical properties can be optimised through variations in composition and heat treatment, to produce a range of microstructures. The starting microstructure will therefore depend on the skill of the manufacturer and their choice of composition and processing route.

An equilibrium iron-carbon phase diagram such as that in Figure 2.2-10 can be used to predict the phases present in plain carbon steels for a given C content and temperature. Although the addition of alloy elements alters the thermodynamics and kinetics of phase change reactions, the iron-carbon binary phase diagram can be used as a guide. The carbon content of the material considered in this thesis is limited to between 0.25 and 0.55 wt%C [77], between these concentrations it is clear from the phase diagram that ferrite and cementite are present at temperatures up to around 723˚C.

Ferrite and cementite can be present as a range of microstructures including pearlite and bainite, dependent on the rate at which steel is cooled from the pure austenite region of the phase diagram. To heat-treat the steel it must first be heated to around 50°C above the A_3 temperature to ensure that single-phase austenite (γ) is present. The steel is then held for a sufficient time for a homogeneous austenite microstructure to form, to ensure uniform composition and temperature. The cooling rate to room temperature is then controlled, to achieve the desired microstructure and thus mechanical properties. The development of an equilibrium microstructure requires an extremely slow cooling rate. This is so that equilibrium adjustments between temperature and the relative chemical

composition of each phase can be made. These adjustments are made by the time-dependent diffusion of elements from one phase to another across phase boundaries. Realistic cooling rates are far higher than those required to produce equilibrium microstructures. In the case of cooling from austenite to ferrite and pearlite the transformed equilibrium microstructure would be that of coarse pearlite with some ferrite at prior austenite grain boundaries.

For a composition of between 0.25 and 0.55 wt%C held at a temperature in the austenite region it can be assumed that all C is in solid solution. In other words, all C atoms occupy interstitial sites between the larger Fe atoms, rather than forming separate clusters of atoms (carbides). During cooling, the microstructure remains fully austenitic, until the temperature is reduced to below the A_3 line (Figure 2.2-10) when it begins to transform to ferrite, which has a lower solubility of C than does the austenite phase. Additionally, ferrite and austenite have different crystal structures. In austenite Fe atoms occupy the corners and face centres of a cube unit cell (face-centred cubic FCC) (Figure 2.5-1(a)), and in ferrite Fe atoms occupy cube corners and centres (body centred cubic BCC) (Figure 2.5-1(b)). Although the atoms are more closely packed in the FCC arrangement the interstitial sites are larger (due to a larger unit cell), and less lattice distortion is required for C atoms to occupy them. This means that more C can be in solid solution in austenite than in ferrite. If the cooling rate is sufficiently slow to allow diffusion to occur ferrite becomes fully saturated with carbon, and the remaining carbon atoms form cementite carbides. The morphology of these carbides, their size and shape, is dependent on the rate at which steel is cooled from austenite, and this determines mechanical properties.

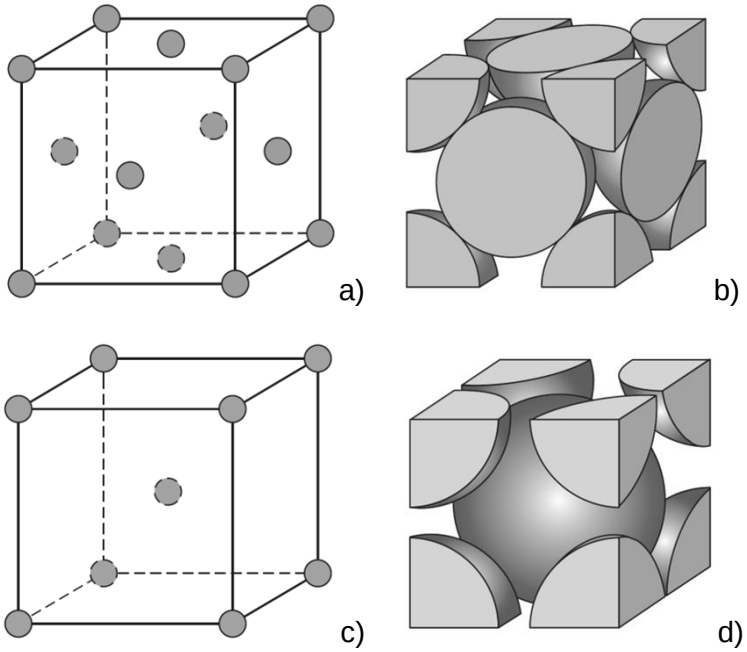

Figure 2.5-1 (a) a reduced sphere FCC unit cell (b) a hard cell FCC unit cell representation (c) a reduced sphere BCC unit cell (c) a hard cell BCC unit cell representation. Copied from Materials Science and Engineering [78]

2.5.1 Pearlite

During slow cooling of pre-eutectoid steel (<0.76 wt%C) ferrite grains nucleate at austenite grain boundaries, once below the A_3 line, and grow until they have rejected so much C into the remaining austenite (at temperatures just above the A_1) that conditions for cementite (Fe_3C) nucleation are more favourable than ferrite growth. Small Fe_3C carbides nucleate at the interface between ferrite and austenite, and grow in co-operation with ferrite in a lamellar morphology called pearlite. Ferrite continuously expels C into Fe_3C lamellae, and the growth continues until pearlite colonies meet. Pearlite can only form when cooling rates are relatively slow, because the transformation is dependent on the diffusion of C. If austenite is cooled more rapidly there is less time for diffusion to take place, and a very fine bainitic microstructure is formed. For very high cooling rates, there is no time for diffusion to take place at all, resulting in the formation of the non-

equilibrium phase martensite, consisting of a body centred tetragonal crystal structure.

The pearlite lamella thickness is dependent on the final temperature to which the steel is cooled. A large undercooling results in a higher Fe_3C nucleation rate, and therefore many finely-spaced lamellae. At low temperatures the diffusion rate of C is low, so lamella spacing is also small to compensate for decreased diffusivity at lower temperatures [57]. At low temperatures, there is also a high driving force for the transformation, so pearlite growth is rapid. The size of pearlite colonies is dependent on the prior austenite grain size, since smaller prior austenite grains provide a greater number of nucleation sites, and therefore smaller colonies. A fine lamellar structure provides improved strength in the same way as fine grains do through grain-boundary or Hall-Petch strengthening [78]. Interfaces between cementite and ferrite lamellae, like grain boundaries, impede dislocation motion and the onset of plasticity, therefore, decreasing lamellar thickness and increasing the number of these interfaces leads to increased yield strength.

2.5.2 Martensite

If steel is cooled rapidly (quenched) from the austenite region the martensite transformation will occur. Typically a liquid quench medium, such as oil or water, is used to achieve the cooling rate required for the martensite transformation. The transformation from austenite to martensite is diffusion-less, due to an extremely fast rate of martensite plate growth [57]; therefore carbon cannot diffuse out of ferrite and back into the remaining austenite upon cooling. The transformed martensite, therefore, has the same chemical composition as the prior austenite, and is supersaturated with interstitial C atoms. A distorted body-centred tetragonal (BCT) crystal structure is formed, rather than the typical BCC crystal structure of ferrite. The strengthening mechanism in this case is lattice distortion due to the

high number of interstitial C atoms impeding dislocation motion. For low-carbon steels up to 0.5 wt% carbon, such as that used in Property Class 8.8 bolts, martensite usually has a lath structure with laths making up a larger packet structure [56]. The temperatures at which martensite transformation starts and stops are determined by chemical composition, most significantly wt%C, and in steels which contain above 0.4 wt%C the martensite finish temperature is likely to be below room temperature, so a certain amount of retained (untransformed) austenite will remain.

Martensite is a metastable phase which decomposes to carbides and other structures if heated, to allow mobility of C atoms during a process called tempering. Tempering is required to introduce ductility to as-quenched martensite which, although high-strength, has very low toughness.

2.5.3 Bainite

Bainite has microstructural and transformation similarities to both martensite and pearlite. Bainite contains a combination of cementite and ferrite but these are present in lath or plate morphologies, unlike the lamellar structure of pearlite. Upper bainite is formed at temperatures just below those of pearlite transformation, and consists of elongated carbides between ferrite laths, while lower bainite forms at temperatures closer to the martensite transformation temperature and consists of very fine carbides within large plates.

2.5.4 Continuous Cooling Transformation (CCT) Diagrams

Continuous cooling transformation (CCT) curves graphically depict the transformation behaviour of a given steel composition by plotting Log time (s) on the x-axis and Temperature (˚C) on the y-axis. A CCT diagram consists of curves plotted to represent the start and finish temperature and time of transformation to

ferrite, pearlite, bainite and martensite. A CCT diagram can be used to determine transformed microstructures for various cooling rates from the intersection of a specific cooling rate with these curves. This determines which transformation products will be formed for the given rate of cooling, and can therefore predict the cooling rate required to bypass high-temperature transformation to products such as pearlite and/or upper bainite. Intermediate cooling rates may lead to the formation of more than one structure, since the material may not have spent sufficient time at a given temperature for full transformation to occur.

For a very slow cooling rate, an equilibrium transformation to pearlite will occur at a high temperature. Lamellar spacing will be coarse due to the high rate of diffusion at high temperatures. At faster cooling rates and lower temperatures the driving force for transformation is high but the rate of diffusion is low, causing lamellar spacing to be small. Below the nose of the diagram carbon can no longer diffuse rapidly enough to form pearlite lamellae, and the non-equilibrium transformation to bainite occurs. Excess carbon forms cementite dispersions within a ferrite matrix. Bainite has comparable ductility to pearlite but has increased strength as a result of dispersion hardening, due to second-phase particles dispersed throughout the iron matrix. If a sufficiently fast cooling rate is used to bypass the transformation to pearlite and bainite, the diffusion-less transformation to martensite occurs below the martensite start temperature.

2.5.5 Hardenability

The hardenability of medium-carbon steels is highly sensitive to chemical composition (particularly C, Mn, Si and residual elements such as P and S) and austenite grain size at the time of quench. Pearlite tends to nucleate at austenite grain boundaries and grain boundary triple points. Therefore, fine austenite grains provide a larger number of nucleation sites and reduces hardenability. Large

austenite grains lead to the deterioration of other mechanical properties such as notch toughness, and therefore prior austenite grain size should be selected carefully, and not as a method of achieving high hardenability.

Although plain carbon steels have sufficient hardenability for thin sections to achieve maximum hardness throughout, small alloy additions are required for larger sections. Mn, Ni and Cu are austenite stabilisers which reduce the Ac_3 temperature (the temperature at which the ferrite-to-austenite phase transformation is completed upon heating), meaning that the steel has a lower austenite to ferrite transformation temperature and associated rate of diffusion upon cooling. These alloy elements do not partition between ferrite and Fe_3C pearlite lamellae, so their effect on reaction rate is assumed to be through their thermodynamic influence on the austenite-to-ferrite transformation alone [79]. Ferrite stabilisers such as Mo, Cr and Si tend to partition in the temperature range of the austenite-to-ferrite transformation. The diffusion rate of the alloying elements is very slow at temperatures below A_1, so pearlite transformation is significantly retarded. Both austenite and ferrite stabilisers lead to the transformation to pearlite at lower temperatures and slower rates of cooling, improving hardenability. Small amounts of many alloying elements are more effective at improving hardenability than large amounts of a few of them. The primary function of these elements is hardenability; however, a secondary function is their contribution to elevated-temperature toughness and corrosion and abrasion resistance.

Hardenability can also be affected by the rate of heating and holding time above the A_3 temperature prior to quenching. Sufficient temperature and time are required to ensure that all C and other alloy elements are in solid solution. If free carbides exist at the time of quenching the chemical composition of the steel will not reflect the amount of carbide-forming elements in solid solution in the austenite,

and any elements not in solid solution will not contribute to the hardenability of the steel. Carbides present in austenite at the time of quenching can actually reduce hardenability by acting as nucleation sites for high-temperature transformation products.

2.5.6 Tempering

During the transformation from austenite to martensite, there is a significant increase in volume as the material transforms from a closely-packed FCC crystal structure to a loosely-packed BCT crystal structure, super-saturated with carbon atoms. Dislocations are generated to accommodate this rapid increase in volume, leading to a very high dislocation density such as that which would be expected from cold working. The interactions between large numbers of dislocations, both with each other, interstitial carbon atoms and strain fields caused by lattice distortions, hinder dislocation motion, inhibiting deformation and resulting in high strength at the expense of ductility. Tempering provides the thermal activation required for interstitial carbon diffusion, leading to the formation and subsequent coarsening of epsilon-carbides and cementite [56]. During tempering, concurrent recovery may occur in which point defects such as excess vacancy concentrations are minimised and the reconfiguration of dislocations into low energy positions takes place [80]. Both of these processes reduce the tetragonality of the lattice and relieve lattice distortions. During tempering, recrystallisation will also occur in which strain-free, equiaxed ferrite grains nucleate and grow [78]. Since the minimum specified tempering temperature of nuts and bolts is fairly low, little grain growth can be assumed. The decrease in dislocation density through recrystallisation and the annihilation of opposing dislocations will lead to reduced hardness and increased ductility, because fewer dislocations can intersect with one another and impede the motion of dislocations behind them. Carbide-forming elements such as

Cr, Mo and V retard softening and raise the tempering temperature required. These effects are balanced by the need for a less drastic quench, to achieve maximum hardness and a greater plasticity at a given hardness, due to the lower C content. The tempering temperature must be greater than the zinc-bath temperature for galvanised products to avoid any further tempering during galvanising.

2.5.7 Galvanising

The standard for hot-dip galvanised coating of fasteners, ISO 10684 [62], specifies a maximum thickness of 98 µm. Minimum local and batch coating thicknesses of 40 µm and 50 µm respectively are specified. The coating is not pure Zn, but actually consists of a number of layers containing different concentrations of Zn and Fe, ranging from pure Zn at the surface to the pure steel substrate (Figure 2.5-2).

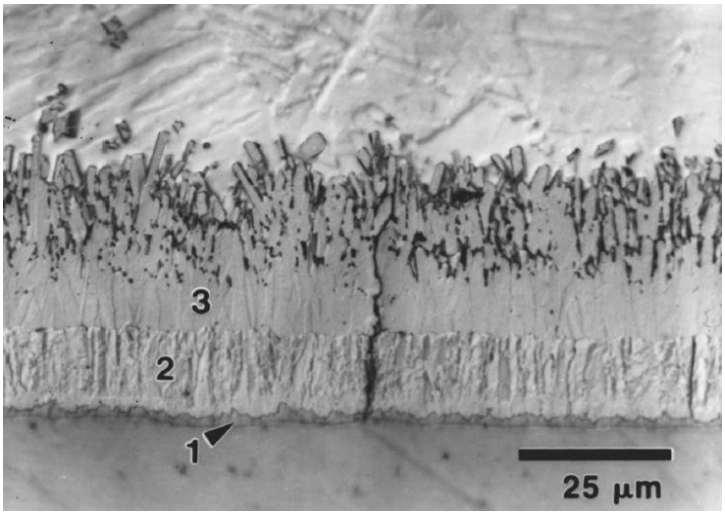

Figure 2.5-2 Microstructure of Zn coating formed after 300 s immersion in a 450 °C Zn bath with eta phase (pure zinc) at the top of the image in addition to(3) zeta (ξ) phase, (2) delta (δ) phase and (1) gamma (Γ) phase. Copied from "The metallurgy of zinc-coated steel" [81]

The thicknesses of these layers depend on bath temperature and immersion time. For fasteners, the normal galvanising temperature range is 455-480°C, while high-temperature galvanising can be used to produce a smoother, thinner coating at 530-560°C [62]. Each layer has not only different mechanical properties, indicated

by different hardness's and melting temperatures, but also different phases (Table 2.5-2).

Table 2.5-2 Zinc alloy layers within a galvanised zinc coating applied to steel [82]

Alloy	Composition	Hardness (DPN)	Melting T (°C)
Eta	Zn	70-72	419
Zeta	FeZn13	175-185	530
Delta	FeZn7	240-300	530-670
Gamma	Fe8Zn10	250	670-780
Steel		150-175	1510

2.6 Summary

This chapter has provided a brief description of the manufacture and heat treatment processes and the relevant bolting standards available, in order to highlight the range of mechanical and geometrical properties available. Property class designation, chemical composition, mechanical properties, quality assurance testing, thread tolerances and external geometry have all been explained.

The literature available in this field has been discussed and gaps in the field highlighted. Most significantly, no single piece of literature has focussed on galvanised structural bolt assemblies containing Grade 8.8 bolts and Property Class 10.9 nuts despite this currently being the most common bolt assembly used in UK construction. The most comprehensive research in this field is that of Kirby [1]. The strength reduction factors currently specified in Eurocode 3 [8] are based directly on his research. However, many differences exist between modern bolt specifications and those which existed at the time when his research was published;

1. Chemical composition limits were only specified for nuts of Grades 4 and 6 in BS 4190 [83] and these only contained maximum limits of C, P, S. The modern limits specified in ISO 898-1 and 898-2 contain detailed chemical composition limits for the bolt and nut respectively, and three different steel types for bolts

of grades 8.8, 9.8 and 10.9; quenched and tempered carbon steel with additives (eg. B, Mn or Cr), quenched and tempered carbon steel, and quenched and tempered alloy steel

2. Structural bolt assemblies did not exist at the time of Kirby's research. Nuts and bolts could be purchased separately and interchangeably, whereas they must now be purchased as an assembly from a single manufacturer in accordance with BS EN 15048-1 [9]
3. The assemblies tested by Kirby had a relatively loose thread tolerance 7H8g, while those currently used are typically 6H6g for uncoated and 6AZ6g for galvanised bolt assemblies

The previously published results described in this chapter will be used later in this thesis, to validate the finite element model and provide a comparison for steady-state tensile tests carried out on bolt assemblies and turned-down bolts from the same batch.

3 Microstructural Characterisation

Microstructural characterisation has been carried out on bolts from different manufacturers and batches, to identify the range of products available in the UK market. These results have also been compared with those of a bolt from the batch used for mechanical testing of bolt assemblies, in order to determine whether the mechanical behaviour of this assembly is likely to be characteristic of other structural bolt assemblies of this grade. Characterisation of bolts from different manufacturers has included chemical composition analyses, Vickers hardness testing, optical and scanning electron microscopy (SEM), prior austenite grain size measurement and calculation of continuous cooling transformation (CCT) curves. Uniaxial tensile testing has been carried out on turned-down bolts at temperatures within the range 20-700˚C and engineering strain-rates of 0.002-0.02 min^{-1} ($3.33x10^{-5}$-$3.33x10^{-4}$ s^{-1}) to determine the tensile behaviour of the bolt material. In these tests the 20 mm diameter bolt shank was reduced to a cylindrical profile of 7 mm diameter, to allow accurate stress and strain measurement, eliminating the effects of thread deformation. Results will reveal the strain-rate and temperature sensitivity of bolt material flow behaviour.

Although ISO 898-1 specifies that bolts should be quenched and tempered with a minimum of 90% martensite at the bolt centre in the as-quenched condition, there is no guidance in the standards regarding the specific processing route. An adequate heat treatment is verified through mechanical testing alone, and metrology is verified through geometrical inspection. This provides scope for large variations between the metallurgies of bolts produced by different manufacturers.

Six M20 Grade 8.8 bolts were chosen from five different UK distributors for this study (Table 2.6-1). Four of these are non-structural, which means that they were not purchased as part of an assembly in accordance with EN 15048-1 [9]. However, the geometrical and material tolerances specified in EN ISO 898-1 [11] still apply. Characterisation is particularly significant at the current time, because all structural bolt assemblies are sourced from overseas due to the high cost of raw materials in the UK [10].

Table 2.6-1 Summary of bolts to be characterised

Ref no.	Marking	Coating	Structural
1	YH	Self-Coloured	N
2	UM	Self-Coloured	N
3	JD	Self-Coloured	N
4	TVS	Zinc Electroplated	N
5	Anon.	Hot Dip Galvanised	Y
6*	Anon.	Hot Dip Galvanised	Y

* Bolt 6 is from the batch of bolts to be used for mechanical testing

Bolt 6 is from the batch used for uniaxial tensile testing of bolt assemblies. The distributor which donated Bolt 6 also donated Bolt 5, and wishes to remain anonymous. This distributor had inspected and tested the bolt prior to distribution, and had placed its own manufacturer's mark on it, as is common. It is therefore regarded as the manufacturer according to ISO 898-1 [11] and, unless it is willing to share this information, the fasteners cannot be traced back further than the UK. The purpose of microstructural characterisation is two-fold; firstly, variations between the five manufacturers have been identified and secondly, the material

properties of the bolt from the batch used for uniaxial tensile testing have been compared to those from other manufacturers.

3.1 Chemical Composition

Composition analyses have been carried out by Tata Steel. Most elements, including B, were measured using spark OES (Optical Emission Spectrometer), while C and S were determined by induction furnace combustion and N by inert gas fusion. The average of three results was taken if there was no significant scatter. If this was not possible the result was considered to be null and was excluded from the report.

Continuous cooling transformation (CCT) curves can be calculated from chemical composition and prior austenite grain size, to predict the cooling rates required for martensite transformation. A wide range of suitable chemical compositions is allowable within the limits specified in ISO 898-1 (Table 3.1-1). The results of chemical composition analyses carried out on bolts are detailed in Table 3.1-2.

Table 3.1-1 Chemical composition and tempering temperature limits of a property class 8.8, carbon steel, quench and tempered [11]

Chemical composition limit (wt%)					Tempering T (˚C)
C max.	C min.	P max.	S max.	B max.	min.
0.25	0.55	0.025	0.025	0.003	425

The compositions of Bolt 1-6 (Table 3.1-2) are typical of low-to-medium plain carbon steels containing <0.6 wt%C and 0.6-1.65 wt%Mn [84] with small additions of Si, Ni, Cr, Mo, V and B for improved hardenability. The most important element for hardenability is C; however, ISO 898-1 [11] states that carbon content may range from 0.25–0.55 wt% in bolts of Property Class 8.8 (Table 3.1-1). This is a large range, considering that the effects of alloy additions to improve hardenability are most significant above 0.3 wt%C [85]. The measured chemical composition analyses show significant variation in C contents, ranging from 0.22 in Bolt 2 to

0.40 in Bolt 4. However, all compositions fall within the prescribed values contained in Table 3.1-1. The low C content of Bolt 2 was balanced by relatively higher levels of Si and Mo. Bolt 6 contained 0.37 wt%C, similar to the average of 0.34 wt%. However, compared to Bolts 1-5, the Si and Mn contents are low and Cr content significantly higher.

Table 3.1-2 Chemical composition analyses of bolts 1-6

	Composition (wt%)									
Ref.	C	Si	Mn	P	S	Cr	Mo	Ni	Cu	Sn
1	0.360	0.120	0.720	0.013	0.004	0.020	<.005	0.030	0.060	0.008
2	0.215	0.270	0.920	0.013	0.009	0.060	0.020	0.110	0.240	0.017
3	0.345	0.120	0.690	0.021	0.006	0.007	<.005	0.005	0.010	0.001
4	0.400	0.170	1.430	0.015	0.017	0.140	<.005	0.040	0.090	0.009
5	0.365	0.210	0.710	0.010	0.007	0.020	<.005	0.008	0.020	0.006
6*	0.370	0.080	0.440	0.014	0.002	0.240	<.005	0.007	0.030	0.001
avg.	0.343	0.162	0.818	0.014	0.007	0.081	0.003	0.033	0.075	0.007

	Composition (wt%)									
Ref.	Al	As	B	Ca	Co	N	Nb	Ti	V	W
1	0.008	0.005	<.0005	0.002	0.006	0.006	<.001	0.0001	<.001	<.001
2	0.038	0.017	0.0005	0.002	0.015	0.010	<.001	0.0520	0.004	<.001
3	0.022	0.003	<.0005	0.002	0.004	0.006	<.001	0.0039	0.004	<.001
4	0.046	0.004	0.0020	0.002	0.005	0.008	<.001	0.0460	<.001	<.001
5	0.052	0.008	<.0005	0.002	0.005	0.004	<.001	0.0037	<.001	<.001
6*	0.020	0.021	0.0025	0.002	0.004	0.006	<.001	0.0070	0.002	<.001
avg.	0.031	0.010	0.001	0.002	0.007	0.007	<.001	0.019	0.002	<.001

* Bolt 6 is from the batch of bolts to be used for mechanical testing

3.2 Vickers Hardness Testing

For quenched-and-tempered Property Class 8.8 bolts, there should be sufficient hardenability to ensure a structure consisting of approximately 90% martensite at the core of the threaded section of a bolt in the 'as-quenched' condition [11]. Because the standards specify mechanical and physical properties, and not heat treatment recommendations, hardness testing can be used to verify that adequate

heat treatment has been carried out. Vickers hardness testing is a feasible quality assurance check carried out for all fasteners which cannot be tensile-tested or to check that the maximum hardness is not exceeded in those which can be tensile tested. For routine inspection the manufacturer may decide whether hardness testing is carried out on a suitable flat surface after removal of any coating, or a transverse section taken at least 1d (where d = shank diameter) away from the end of the shank (Figure 3.2-1). The maximum and minimum hardness limits specified in ISO 898-1 are 255 and 335 HV respectively and the difference in hardness values within the half-radius area (a circle with its origin at the bolt centroid and a radius of 0.5 x bolt shank radius) should be greater than 30 HV.

Figure 3.2-1 A transverse section taken through the bolt shank for Vickers hardness testing

For this study Vickers hardness testing has been carried out on transverse sections, mounted in Bakelite and ground to obtain a level surface, using an applied force of 10 kgf and a dwell time of 15 s in accordance with ISO 6507-1 [66] and sub-clause 9.9 [11] to determine whether martensite is present through the entire bolt cross section. At least 70 indentations were made per bolt at 0.5 mm spacing. These were sorted in distance order, and the data was averaged so that there were 11-12 data points per curve. This resulted in averages taken from 6 values of Vickers hardness for Bolt 6, 14 readings for Bolt 5 and 10 readings for Bolts 1-4, per data point. These average values of hardness were plotted against

average distance from the bolt centre, and compared with the maximum and minimum permissible values of hardness prescribed in ISO 898-1 (255 and 335 HV respectively). The error bars represent the standard deviations of these values.

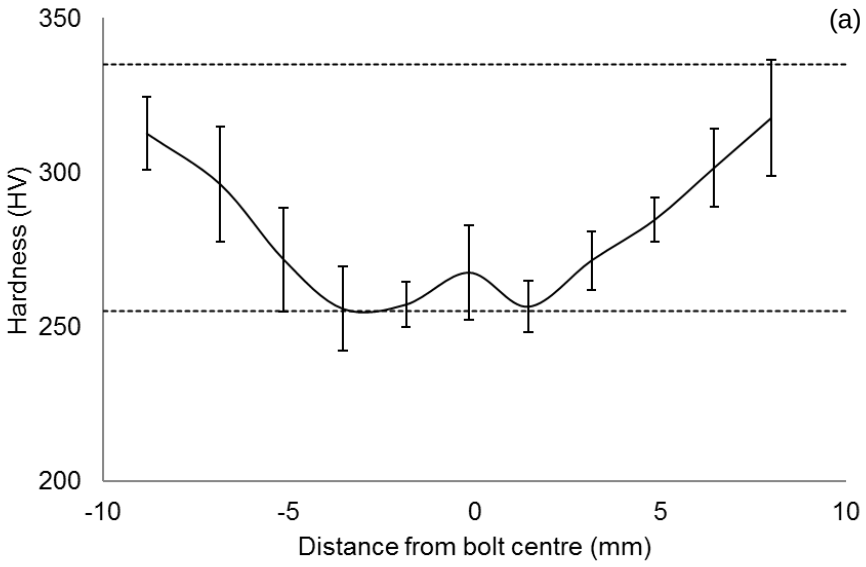

Bolt 1

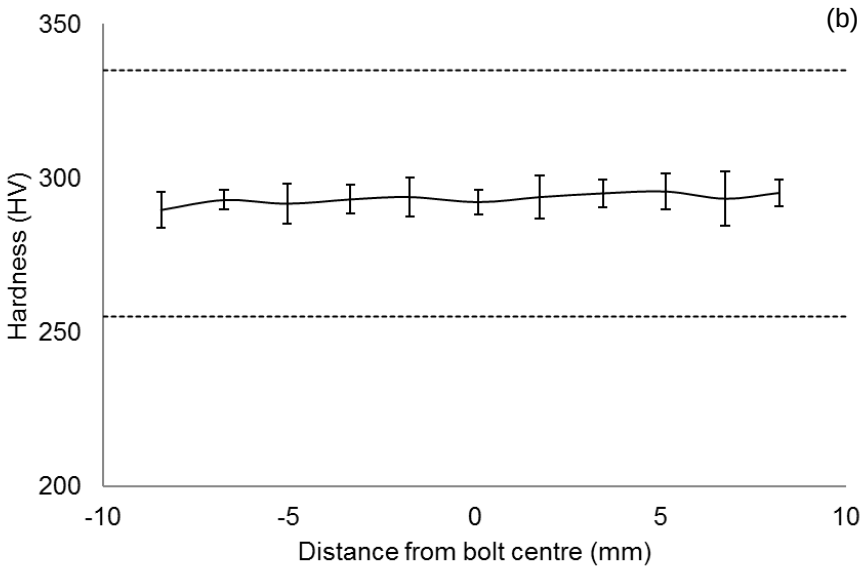

Bolt 2

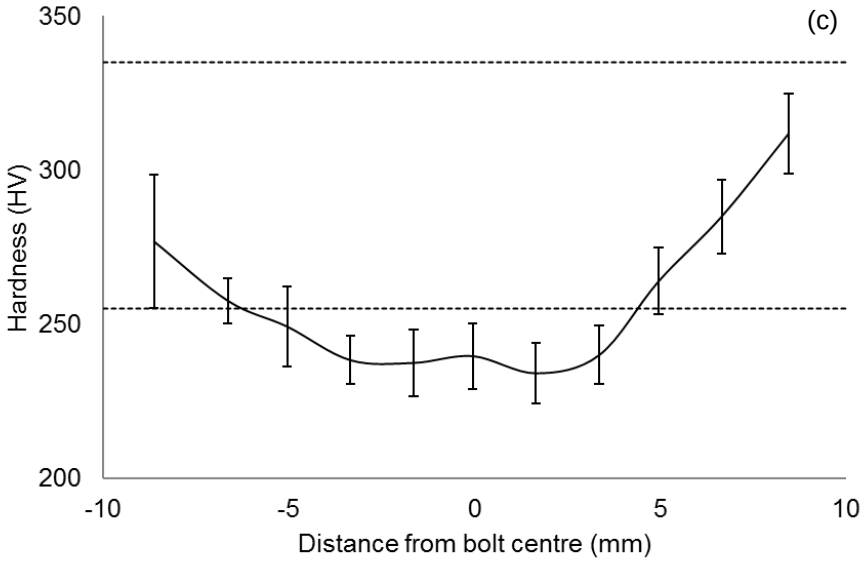
(c)
350
300
250
200
Hardness (HV)
-10
-5
0
5
10
Distance from bolt centre (mm)

Bolt 3

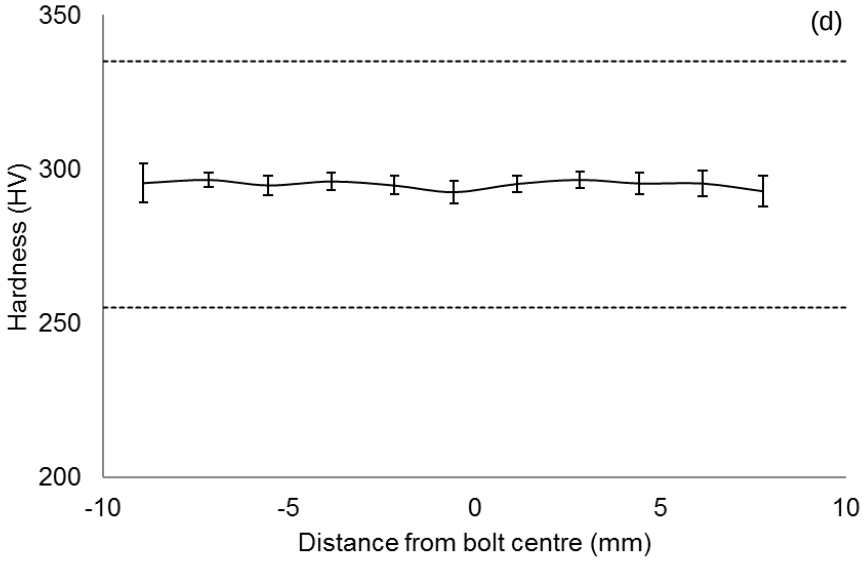
(d)
350
300
250
200
Hardness (HV)
-10
-5
0
5
10
Distance from bolt centre (mm)

Bolt 4

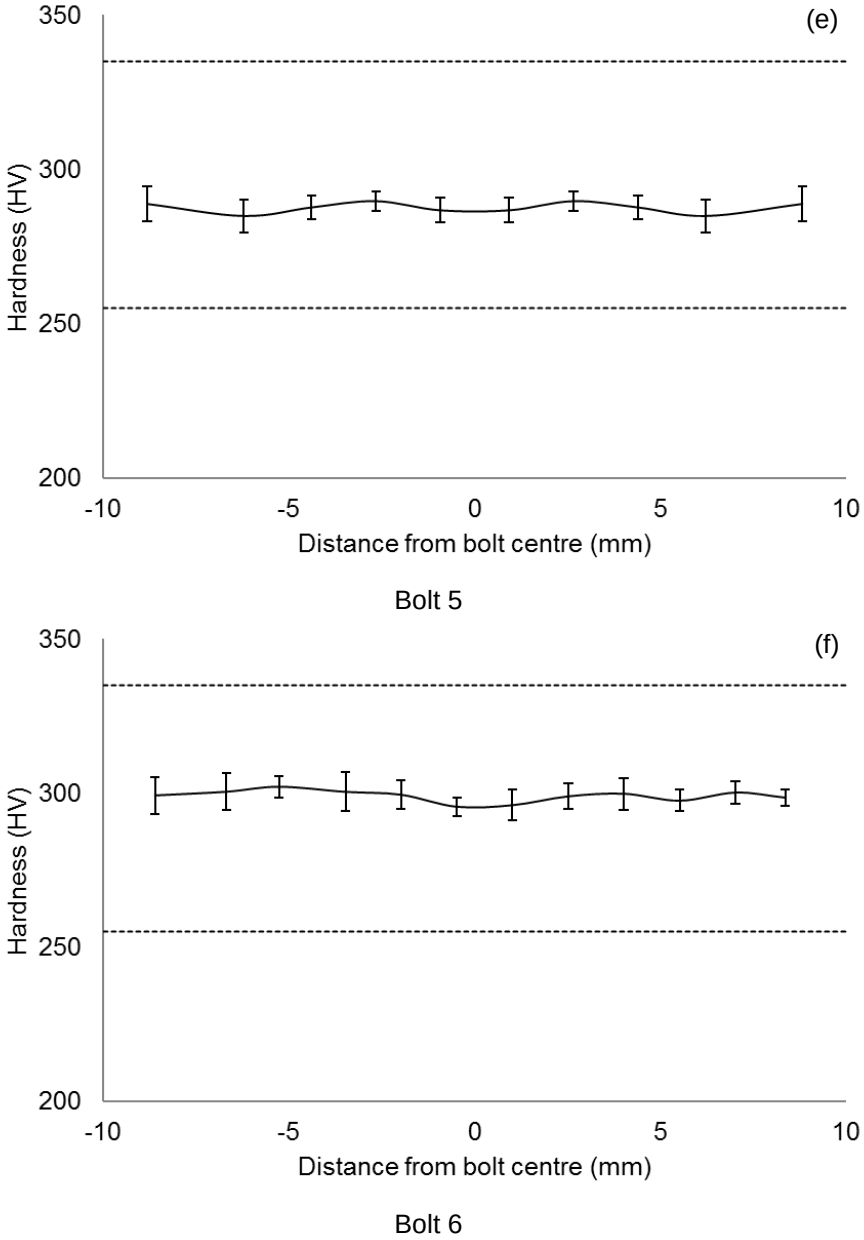

Figure 3.2-2(a-f) Hardness profiles of bolts 1-6 respectively

The most notable difference between the hardness profiles plotted is that Bolts 1 and 3 (Figure 3.2-2(a) and (e)) show low hardness at their centres and large standard deviations. Some of the hardness values for Bolt 1 and most of the hardness values in the central half of Bolt 3 fell below the minimum hardness limit, and the ranges of hardness measured for these bolts were greater than 50 HV and therefore do not comply with ISO 898-1. Bolts 2, 4, 5 and 6 had consistent

hardness between 280-300 HV throughout their cross sections, with very small standard deviations.

The chemical compositions of Bolts 1 and 3 (Table 3.1-2) are unremarkable compared with the other bolts, with C contents, both greater than 0.3 wt%, similar to the average of all six bolts. Since the compositions of Bolts 1 and 3 are fairly typical within the range of compositions measured within this study, the drop in hardness observed at their centres is most likely due to the heat treatment process used during their manufacture, and not due to poor hardenability.

3.3 Optical Microscopy

Although not a requirement of ISO 898-1 [11], optical microscopy has been carried out on a Polyvar optical microscope at magnifications of 500x to identify the microstructures present across the bolt cross-sections. Preparation of metallographic specimens involved hot-mounting in Bakelite transverse sections taken at least 1d away from the end of the shank. Specimen surfaces were ground with water-lubricated metallographic abrasive paper from 240 to 2400 grit, and polished using water-based 3μm and 1μm Diamet suspension, followed by a final colloidal silica step. A Nital etch was used to reveal the final ferrite microstructure. The threads of all bolts appeared to contain a tempered martensite microstructure (Figure 3.3-1(a-f(ii))). Packets of martensite laths and small carbide precipitates which have formed during tempering are visible. No ferrite grains are present, suggesting a complete martensitic transformation upon cooling from the austenite phase.

The centres of Bolts 4-6 Figure 3.3-1(d-f(i))) are very similar to the surface microstructures, and therefore, the through-hardness of these bolts was good. The centres of Bolts 1, 2 and 3, however, show pale regions of ferrite visible in the form

of allotriomorphic and/or Widmanstätten ferrite at the prior-austenite grain boundaries. Vickers hardness testing of Bolt 2 indicated good hardenability, however, suggesting that a uniform microstructure was present throughout its cross section (Figure 3.2-2(b)). Widmanstätten ferrite can be identified by its sawtooth morphology, with parallel plates extending into the prior austenite grains. The microstructure at the austenite grain interior is very fine, making it difficult to identify whether pearlite, bainite or a combination of the two are present. The appreciable drop in hardness at the centres of Bolts 1 and 3 in Figure 3.2-2(a) and Figure 3.2-2(c) respectively can be explained by the relatively large regions of low-carbon ferrite and the coarse carbides present in a pearlitic/bainitc microstructure. These are less effective at impeding dislocation motion than are the small carbides and the strained ferrite matrix present in a tempered martensite microstructure, resulting in lower hardness.

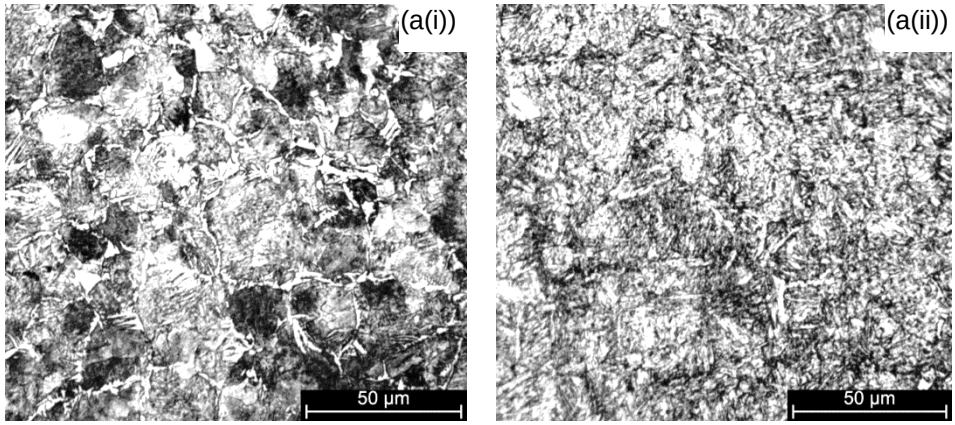

Bolt 1

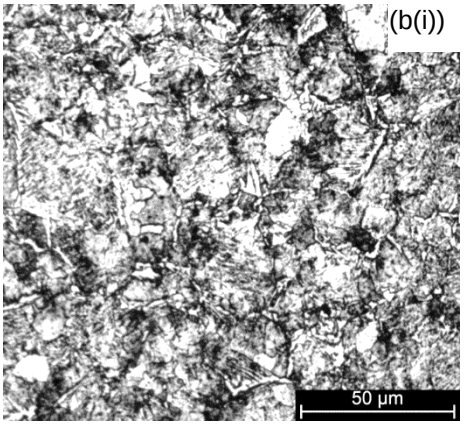

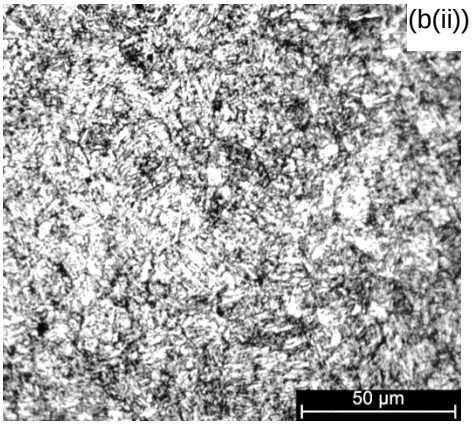

Bolt 2

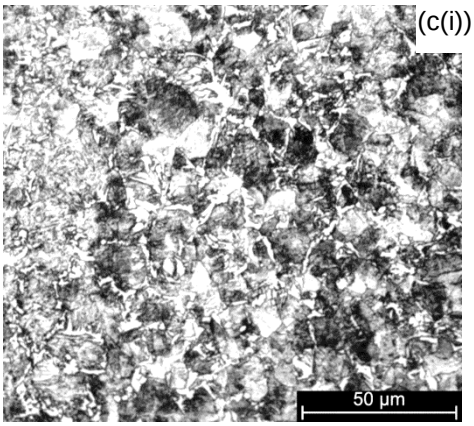

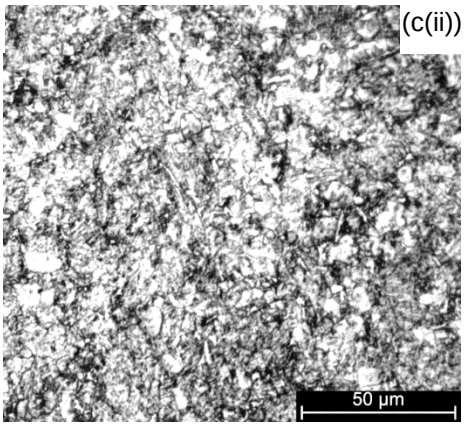

Bolt 3

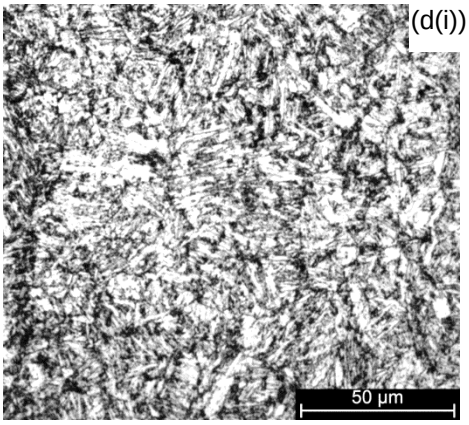

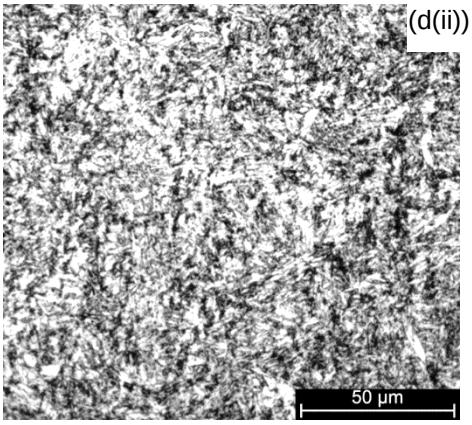

Bolt 4

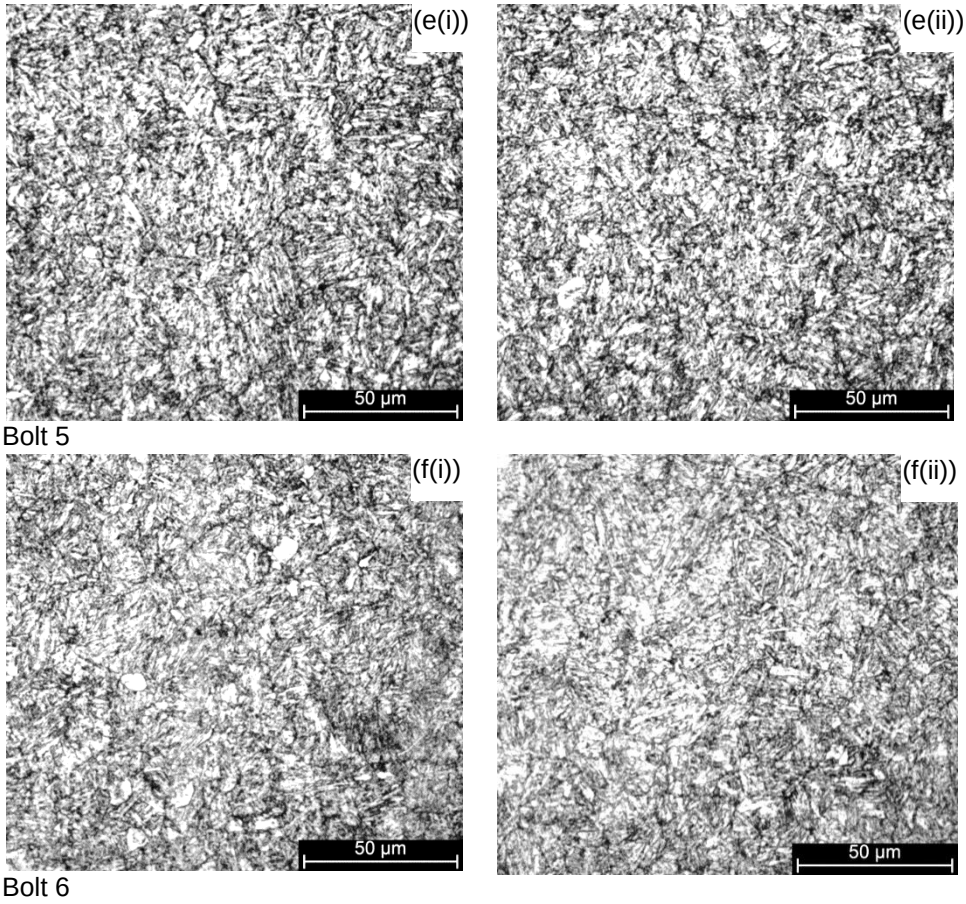

Figure 3.3-1 Optical micrographs taken at bolt centres (i) and surfaces (ii) of bolts 1-6 (a-f) respectively

3.4 Scanning Electron Microscopy

In order to identify the microstructure at the centres of Bolts 1 and 3, scanning electron microscopy (SEM) has been used to allow far greater magnification. This microscopy method does not depend on the reflection of light from the surface topography, but instead detects the interaction between an electron beam and atoms at the specimen surface, allowing high-resolution imaging. An Inspect F FEG (field emission gun) SEM was used with an accelerating voltage 10kV and spot size of 3.

Pearlite can be identified by the lamellar structure caused by the co-operative growth of ferrite and cementite. At fast cooling rates and low transformation

temperatures the driving force of transformation is high, and therefore there is a high nucleation rate of pearlite and many pearlite colonies with different orientations may exist within each austenite grain. Under these conditions the diffusion rate of carbon atoms is low, producing fine, broken-up pearlite lamellae. At slower cooling rates fewer, larger pearlite colonies are formed, and the diffusion rate of carbon atoms is high, leading to coarser pearlite lamellae. From the SEM images obtained it is clear that at the centre of Bolt 1 (Figure 3.4-1(a)) there is a mixed microstructure. Some regions of very fine, broken-up pearlite (P) can be seen, as well as areas of what appears to be lower bainite (B) consisting of cementite precipitates within bainitic ferrite laths between Widmanstätten ferrite. In the bottom right-hand corner of Figure 3.4-1(a) there is a region of high disorder and fine carbide precipitates characteristic of tempered martensite (M).

At the centre of Bolt 3 (Figure 3.4-1(b)) large colonies of coarse pearlite are present, indicating a slower transformation and higher transformation temperature than for Bolt 1. Also present at the centre of Bolt 3 are large regions of ferrite, not only at the prior-austenite grain boundaries, but also within the prior-austenite grains in the form of idiomorphic ferrite. This has most likely nucleated at non-metallic inclusions present in the steel, due to an “unclean” smelting process during steel making. The large ferrite grains and coarse pearlite microstructures are reflected by the low hardness measured at the centre of Bolt 3.

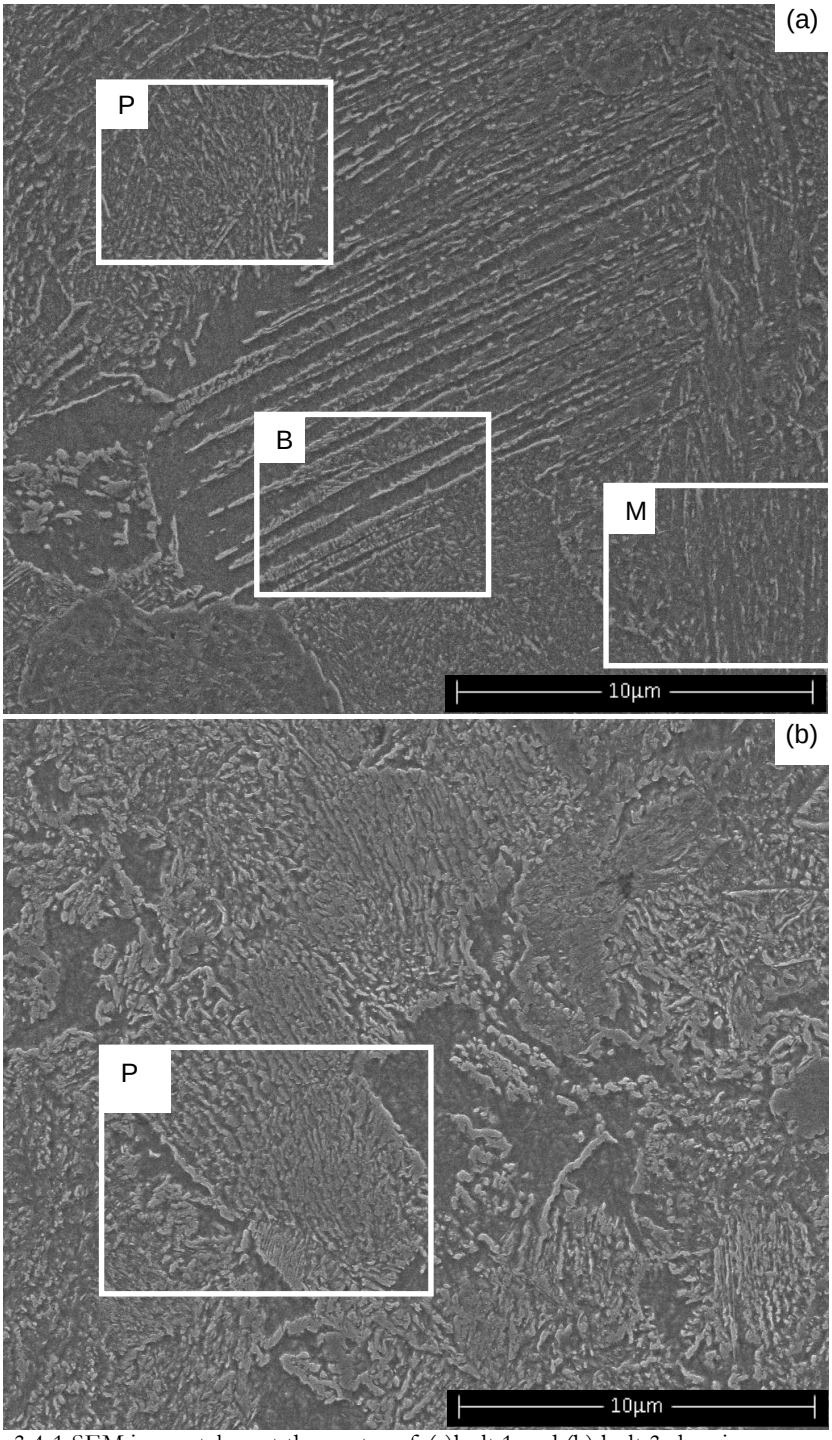

Figure 3.4-1 SEM image taken at the centre of (a)bolt 1 and (b) bolt 3 showing areas of fine pearlite and lower bainite

The mixed and pearlitic microstructures present at the centres of Bolts 1 and 3 respectively are due to slow cooling at their centres (since poor hardenability has

been ruled out by the similar compositions of all bolts considered). Bolts are batch-quenched, and therefore bolts at the centre of the batch can be assumed to cool more slowly than those at the edge of the batch, due to heat transfer from the hot bolts surrounding them. If the quench medium is not cool enough to ensure a rapid enough cooling of the bolts at the centre of the batch, a martensitic transformation will not occur.

3.5 Prior-austenite Grain Size

The prior-austenite grain size is important, as it strongly influences the hardenability. The smaller the grain size the higher the number of pearlite nucleation sites, and therefore the lower will be the steel hardenability [80]. However, as large grains also lead to reduced toughness, the austenite grain coarsening should be managed in order to ensure adequate hardenability and toughness.

Bolts 1-6 were etched to reveal the prior-austenite boundaries using a picric acid etch containing 80 % concentrated picric acid, 20 % Teepol and 2 drops of HCl. A number of optical microscopy images were taken at 200x or 500x magnification, dependent on prior-austenite grain size. An example of the revealed prior-austenite grain structure is given in Figure 3.5-1 for Bolt 2. The grain size was determined using the manual linear intercept method, with lines drawn across each image with a line-spacing similar to the maximum grain size per image, to ensure that no grain was measured more than once. The number of times each line intercepted grain boundaries was counted, and the average grain size was then calculated. At least three images containing between 6 – 9 lines were used to calculate the grain size for each bolt. An average was taken for each bolt, and the 95 % confidence limit was calculated by multiplying the standard error by the relevant t-value for the total number of lines considered for each bolt (Table 3.5-1).

Clearly, large variations in the austenitising treatment also exist between the six bolts, with Bolt 5 producing an average grain size of half that obtained for Bolts 1, 2, and 4. This could be due to the use of a lower austenitising temperature or a shorter holding time during hardening.

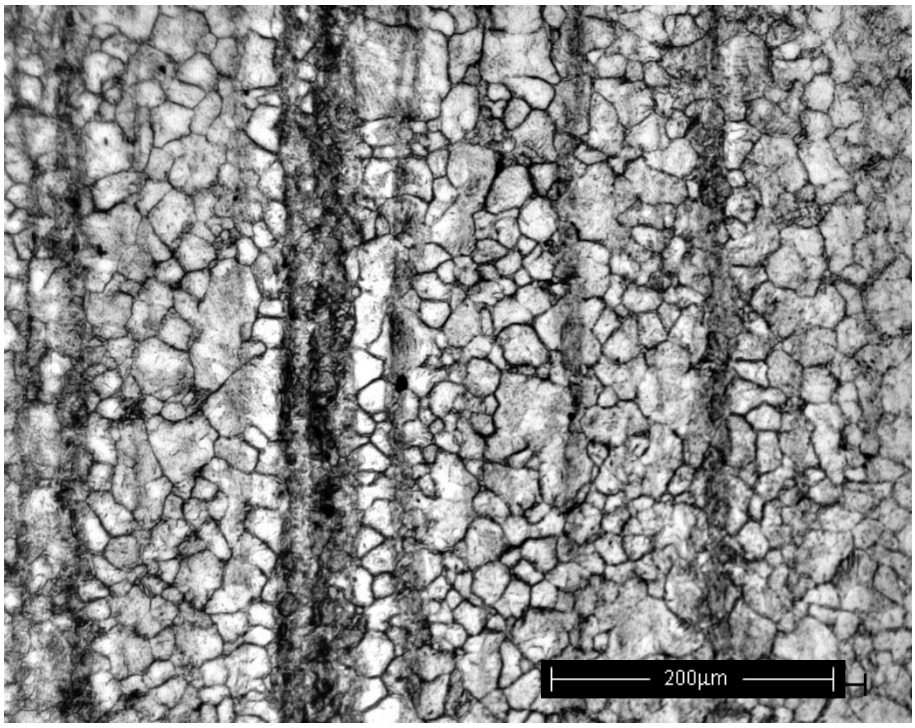

Figure 3.5-1 Prior-austenite grain boundaries in Bolt 2 revealed with picric acid etch

Table 3.5-1 Average prior-austenite grain size and 95% confidence limit for Bolts 1-6

Bolt	Average γ grain size (µm)
1	22.8 ± 0.94
2	22.8 ± 1.00
3	16.1 ± 1.03
4	20.7 ± 1.17
5	10.6 ± 0.59
6	16.1 ± 0.63

3.6 Continuous Cooling Transformation (CCT) Curve Calculation

A software programme called JMatPro has been used to calculate the CCT diagrams of the 6 bolts being considered. These are used to predict the austenite-

to-ferrite transformation at a given cooling rate on a graph with temperature on the y-axis and typically a logarithmic time-scale on the x-axis. The CCT software, included in JMatPro, uses the Johnson-Mehl-Avrami-Kolmogorov (JMAK) equation as a basis [86]. Chemical composition and prior-austenite grain size from previous microstructural characterisations were input, and austenitising temperatures 50˚C above each calculated austenite transformation temperature were assumed. The CCT curves for Bolts 1, 3, 5 and 6 were very similar, due to their similar compositions (Figure 3.6-1). Due to the similarities between these four bolts, all four have been plotted together, with the CCT curve for Bolt 6 highlighted in red. Three cooling rates, of 100, 10 and 1˚C/s, have also been added to the CCT diagrams to indicate which transformations will occur at these cooling rates. The CCT curve of Bolt 6 has been highlighted in red, and falls between the CCT curves of the other three bolts of similar composition. The hardenability of Bolt 6 can therefore be assumed to be characteristic of others on the market, with the exception of Bolts 2 and 4.

The shapes of the CCT curves plotted for Bolts 2 and 4 (Figure 3.6-2(a-b)) are very different from those of Bolts 1, 3, 5 and 6 (Figure 3.6-1) because these bolts have significantly different carbon contents to the other bolts. Individual plots for bolts 1, 3, 5 and 6 can be found Appendix A1. As explained in Section 2.5.5, hardenability is dependent on composition, and while the C content of Bolt 2 is very low compared to the other 5, this bolt contained high levels of Si, Mn and Ni, which improve hardenability. The CCT diagram for Bolt 2 in fact suggests better hardenability than Bolts 1, 3, 5 and 6, with a 100˚C/s quench bypassing all of the high-temperature transformation products and producing a fully martensitic microstructure (Figure 3.6-2(a)). Bolt 4, which contained a relatively high C content

also produced a CCT curve characteristic of good hardenability, which is typical of high C contents (Figure 3.6-2(b)).

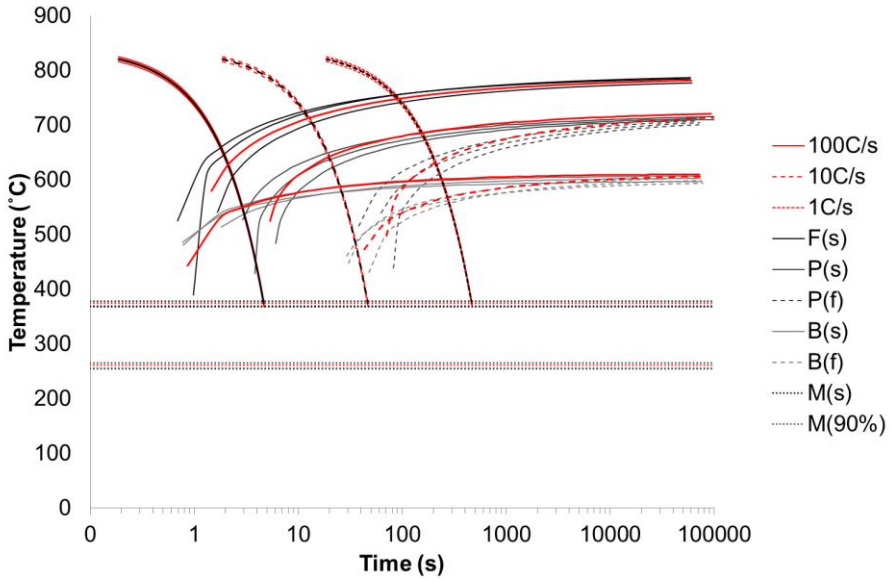

Figure 3.6-1 CCT curves calculated using JMatPro software for Bolts 1, 3, 5 and 6. Bolt 6 is highlighted in red (and black for the three cooling rates) where F(s), P(s), B(s) and M(s) refer to the start of transformation to ferrite, pearlite, bainite and martensite respectively, P(f) and B(f) refer t othe end of transformation to pearlite and bainite respectively and M(90%) refers to 90% transformation to martensite

The austenitising temperature of Bolt 4 was calculated as being significantly higher than that of the other five bolts, at around 1500˚C. This is expected to be due to a "glitch" in the software, as this is unrealistically high. The A_3 line on the Iron-Fe_3C phase diagram (Figure 2.2-10) at 0.4 wt% carbon is at approximately 780˚C, and therefore the austenitising temperature assumed in CCT curve calculation should have been around 830˚C. These CCT curves have been calculated on the basis of the prior-austenite grain size and chemical composition. However, the holding time at the austenitising temperature is also a significant factor in steel hardenability. The holding time must be sufficient for the complete dissolution of C and all other alloy elements to ensure that all alloy elements are in solid solution with austenite.

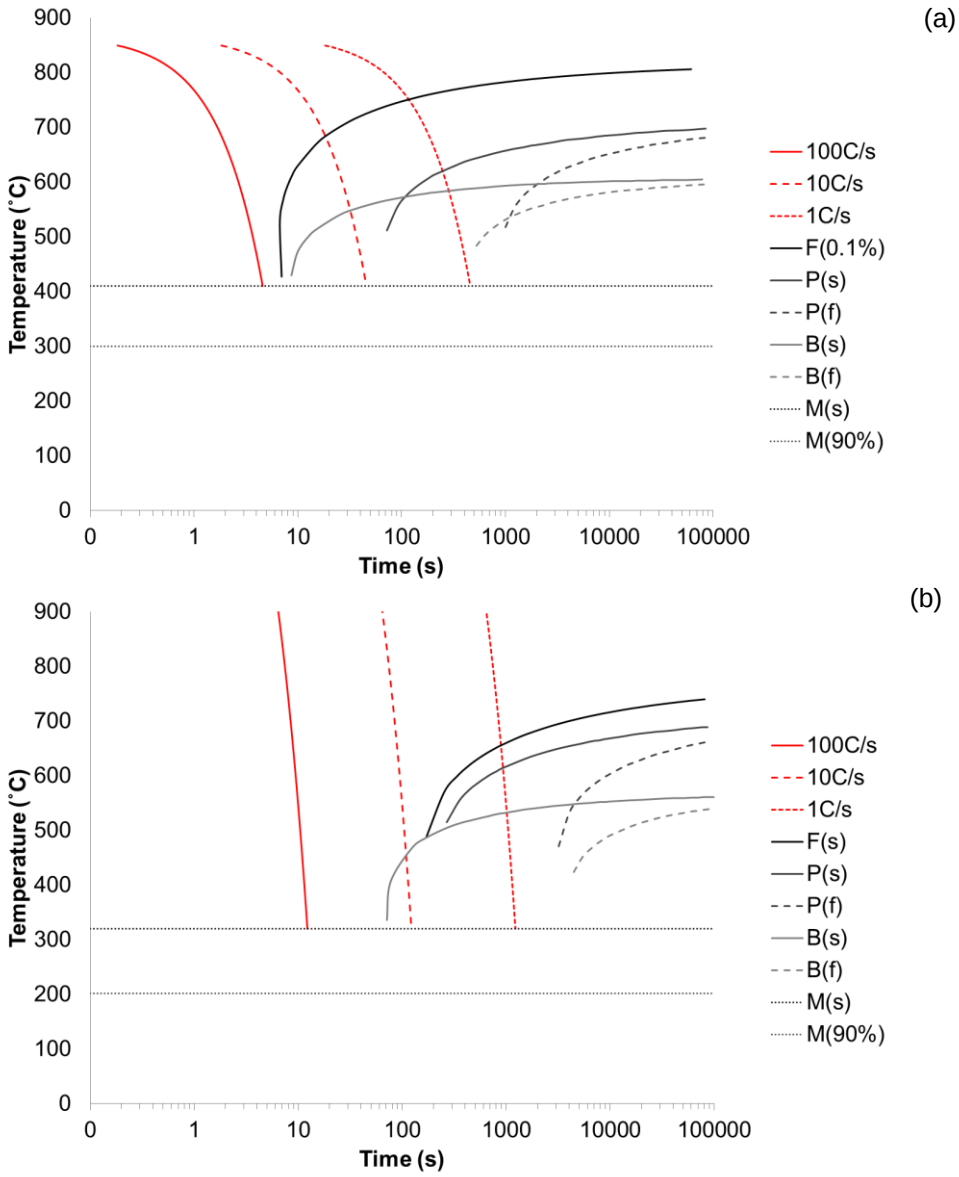

Figure 3.6-2 CCT curves calculated using JMatPro software for (a) Bolt 2 and (b) Bolt 4

3.7 Uniaxial Tensile Testing of Turned down Bolts

3.7.1 Experimental Methods

Testing has been performed under displacement-control and steady-state conditions at a constant temperature and engineering strain-rate. An ESH test machine capable of applying tensile forces up to 1000 kN was used, with grips originally made for the bolt assembly testing carried out by Hu [3]. These grips

have un-threaded central holes which can accommodate an M20 bolt. For a bolt assembly, the bolt passes through both holes and a nut is secured to the end of the threaded bolt shank. The top grip travels at a constant velocity while the bottom grip holds the bolt head stationary. The same set-up was used for turned-down bolts; however, for these tests, the specimen was screwed into two internally-threaded extenders, held in place between the two grips (Figure 3.7-1).

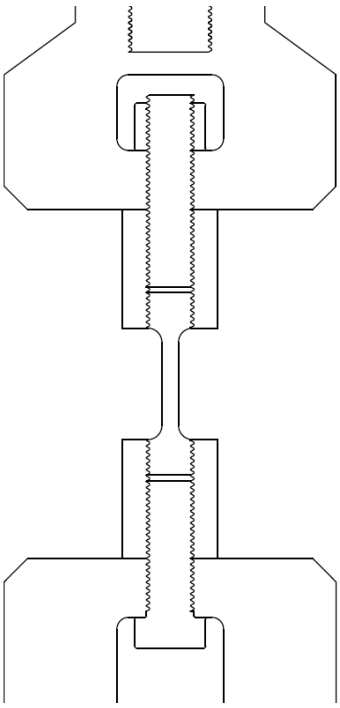

Figure 3.7-1 Apparatus used for turned-down bolt tests

Structural members are typically only stressed within their elastic range, in which case strain is independent of strain-rate. During a fire, however, structural members including steel fasteners typically undergo significant plastic deformation, which usually occurs at a high rate of strain [87]. It was therefore decided that three strain-rates would be considered in addition to four temperatures (Table 3.7-1). A single test has been carried out per strain-rate and temperature combination.

Table 3.7-1 Temperature and strain-rate combinations used for turned-down bolt tests

$\dot{\varepsilon}$	v	Temperature (˚C)			
(min^{-1})	(mm/s)*	20	550	620	700

0.002	6.6733×10^{-4}	x	x	x	x
0.01	3.3501×10^{-4}	x	x	x	x
0.02	6.7338×10^{-3}	x	x	x	x

* Based on a 20 mm gauge length where $v = \frac{L_0}{\dot{\varepsilon}}$

3.7.1.1 Temperature

Test temperatures of 550 and 620°C were chosen, using current guidelines produced by the Association for Specialist Fire Protection (ASFP) in the 'Yellow Book' [88] which prescribes 550˚C and 620˚C as the limiting steel temperatures for columns and beams carrying concrete slabs, respectively. Fire protection thicknesses are specified so that these temperatures are not exceeded in structural members within designated fire resistance times. A higher temperature of 700˚C was chosen as the maximum temperature that unprotected connections are likely to reach in a building fire.

A large wrap-around convection furnace was used to heat the samples. In order to determine where to place the thermocouples, and to measure thermal gradients within the test-piece, an unloaded specimen was heated until the furnace reached 700˚C. The results are shown in Figure 3.7-2 for five thermocouple locations. Heating times to specimen temperatures of 550-700˚C were of the order of 3-6 hours, which meant that thermal gradients were within 1˚C at bolt temperatures greater than 550˚C. As a result of these tests it was decided that temperature would be measured from a thermocouple in the bottom shoulder of the specimen, where it could remain stationary throughout the test without being detrimental to strength. No holding time was required once the temperature had stabilised, due to the small thermal gradients which existed.

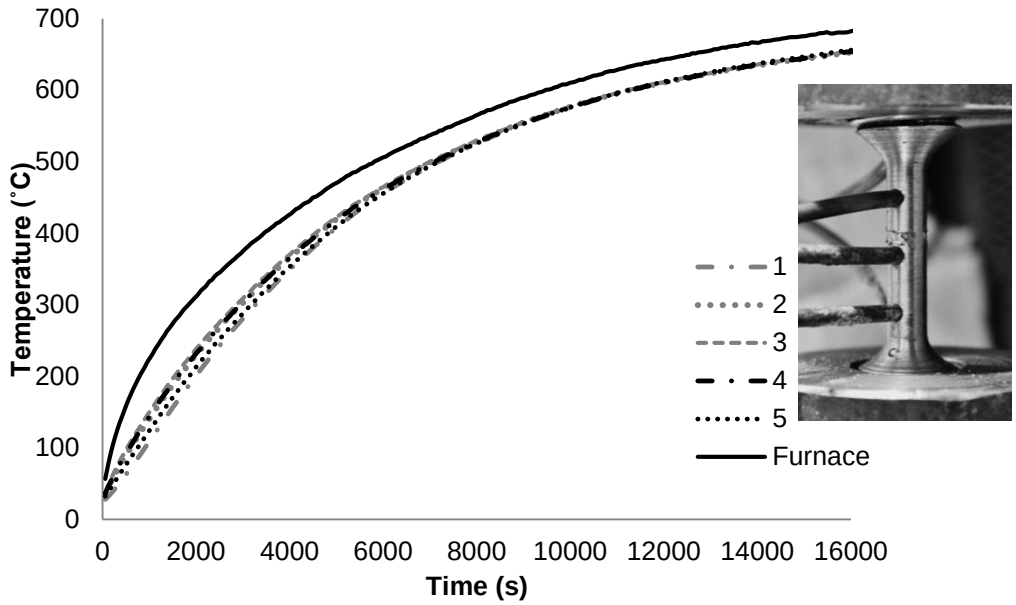

Figure 3.7-2 Temperature during heating of the furnace to 700˚C for five thermocouple locations

3.7.1.2 Strain Rate

A limiting rate of deflection of $L^2/9000d$(mm/min) at the mid-span of a simply supported beam subjected to an evenly distributed load is prescribed in BS 476-20 [89]. This is approximately equivalent to a maximum strain-rate of 0.0005 min^{-1} (Appendix A2). This value is conservative, however, in order to ensure the safety of the fire testing procedure. The slowest strain-rate chosen for the study was therefore 0.002 min^{-1}, which is within the 0.001-0.003 min^{-1} range used by Kirby [1]. Unlike the previous material tests carried out by Kirby [1] and González [4], who respectively increased their strain-rates once the stress level was above the 5% and 2% proof stress levels, the strain-rate was maintained up to rupture. Since the flow behaviour is known to be strain-rate dependent, it was decided that a constant strain-rate would provide more accurate ultimate tensile strength and total strain data. Two faster strain-rates were also chosen, since the strain-rate increases during heavy plastic deformation (Table 3.7-1).

Testing was carried out at constant velocity, where velocity is defined as gauge length ÷engineering strain-rate, based on a gauge length of 20 mm. The true strain-rate will decrease throughout the test, as the gauge length of the test specimen increases in accordance with the empirical relationship in Eq (1), except for a sharp rise at the onset of necking [90] due to a sudden increase in local elongation. Creep effects have been neglected due to the relatively short test durations.

$$\dot{\varepsilon} = \frac{d\varepsilon}{dt} = \frac{1}{L}.\frac{dL}{dt} \quad (1)$$

Where ε̇ = true strain-rate, ε = true strain and L = gauge length.

3.7.1.3 Geometry

The suggested geometry for a test piece with a threaded M20 grip, according to ISO 6892-2, [91] includes a gauge length of 100 mm and parallel length of 191 mm which could not be achieved with the available bolt length of 90 mm. A non-standard geometry was designed with at least 20 mm of the threaded grip remaining at each end of the test piece after machining. The remaining length was 50 mm. The following limits from Annex D of ISO 6892-1 [92] were considered during specimen geometry deign:

$$L_0 = k\sqrt{S_0} \quad (2)$$

$$r \geq 0.75 d_0 \quad (3)$$

$$L_c \geq L_0 + \frac{d_0}{2} \quad (4)$$

A gauge length of 20 mm results in a radius of 2 mm in order to comply with Eq (2). However, the equivalent ultimate tensile load for a 2 mm radius based on nominal

stress area = 245 mm^2 and minimum ultimate tensile load = 203 kN for an M20 Grade 8.8 bolt [11] is just 10 kN (Eq(6)).

$$\sigma = \frac{F}{A} \tag{5}$$

$$\frac{203kN}{245mm} = \frac{F}{\pi x 2^2} \tag{6}$$

This value would be significantly lower for a test carried out at elevated temperature, and was decided to be too small to ensure accurate results, given the high load capacity of the ESH tensile test machine. A diameter of 7 mm was chosen as a compromise between giving a sufficiently high ultimate load capacity at ambient temperature (equivalent to 32 kN for a 7 mm diameter) and having a cross-sectional area sufficiently small to ensure that no thread deformation occurred at that load. The chosen geometry is shown in Figure 3.7-3.

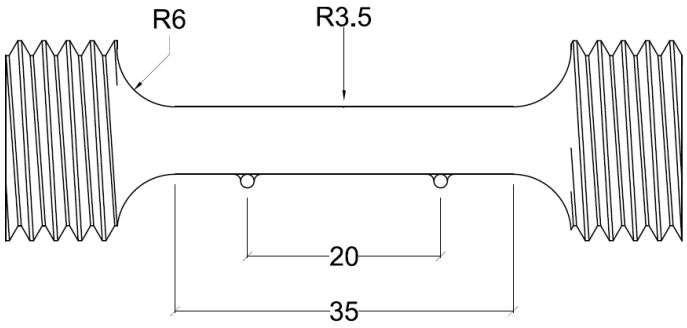

Figure 3.7-3 Turned-down bolt specimen geometry

This geometry complies with Eq(3) and (4), despite using a gauge length smaller than that calculated using Eq(2).Test velocities were calculated for each chosen strain-rate on the basis of this 20 mm gauge length (Table 3.7-1).

3.7.1.4 Data Acquisition

In the turned-down bolt tests the ends of the gauge length were marked with glass beads attached to the surface with fire cement. The silhouettes of these beads were clearly visible against the back of the furnace. During testing, strain was

measured using two-dimensional digital image correlation (DIC), a method chosen to allow strain to be measured up to failure. A Canon EOS 1100D camera, with an 18-55 mm lens, was placed on a tripod, so that the gauge length could be seen through a small window in the front of the furnace. An automatic trigger system connected to a Labview module was used to trigger the shutter at the same time as the force data was recorded to file. Displacement was calculated for both beads, so that the bottom reading could be subtracted from the top to eliminate any tripod movement. The gauge length and cross-sectional diameter were measured three times per specimen prior to testing, and an average was taken to allow accurate strain and stress calculations.

Approximately 500 images were taken per test, to ensure that an adequate number of readings were taken during elastic deformation. The data acquisition rates used are given in Table 3.7-2.

Table 3.7-2 Data acquisition rate (s^{-1}) per test

$\dot{\varepsilon}$	Temperature (˚C)			
(min^{-1})	20	550	620	700
0.002	0.1	0.05	0.04	0.02
0.01	0.5	0.25	0.2	0.1
0.02	1	0.5	0.4	0.2

The pixel resolution was 4272 x 2848 and the gauge length was approximately 400 pixels in length, equating to 20 pixels/mm. Elongation was calculated from the images using GeoPIV [93], a Matlab module developed for the Geotechnical measurement of strains in soil. The GeoPIV Matlab code was run for each bead for each set of images. The patch size and location were generated in an initial mesh file for the first image; in this case a single patch of 20 x 20 pixels was used per bead. GeoPIV then searched for this patch, and was able to locate the area most similar to the previous patch with sub-pixel precision [93]. In more complex studies an array of patches can be used to calculate strains over a large area. A .txt output

file was generated for each analysis, and the displacement in pixels was calculated by subtracting the vertical displacement generated for the bottom bead from that generated for the top bead. The image processing software, ImageJ, was then used to measure the gauge length in pixels and convert elongation from pixels to mm and allow strain calculation.

3.7.1.5 Argon Atmosphere

In order to prevent excessive oxide-scale build-up on the surface of the test-piece during slow heating and long tests at 700˚C a ceramic surround was made to fit between the two grips and partially encase the test piece, so that the gauge length markers are still visible to the camera lens (Figure 3.7-4).

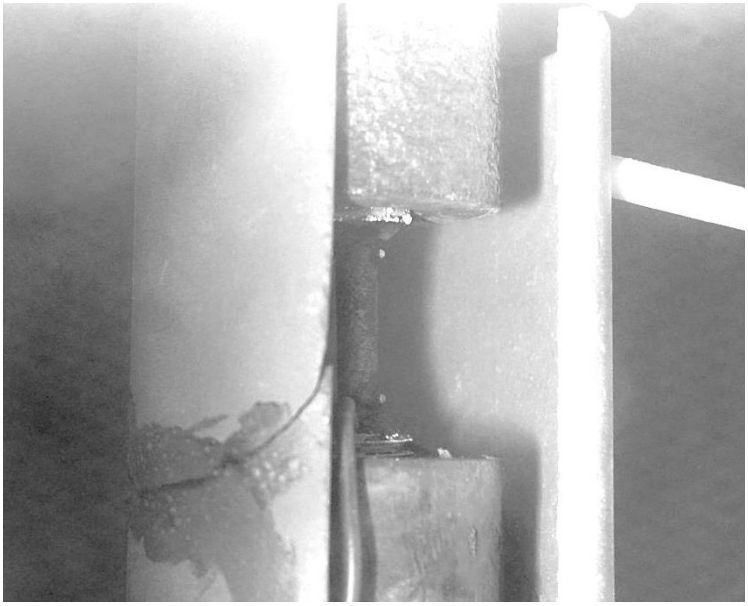

Figure 3.7-4 Ceramic surround for use with Argon at 700 ˚C

This was filled with a steady stream of Argon through a ceramic tube fed through the wall of the furnace during heating and testing. Scale not only reduces accuracy by preventing gauge markers on the scale surface from accurately tracking displacement of the same points on the substrate material, but also reduces the

effective cross-sectional area of the test piece, leading to inaccurate stress calculation.

3.7.1.6 Post-Processing

At the start of testing, the rate of loading was slow, due to initial adjustments of the position of the test-piece and the test rig itself. This effect was removed by calculating the gradient between ¼ and ¾ of the UTS, extrapolating this gradient backward to zero force and zeroing displacement (Figure 3.7-5).

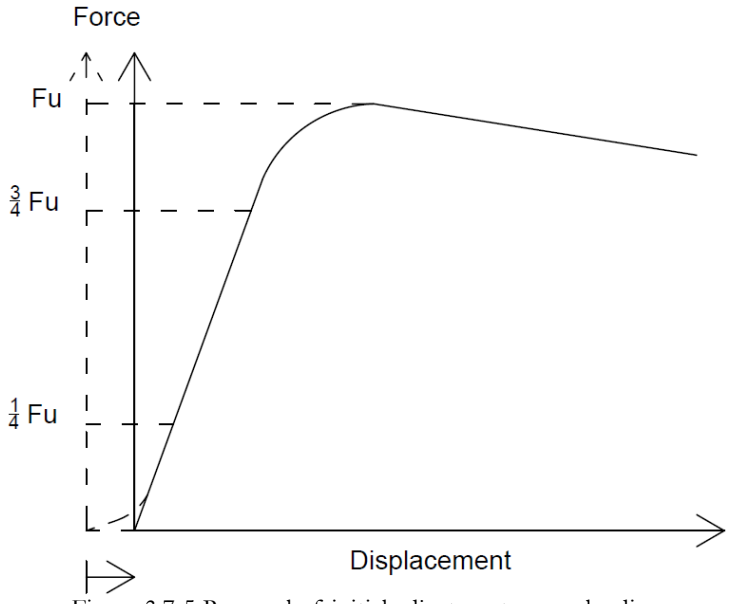

Figure 3.7-5 Removal of initial adjustments upon loading

3.7.2 Experimental Results

The first three tests at all three strain-rates were performed at ambient temperature, and the resulting stress-strain curves were plotted in Figure 3.7-6. In these curves, and in subsequent results, the terms “stress” and “strain” refer to true stress $\sigma = s(1+e)$ and logarithmic strain $\varepsilon = \ln(1+e)$ where e = engineering strain and s = engineering stress.

The nominal tensile strength of 800 MPa prescribed in ISO 898-1 is shown in Figure 3.7-6 by a dotted line, and it can be seen that all three data sets exceeded this value. Typically, strength is a function of deformation rate, with higher strain-rates producing higher strength and reduced ductility. Although this effect could be inferred from Figure 3.7-6, the shapes of the curves are very different from one another.

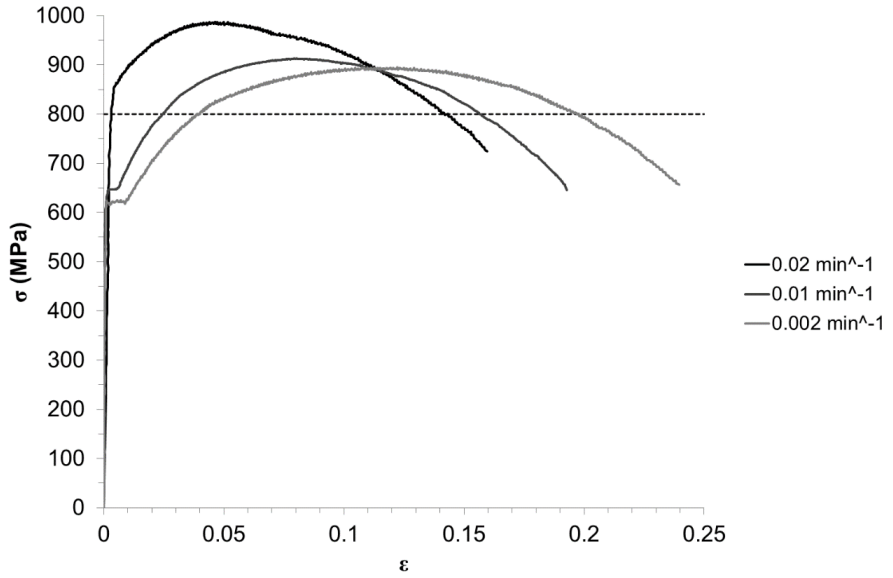

Figure 3.7-6 Flow curves obtained at ambient temperature at 0.02, 0.01 and 0.002 min^{-1}, exhibiting behaviour characteristic of martensite, bainite and pearlite respectively presented with the nominal ultimate tensile stress based on the temperature-dependent strength reduction factors prescribed in EN 1993-1-2

The fastest strain-rate produced a smooth transition from elastic to plastic behaviour, which is characteristic of a martensitic microstructure. The medium and slowest rates, however, produced discontinuous behaviour in the form of a yield plateau at a significantly lower yield point, which is characteristic of pearlite and bainite microstructures [40]. This is surprising, as ISO 898-1 specifies that quenched and tempered M20 Grade 8.8 bolts should contain at least 90% tempered martensite at their centres. Since all three bolts were taken from the same batch, they have been assumed to have similar chemical compositions, and the variations in microstructure are therefore attributable to differences in cooling

rates during heat treatment. A transverse section was cut through the threaded part of each specimen tested, and the average of fourteen hardness readings across each cross-section was calculated to confirm the presence of different microstructures. The average values for the 0.02, 0.01 and 0.002 min^{-1} rates were 313.1+/-5.3, 262.4+/-13.0 and 268.4+/-15.5 HV respectively, with the lowest readings obtained for the two slower strain-rates falling below the minimum limit of 255 HV given by ISO 898-1**.** In order to ensure consistent results, and to provide worst-case mechanical properties, it was decided that these three tests would be repeated. The subsequent three specimens were machined from bolts for which the centre of the underside of the bolt head had hardness values of 250.1, 241.8, and 247.1 HV, lower than the specified minimum [11] and indicating a non-martensitic microstructure. The results of these tests were far more consistent with one another, with all three specimens exhibiting a yield plateau at between 600-650 MPa (Figure 3.7-7).

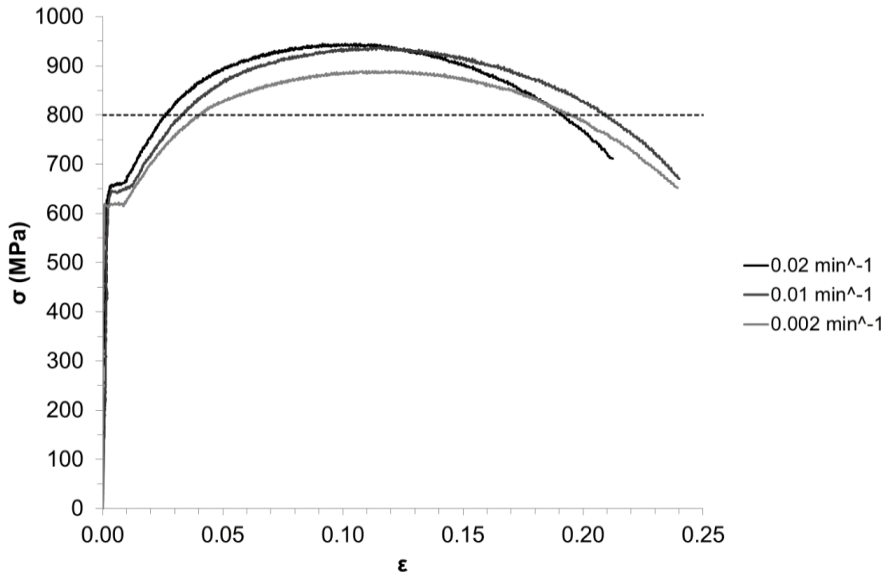

Figure 3.7-7 Flow curves obtained at ambient temperature at 0.02, 0.01 and 0.002 min^{-1} for bolts exhibiting hardness' below the minimum values specified in ISO 898-1 presented with the nominal ultimate tensile stress based on the temperature-dependent strength reduction factors prescribed in EN 1993-1-2

There were slight variations in ultimate tensile, and yield stress for the three different strain-rates but these were not significant enough to suggest a strain-rate sensitivity of stress at ambient temperature. However there was a significant strain-rate sensitivity of strength and ductility in elevated-temperature tensile test results (Figure 3.7-8), most significantly at 550˚C (Figure 3.7-8(a)). The nominal ultimate tensile strength has also been plotted on these charts on the basis of the nominal ultimate tensile strength at ambient temperature of 800 MPa [11] and the strength reduction factors prescribed in Table D of EN 1993-1-2 [8]. All results obtained fell below this value, most notably so at slower strain-rates. The ultimate tensile strength results obtained at 0.002 min^{-1} were approximately half of the nominal value for every elevated-temperature test. At strain-rates of 0.02$min^{-1,}$ the values obtained were closer to the nominal values. At 550˚C the difference between the two was still over 50MPa.

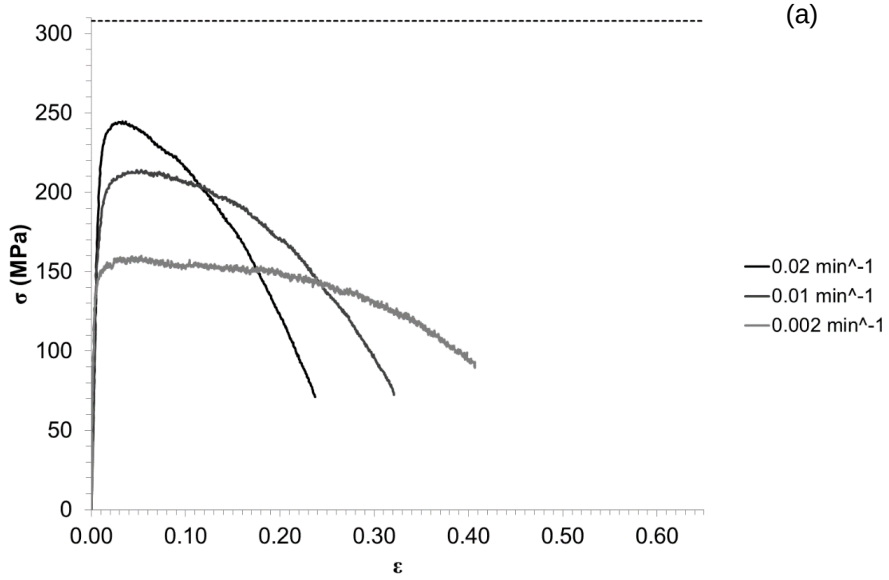

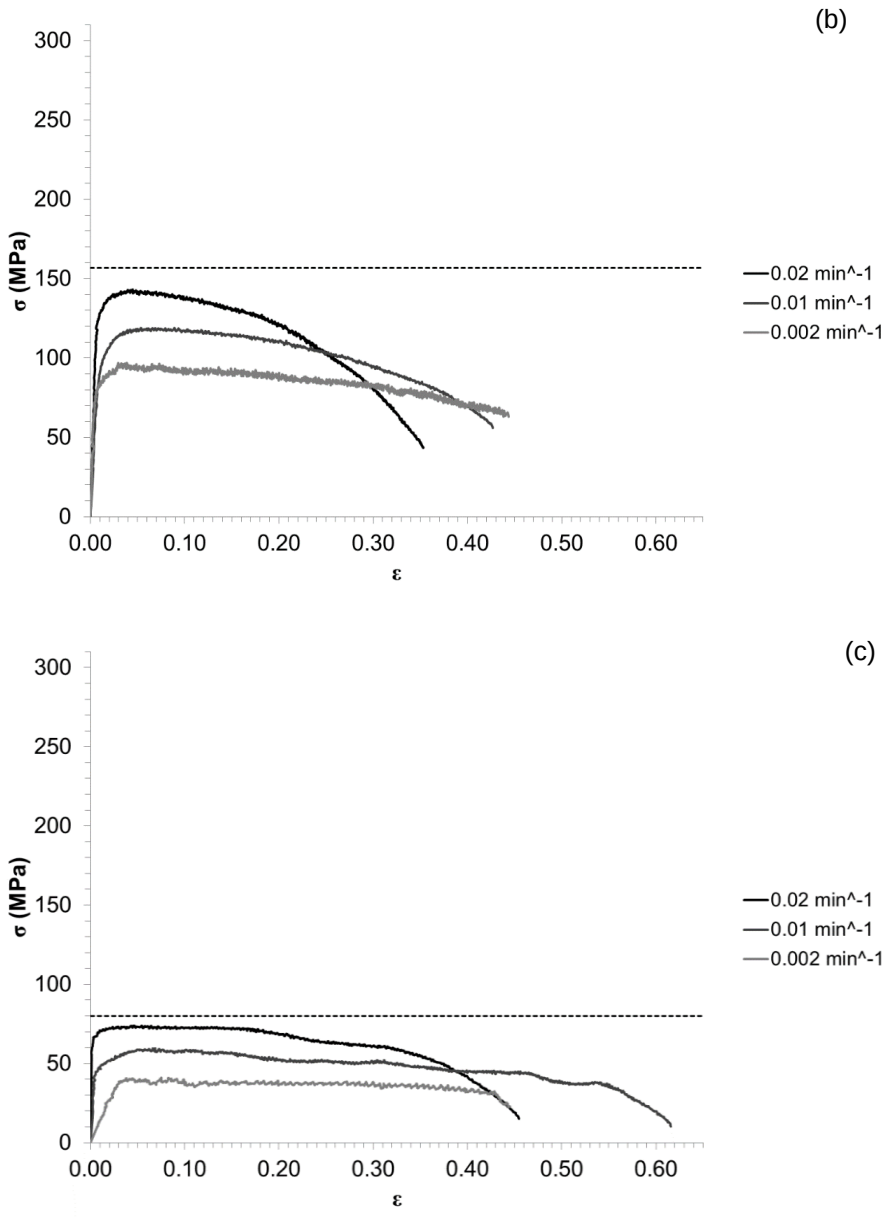

Figure 3.7-8 Flow curves obtained at (a) 550˚C, (b) 620˚C and (c) 700˚C at 0.02, 0.01 and 0.002 min^{-1} presented with the nominal ultimate tensile stress based on the temperature-dependent strength reduction factors prescribed in EN 1993-1-2

A summary of the strain-rate and temperature-dependent mechanical properties of the bolt material is given in Table 3.7-3 including Young's modulus, ultimate tensile strength, 0.2% and 2% proof strains.

Table 3.7-3 Ultimate tensile strength, 0.2% proof and 2% proof stress calculated for each temperature (°C) and strain-rate (min^{-1}) combination

(MPa)	20			550		
	0.002	0.01	0.02	0.002	0.01	0.02
σ(0.2%)	615.1	643.8	654.9	141.5	182.7	219.3
σ(2%)	703.3	738.0	767.0	156.2	210.2	244.3
σ(UTS)	889.5	938.1	944.7	160.0	214.1	244.7

(MPa)	620			700		
	0.002	0.01	0.02	0.002	0.01	0.02
σ(0.2%)	82.0	96.7	124.7	35.9	46.7	66.1
σ(2%)	92.5	115.2	140.3	39.5	54.1	72.4
σ(UTS)	96.9	119.0	143.2	41.0	59.6	73.3

Each value of 0.2% and 2 % proof stress and ultimate strength was normalised with respect to their ambient-temperature values for each strain-rate and temperature (Table 3.7-4). These results have been compared to the strength reduction factors prescribed in EN 1993-1-2 and also the results from previous research contained within Figure 2.2-14. It can be seen from Figure 3.7-9 that the strength reduction factors obtained for Bolt 6 are well below the bolt strength reduction factors prescribed in Eurocode 3, most markedly so for the slowest strain-rate. This may be due to the slow heating and long test times in this study, which allowed greater recovery of the bolt material than was possible in Kirby's tests, which were heated at 5-10 °C/min with the strain-rate being increased to 0.01 min^{-1} to rupture beyond the 5 % proof stress. Differences in chemical composition would also lead to differences in strength, as less heavily alloyed steels rely more on heat treatment to achieve their strength. The strength reduction factors calculated in Table 3.7-4 must be treated with caution, because the ambient-temperature results obtained in Figure 3.7-7 were obtained from bolts containing a pearlitic microstructure. The strength values obtained were, therefore, significantly lower than would be expected from that of a tempered martensitic steel. If the elevated-temperature results were normalised with respect to the value obtained

from the martensitic steel in Figure 3.7-6, these strength reduction factors would be even lower than those presented in Table 3.7-4.

Table 3.7-4 Strength reduction factors calculated by normalising elevated-temperature (°C) properties with respect to ambient-temperature values.

	0.002				0.01				0.02			
	20	550	620	700	20	550	620	700	20	550	620	700
σ(0.2%)	1.00	0.23	0.13	0.06	1.00	0.28	0.15	0.07	1.00	0.33	0.19	0.10
σ(2%)	1.00	0.22	0.13	0.06	1.00	0.28	0.16	0.07	1.00	0.32	0.18	0.09
σ(UTS)	1.00	0.18	0.11	0.05	1.00	0.23	0.13	0.06	1.00	0.26	0.15	0.08

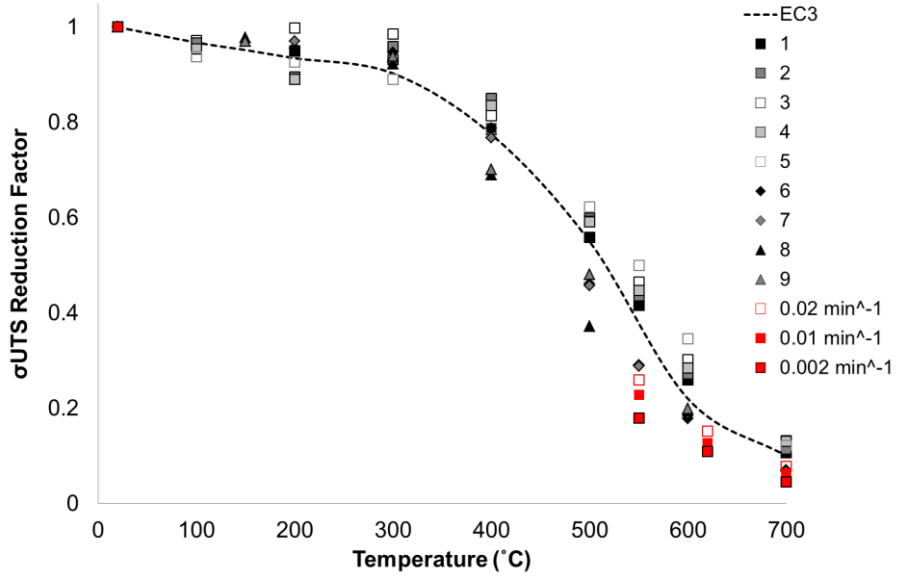

Figure 3.7-9 Strength reduction factors obtained by normalising elevated temperature ultimate tensile strengths with respect to the ambient-temperature value in relation to those prescribed in EN 1993-1-2 and previously published data (Table 2.2-3)

3.8 Summary

It is clear from the research reported in this chapter that there could potentially be a large number of M20, Grade 8.8 bolts currently in use in steel-framed buildings which contain a non-martensitic microstructure. This is due, in part, to the range of permissible chemical compositions and hardness values prescribed by ISO 898-1. Although Bolt 1 contained a large amount of ferrite at its centre, only a small proportion of the Vickers hardness readings obtained fell below the minimum limit

prescribed in ISO 898-1, suggesting that the minimum value should be raised from 255 HV. Three of the six bolts considered contained ferrite at their centres, and two showed significant variations in hardness across their cross-sections, suggesting that this is a widespread problem. Bolt 6, which gave uniform hardness and tempered martensite throughout its cross-section, was from the same batch of bolts used for uniaxial tensile testing. Two of the three specimens initially tested under tension at ambient temperature produced yield plateaus in the range 625-650 MPa, while the minimum prescribed 0.2% proof stress is 660 MPa [11]. Microstructural variations, therefore, not only exist between different manufacturers, but also within a single batch of bolt assemblies.

At ambient temperature, microstructural variations led to different flow behaviour. The bolt containing a tempered martensitic microstructure and having a hardness of 313 HV produced a smooth transformation between elastic and plastic behaviour, a yield strength of approximately 850 MPa, and an ultimate tensile strength of almost 1000 MPa. The bolts containing non-martensitic microstructures produced yield plateaux in the range 600-650 MPa and ultimate tensile strengths between 850-950 MPa. Despite visible differences in mechanical behaviour, all of the turned-down bolts tested at ambient temperature produced ultimate tensile strengths greater than the nominal value of 800 MPa specified in ISO 898-1.

At elevated temperatures all results produced smooth yield transitions and similarly-shaped flow curves. These, however, produced much lower ultimate tensile strengths than expected on the basis of nominal strength and the temperature-dependent strength reduction factors prescribed in EN 1993-1-2. This was highlighted in Figure 3.7-9, in which strength reduction factors were compared to those provided in EN 1993-1-2. Although literature produced since the inclusion of strength reduction factors in EN 1993-1-2 by Hu [3] and Gonzalez [5] also fall

below those obtained by Kirby [1], the results produced in this study were significantly lower. It must be noted that these reduction factors would be lower still, had they been normalised with respect to the ultimate tensile strengths obtained for the turned-down bolt containing a tempered martensite microstructure and not a pearlitic one.

Despite the range of microstructures identified in this study, every turned-down bolt tested at ambient temperature produced an ultimate tensile strength within the limits prescribed in ISO 898-1 and yield strengths similar to the nominal value prescribed. While a minimum of 90% martensite in the as-quenched condition is specified, those containing large regions of ferrite and pearlite do not fall far below the minimum mechanical properties prescribed at ambient temperature. The similarly shaped curves produced at elevated temperatures suggest that at 550˚C, carbides might have coarsened sufficiently in both the pearlitic and martensitic microstructures to produce similar flow behaviour. The effect of ambient-temperature microstructure can therefore be assumed to have a negligible effect on elevated-temperature properties once the tempering temperature of the bolts has been exceeded.

Page Intentionally Left Blank

4 Mechanical Testing of Bolt Assemblies

Uniaxial tensile testing of bolt assemblies from the same batch used for turned-down bolt specimens, Bolt 6 of the material characterisation, has been carried out in order to investigate the influence of different variables, including strain-rate, temperature and thread tolerance, on the failure modes and ultimate tensile strengths of bolt assemblies under pure tension.

4.1 Experimental Methods

The same ESH test machine, furnace and strain-rate and temperature combinations used for turned-down bolt testing have been used, with the exception of 620 ˚C which was excluded. Each test has been repeated at least three times. The test velocity and the frequency at which images were taken were altered to reflect the longer gauge length of 90 mm bolts (Table 4.1-1).

Table 4.1-1 Image frequency (s-1) for all temperature and strain-rate combinations used for bolt assembly tests

$\dot{\varepsilon}$	v	Temperature (˚C)		
(min^{-1})	(mm/s)*	20	620	700
0.002	2.0667×10^{-3}	0.1	0.04	0.02
0.01	1.0333×10^{-2}	0.5	0.2	0.1
0.02	2.0667×10^{-2}	1	0.4	0.2

* Based on a 62 mm gauge length where $v = \frac{L_0}{\dot{\varepsilon}}$

The same grips were used as for the turned-down bolt tests. In these tests, however, two spacers were machined from stainless steel, and were respectively

placed under the bottom surface of the nut and above the bolt head (Figure 4.1-1). These spacers had a slot cut from their front faces to allow the threads to be visible at both ends of the bolt shank, for strain calculation in the case of necking failure under tension.

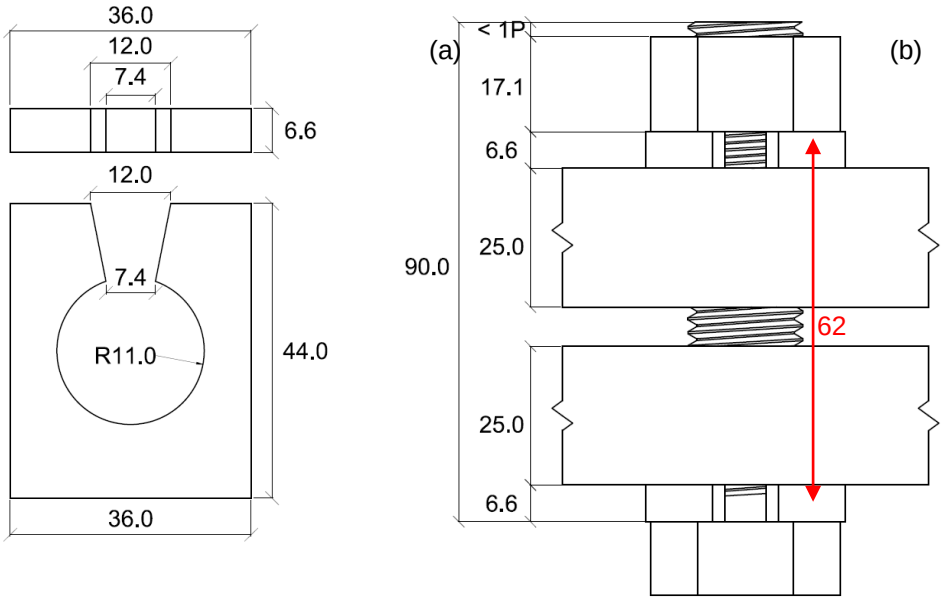

Figure 4.1-1 (a) Spacers to enable visibility of gauge length and (b) bolt assembly test setup using these spacers

The 62mm distance between the centres of these two spacers determined the gauge length used for calculating test velocity (Table 4.1-1), with a uniform cross-sectional area of 245 mm^2 [11], when less than one bolt thread pitch was visible above the top surface of the nut. In the case of thread-stripping failure, for which deformation occurred outside the gauge length, strain could not be calculated, and displacement and force readings were recorded. In this case any area of high contrast on the nut and bolt head could be used for calculating elongation using digital image correlation.

The nut was always placed above the top grip, so that a force was applied to the underside of the nut while the bolt head was restrained for consistency. The nut was hand-tightened so that less than one thread pitch was visible above the top

surface of the nut in accordance with EN 15048-2 [7]. The effect of scale was neglected in bolt assembly tests, because of the relatively large cross-sectional area.

4.1.1 Thread Tolerance Measurement

Since the tolerance between the nut and bolt threads is thought to influence the failure mode, a simple test was carried out prior to testing of each assembly, in order to determine the minimum clearance between the nut and bolt threads (Figure 4.1-2).

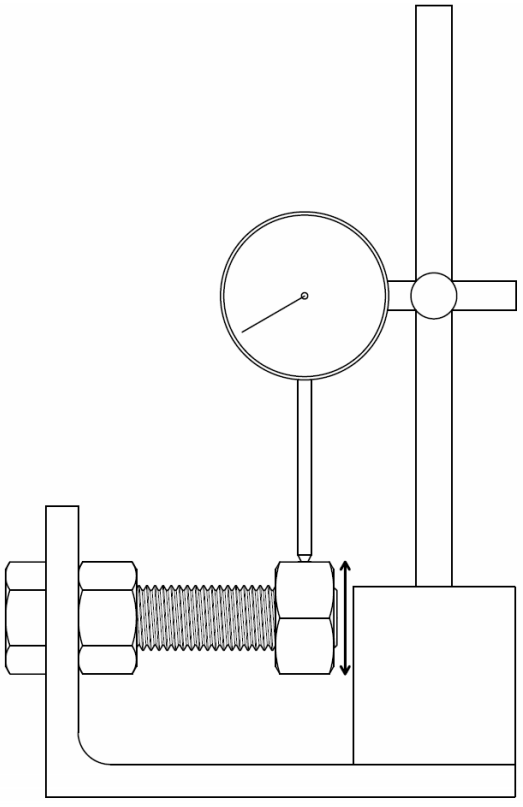

Figure 4.1-2 Method of thread clearance measurement

Each bolt specimen was slotted through a hole in a right-angle steel section and a nut was then tightened mechanically, using an impact driver, against the steel section so that the bolt was firmly held in place. The nut to be tested was then

tightened by hand to a position approximately one thread pitch (2.5mm) from the end of the bolt shank with a flat face at the top. A dial gauge was attached to the steel section, using a magnetic base to eliminate the displacement of the steel-angle, and the maximum and minimum readings were noted as the nut was moved up and down by hand. The differences between these readings were halved in order to give the thread tolerance for each assembly tested.

4.2 Results

4.2.1 Effect of strain-rate and temperature

The results of tensile testing carried out at three temperatures and three strain-rates are summarised in Figure 4.2-1(a-c). The results are plotted as force against displacement, because the majority of failures were due to thread-stripping, and therefore accurate strain measurements could not be calculated from the displacement of threads visible through the spacer slots shown in Figure 4.1-1.

At ambient temperature both failure modes were observed (Figure 4.2-1(a)). In previous literature necking failures are reported as tending to occur at loads greater than, or equivalent to, those for thread-stripping [1] (Table 2.2-3). It was surprising, therefore, to see that necking occurred at significantly lower loads in this study. None of the assemblies tested at ambient temperature showed a significant strain-rate effect on either the ultimate tensile force or total elongation. The low tensile strength of necking failures was found to be a result of the same microstructural variations observed for turned-down bolts (Figure 3.7-6). Average Vickers hardness readings taken from three indents at the centre of the cross-section revealed that the three bolts which failed due to necking had significantly lower hardness values. These were; 245.7, 249.9 and 248.3HV for 0.01a, 0.002b and 0.002d respectively, all of which fell below the minimum specified in ISO 898-1,

and were comparable to the values measured previously for turned down bolts which contained pearlitic and/ or bainitic microstructures. From these observations it is clear that, for those assemblies which contained soft, ductile material, necking was the more likely failure mechanism. Those which contained hard, brittle material were more likely to fail through thread-stripping at higher loads.

Despite the existence of material-dependent failure modes at ambient temperature, all ultimate load capacities were greater than the specified minimum of 203 kN prescribed in ISO 898-1, as shown by the dotted line in Figure 4.2-3(a). At ambient temperature ductility is less important than strength in standard applications, due to the very small beam deflections which are permissible, and so the variations in mechanical properties due to different microstructures are not very significant at ambient temperature. The ultimate load capacities of those assemblies which failed through thread-stripping were in the region 230-242 kN, with an average of 236 kN, and are significantly higher than any of the load capacities obtained, either through necking or thread-stripping, by Kirby [1] (Table 2.2-3) who tested bolt assemblies provided to BS 4190 with the looser thread tolerance class combination, 8g7H.

At elevated temperatures ductility becomes far more critical in bolt assemblies, which must continue to transfer loads effectively from beams to columns during thermal expansion and subsequent sagging of beams during the growth of a fire. The results of elevated-temperature testing (Figure 4.2-1(b-c)) show again that the effect of strain-rate is most pronounced at elevated temperatures, with higher strain-rates producing higher ultimate load capacities in all cases. Ductility was not affected by strain-rate, however, because all assemblies failed through thread-stripping at approximately 5mm extension at 550˚C (Figure 4.2-1(b)) and 7.5-10mm at 700 ˚C (Figure 4.2-1(c)).

The forces obtained at elevated temperatures were compared with those predicted by using the strength reduction factors prescribed in EN 1993-1-2 applied to the nominal ambient-temperature ultimate load capacity. This calculated failure load is plotted in (Figure 4.2-1(a-c)) as a dotted line. At 20˚C bolt assemblies which failed due to bolt breakage failed at failure loads comparable to the nominal value prescribed in ISO 898-1. At elevated temperatures the results obtained were much lower than those predicted using the Eurocode 3 strength reduction factors and the nominal load capacity (Figure 4.2-1(b-c)). The strength reduction factors were as also found to be unconservative by Hu [3] and Gonzalez [5] (Figure 2.2-14)**.** The difference between predicted failure load and test failure load was greatest for the lower strain-rates, for which failure occurred at less than 50% of the capacity predicted.

(a)

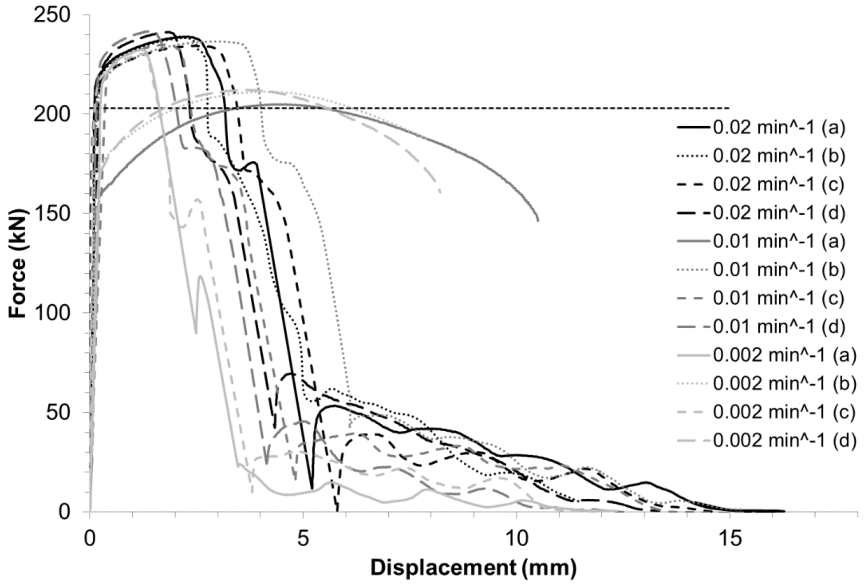

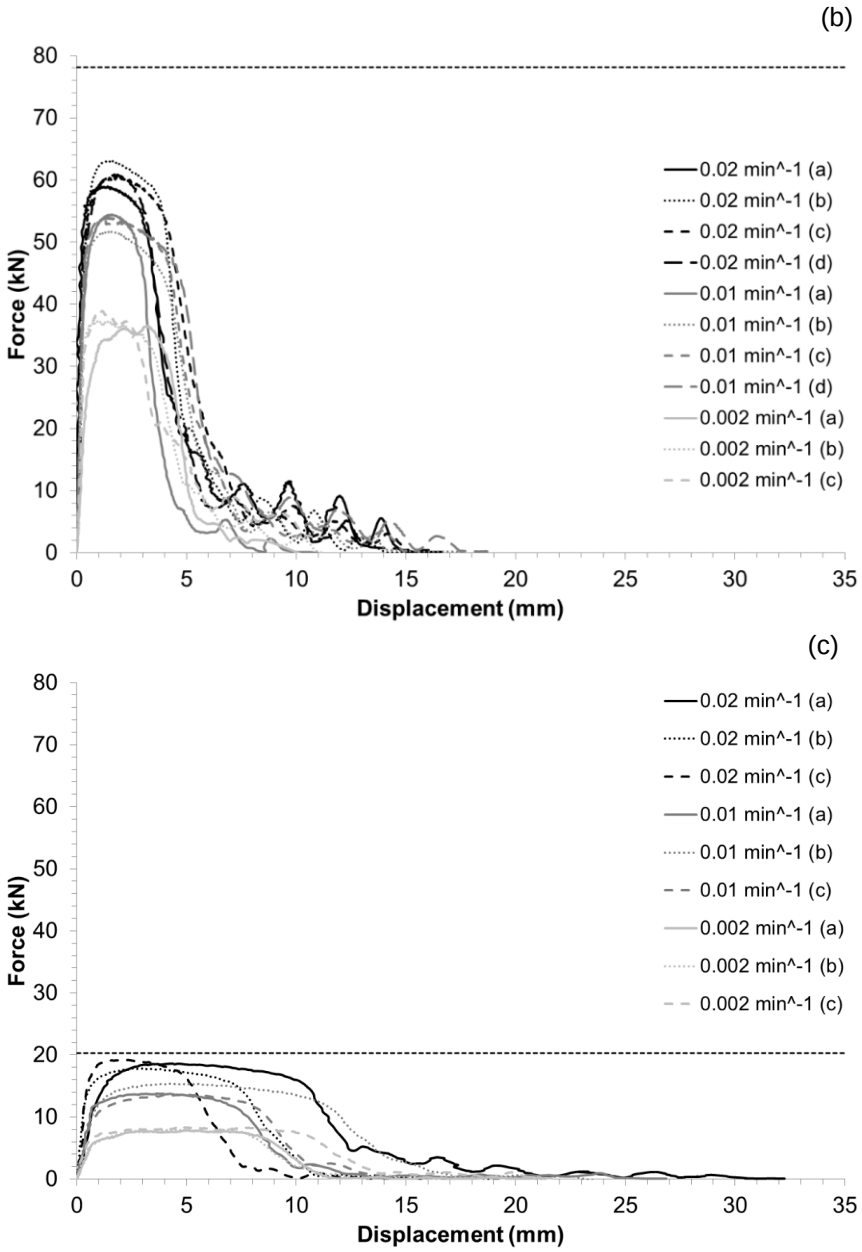

Figure 4.2-1 Force-displacement curves obtained at (a) 20˚C (b) 550˚C and (c) 700˚C at 0.02, 0.01 and 0.002 min^-1 presented with the nominal ultimate tensile force based on the temperature-dependent strength reduction factors prescribed in EN 1993-1-2

In elevated-temperature tests, temperatures far exceeded the tempering temperature used during heat treatment, and therefore any variations in microstructure at ambient temperature become less significant after further tempering to 550°C or 700˚C. The softening of the bulk material seems to have been outweighed by the softening of the threads and subsequent increase in

thread deformation. Alternatively, since all bolts were galvanised, there will have been a marked increase in effective thread clearance at temperatures above the melting point of the zinc coating. The eta and zeta layers will have melted by 550°C, and by 700°C the delta (and gamma) layers will have melted (Table 2.5-2). At 700°C little more than the substrate material will remain, as the gamma layer which melts at 670-780°C is very thin.

The bolt assemblies investigated by Gonzalez [5] were also galvanised. However, they were high-strength assemblies suitable for pre-loading, and the nuts and bolts were of comparable strength, with a Grade 10.9 bolt and Property Class 10 nut. In order to compare the results obtained in this chapter with those obtained in the literature, strength reduction factors were again calculated with respect to ambient-temperature strength. Since two failure modes were observed at ambient temperature, the strength reduction factor was calculated on the basis of the tensile necking failures. The average values of ultimate tensile strength, and the strength reduction factors for each strain-rate and temperature, are summarised in Table 4.2-1 and plotted against those obtained in literature (Figure 4.2-2). The ambient-temperature average was calculated from those assemblies which failed by bolt fracture, and excludes those which failed by thread-stripping. Strength reduction factors obtained for the slowest strain-rate, 0.002 min^{-1}, produced strength reduction factors significantly lower than those prescribed in Eurocode 3 and those obtained from literature. Although previous bolt assembly tests used strain-rates of 0.001-0.003 min^{-1} [1, 5], the strain-rates used by Gonzalez [5] were increased to 0.025 min^{-1} to rupture, beyond the 2% proof stress. These results may have given misleadingly high values of ultimate load capacity, since the strain-rate in the work-hardening region of the flow curve was increased. The strength reduction factor

calculated at 550°C for a strain-rate of 0.002 min^{-1} was significantly lower (less than half) the strength reduction factor prescribed in Eurocode 3.

Table 4.2-1 Average ultimate tensile strengths and strength reduction factors calculated for each temperature and strain-rate tested

T (°C)	20		550			700	
$\dot{\varepsilon}$ (min^{-1})	N/A	0.02	0.01	0.002	0.02	0.01	0.002
Load Capacity (kN)	209.52	60.85	53.39	37.55	18.55	14.24	8.07
Reduction Factor	1.000	0.290	0.255	0.179	0.089	0.068	0.039

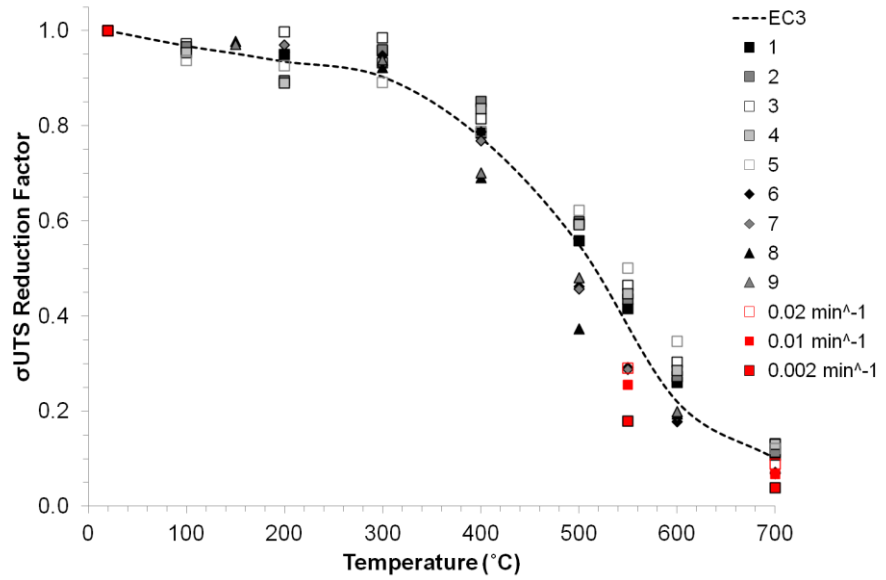

Figure 4.2-2 Comparison between average strength reduction factors obtained for bolt assembly tests at three strain-rates with those prescribed in EC3 [8] and in literature [1, 3, 5] (Table 2.2-3)

4.2.2 Effect of Thread Clearance

The measured thread clearances were plotted against ultimate tensile force; a) to determine whether the method of measuring thread tolerance was sufficiently accurate to identify a trend between thread clearance and load capacity, and b) to see what the effect was (Figure 4.2-3(a-c)). Clearance in this case is the total amount of vertical displacement of the nut positioned one thread pitch from the end of the bolt shank, divided by two. This clearance obviously excludes the thickness

of the galvanised layer and is unconservative, as it measures the smallest possible clearance between the two thread profiles.

Thread tolerance has been reported to influence failure mode [44], however, the influence of thread clearance on ultimate tensile force is unlikely to affect the bolt fracture strength due to localised stress build-up within the necking area. For thread-stripping failures, which constituted the failure mode for every elevated-temperature tensile test, the effect of thread clearance on ultimate load capacity should be significant. Surprisingly no trend was observed between thread clearance and ultimate tensile force (Figure 4.2-3) at any temperature, suggesting that the method for testing thread clearance was inadequate. This could be explained by a localised build up in zinc thickness providing a misleadingly low value of clearance, when in fact the steel-to-steel thread clearance was large. Another explanation for a low clearance measurement could be flank distortion during the cold-rolling of bolt threads, reducing thread clearance at the external thread pitch diameter.

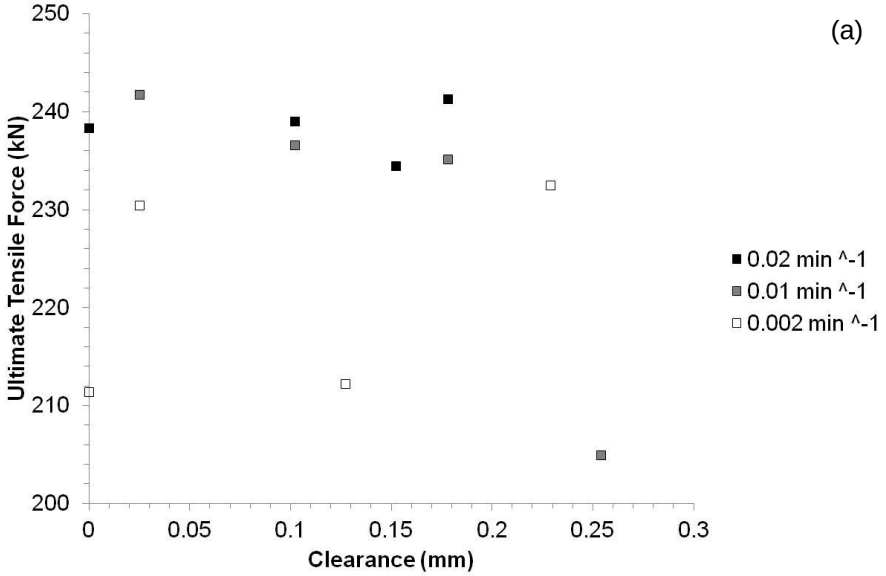

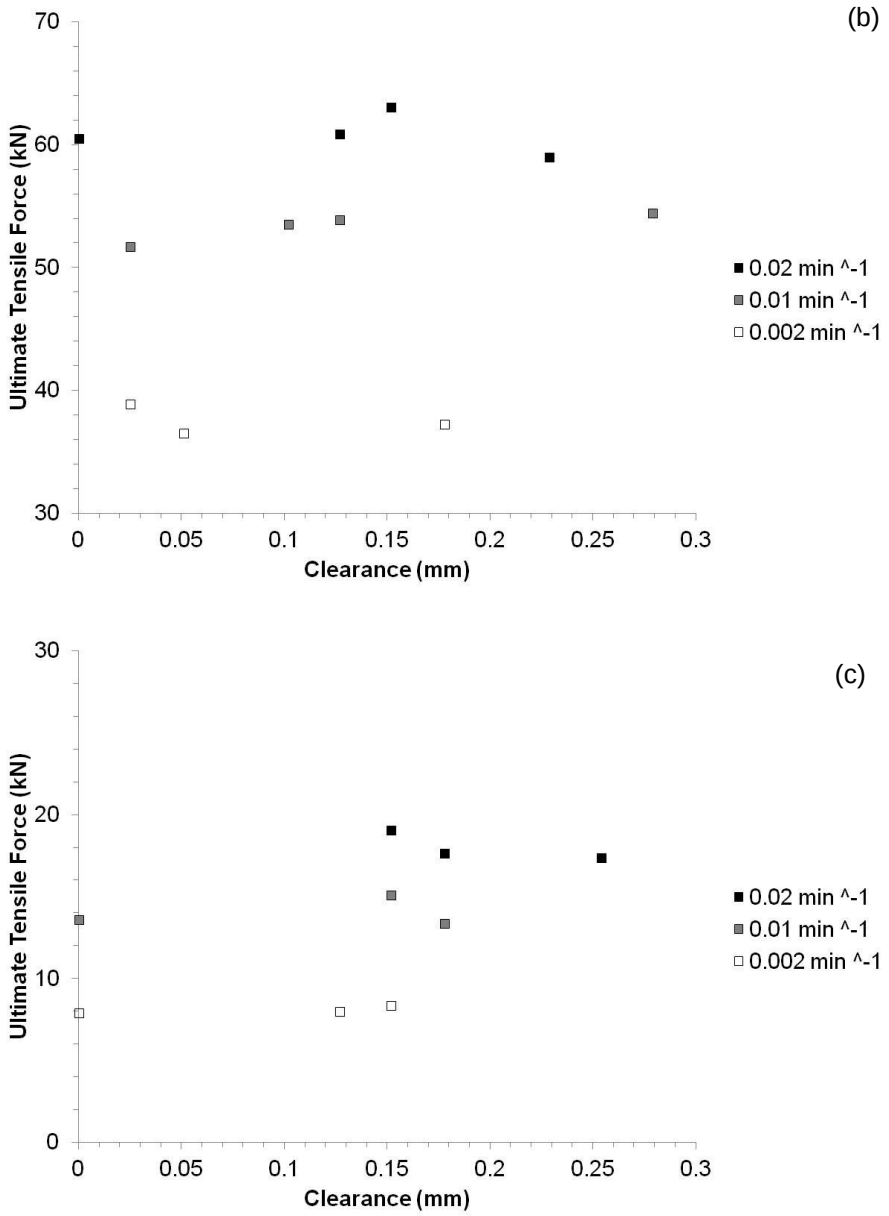

Figure 4.2-3 Effect of measured thread clearance on ultimate tensile strength at (a) 20°C, (b) 550°C and (c) 700°C

There are many reasons that could explain the unreliability of thread clearance measurement using this method including uneven zinc coating thickness. The effect of thread clearance will therefore be investigated further through finite element modelling in the next chapter.

4.2.3 Thread Deformation

In order to investigate the mechanism of thread-stripping a section was milled-out of a nut and bolt to reveal the thread contact interface (Figure 4.2-4 (a)). This was then tested under displacement control at ambient temperature, at the same velocity used for the bolt assemblies tested at $0.02min^{-1}$. In this case, the nut was positioned below the bottom of the lower grip and the bolt head above the upper grip, so that the nut remained stationary. The thread deformations observed explain the force peaks which follow the sudden initial drop in load capacity. At the start of loading, the threads make contact (Figure 4.2-4(b-c)), and begin to plastically deform and work-harden (Figure 4.2-4(d-e)). Work-hardening relates to the increase in strength caused by an increase in both dislocation density and dislocation interactions during plastic deformation, and the rate of work-hardening is most rapid at ambient temperature. The effect of work-hardening can be clearly seen in Figure 4.2-1(a), as the slope between yield and ultimate tensile capacity. Within this region of the graph, dislocations interact with one another and other defects in the crystal lattice; this impedes further dislocation motion. During plastic deformation, the number of dislocations also multiplies, leading to a greater number of dislocation interactions and increased strengthening. At the onset of thread-stripping, sufficient plastic deformation has occurred for the threads to slide over each other (Figure 4.2-4(f-g)).

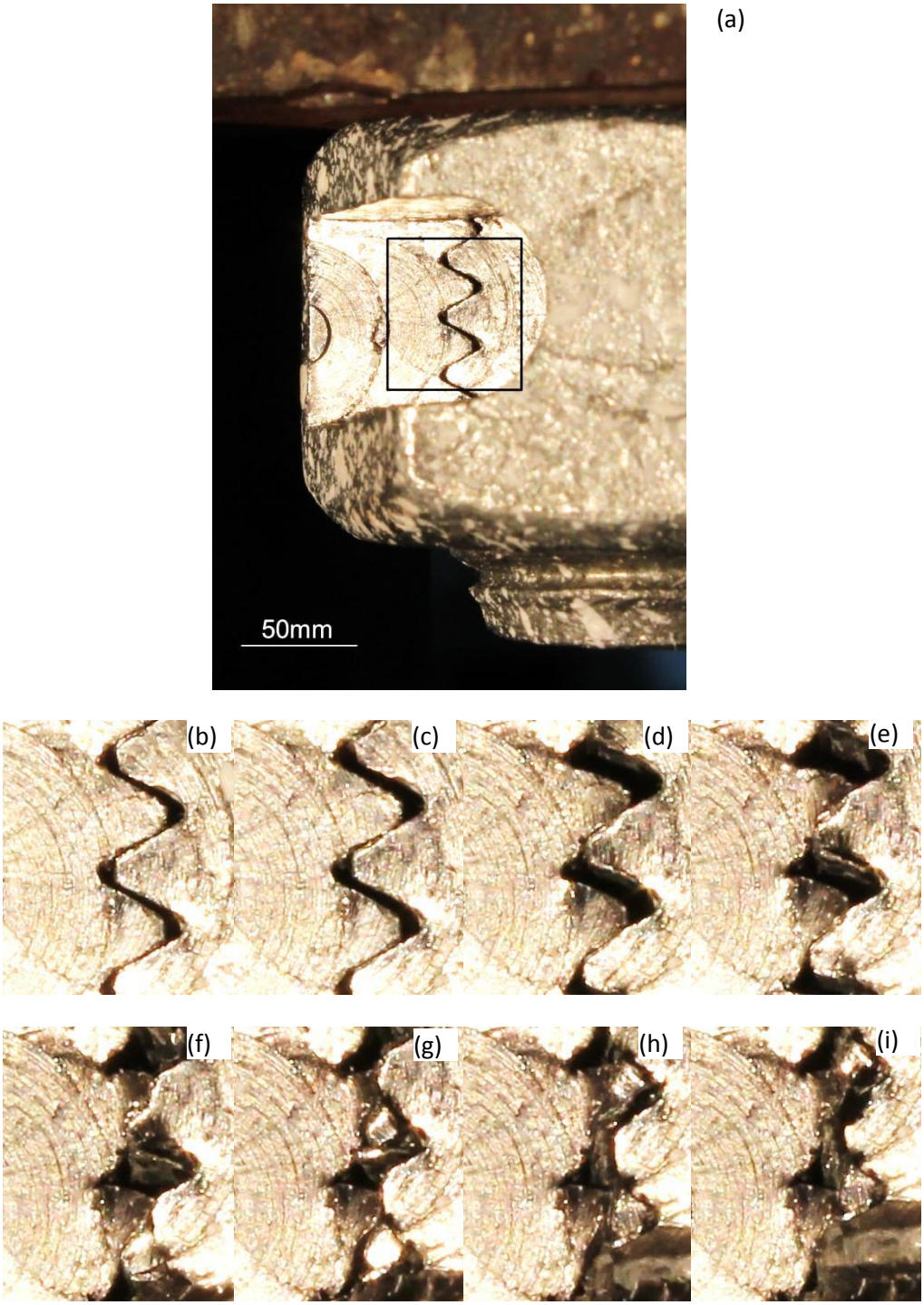

Figure 4.2-4 (a) Specimen tested with section milled-out to reveal thread interface and (b-i) images taken at different stages of the thread-stripping process

All of the threads which were previously engaged are now heavily deformed, and therefore the force drops abruptly. Material which has sheared from a thread tip is

then pushed up against the flank of the next thread, where plastic deformation and work-hardening leads to a slight increase in force (Figure 4.2-4(h-i)). As any thread moves over the second adjacent thread, there is another drop in force. These fluctuations in force continue, with the force reducing slightly each time until the nut has completely pulled off the bolt shank.

4.3 Summary

This chapter has highlighted the importance of tight controls during the manufacture and heat treatment of the components of bolt assemblies in ensuring consistent microstructural properties within the same batch. The failure mode at ambient temperature, in this batch of bolts, was dependent on microstructure. Tempered martensite led to thread-stripping, and bainite and/or pearlite led to necking at significantly lower force levels.

To ensure transformation to martensite during heat treatment, all bolts in a batch must be quenched rapidly. Since all bolts tested in this study were from a single batch, it is likely that those containing weaker microstructures were at the centre of the batch during quenching, and cooled less rapidly due to the temperatures of the bolts surrounding them as opposed to variations in chemical composition. Although hardness values measured at the centres of the bolt heads of the three assemblies which failed through necking fell below the recommended minima, all ambient-temperature failures occurred above the specified minimum ultimate tensile load capacity.

Although microstructure-dependent failure modes were observed at ambient temperature, all assemblies failed due to thread-stripping at elevated temperatures. These failures occurred well below the load predicted using strength reduction factors in Eurocode 3. At these temperatures the clearance is larger than at

ambient temperature due to the melting of galvanised zinc layers, suggesting that thread tolerance has a greater effect on failure mode than as-received microstructure at elevated temperature.

In order to ensure that bolt assemblies contain a tempered martensite microstructure, a more stringent testing procedure may be required, since the current hardness and tensile strength limits prescribed in ISO 898-1 clearly allow for some bolts containing a pearlite/bainite microstructure to be deemed acceptable. In order to ensure necking failure of assemblies containing tempered martensite, a higher tempering temperature would improve ductility at the expense of strength, and may shift the failure mode from stripping to necking. This would, however, contradict the theory of Alexander [44], who suggested that when the length of thread engagement is long, and both thread sets are of comparable strength, the failure mode is likely to be bolt fracture. Clearly, reducing the strength and increasing the ductility of the bolt would increase the difference in strength between the bolt, which is Grade 8, and the nut which is property Class 10. It is interesting, therefore, that the bolts containing the weakest material cause necking failure, and those containing material of strength similar to that in the nut threads failed by thread-stripping. This is unless, of course, the nut material is also softer than expected.

Page Intentionally Left Blank

5 Finite Element Modelling

Finite Element Modelling (FEM) has been used to determine the influence of parameters which could not easily be investigated though mechanical testing. These parameters include the relative strengths of the two thread sets, nut height (and thus the number of threads engaged) and the clearance between threads.

5.1 Input Parameters

5.1.1 Geometry

An axisymmetric model has been chosen, neglecting the helix angle and bolt head, and assuming a cylindrical nut in order to reduce computational time. The chosen geometry has been used for axisymmetric models and a 90˚ revolution applied to it for 3D models (so that the cut planes can be restrained in the global co-ordinate system). The model includes; a full-height bolt excluding the bolt head, an analytically rigid plate, and a full-height nut.

5.1.1.1 Thread Geometry

In order to determine the geometry of the parts, the real thread geometries of three bolt assemblies from the batch of bolts used for mechanical testing were measured and compared to the nominal thread dimensions of thread tolerance class

combination 6AZ6g provided in BS 3643-1[67] and BS 3643-2[68] and discussed in Section 0 “Thread Tolerance” (Figure 5.1-1).

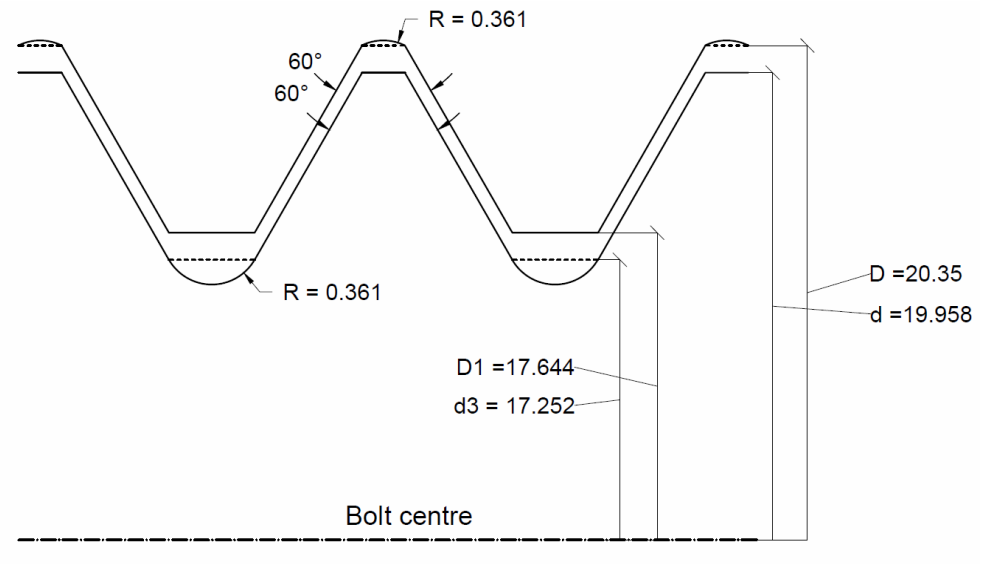

Figure 5.1-1 Nominal thread dimensions for thread tolerance class combination 6AZ6g

A transverse section was cut through the centres of three mated nut/bolt assemblies, for which where the bottom nut face was aligned with the base of the bolt shank (Figure 5.1-2(a-c)).

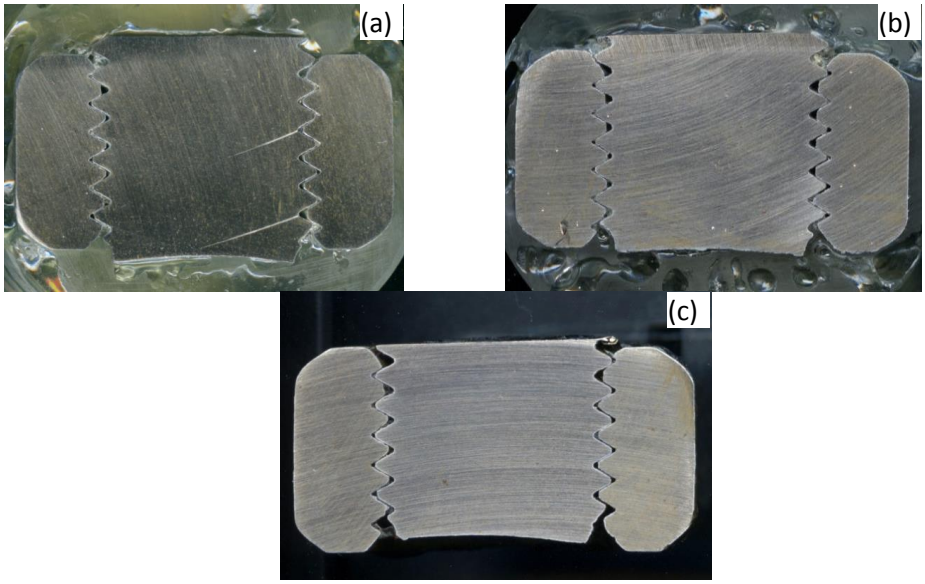

Figure 5.1-2 Transverse sections (a) A, (b) B, and (c) C, used to measure real thread geometries of three bolt assemblies from the batch

Care was taken to cut directly through the centre of the bolt, to ensure that the cut surface ran down the bolt's centroidal axis to avoid distortion of the visible thread profile. Due to the sizes of the cross-sections they were mounted in epoxy resin and were coarsely ground to produce a flat surface, which was then scanned using an Epson Perfection V700 scanner. The dimensions shown in Figure 5.1-3 were then measured from the scanned images using Image J image processing software. These dimensions were measured in pixels and then converted to mm for each section by measuring nut height in mm with a vernier caliper and pixels with Image J to determine pix/mm. Each dimension was measured at five different locations per section and the average taken; these are given in Table 5.1-1

.

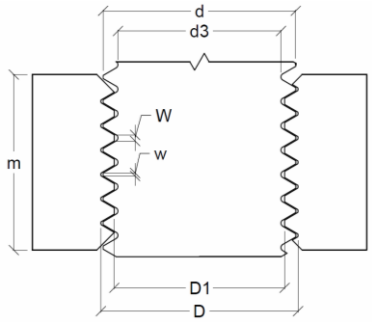

Figure 5.1-3 Dimensions measured for sections A, B and C (w = flat width).

Table 5.1-1 Average measured dimensions for sections A-C

ref.	Nut dimensions (mm)				Bolt dimensions (mm)		
	m	D	D1	W	d3	d	w
A	17.4	20.7	17.7	0.5	16.9	20.1	0.4
B	17.6	20.9	18.3	0.7	17.2	20.2	0.4
C	17.3	20.9	18	0.5	17.1	20.2	0.5

The associated thread profiles were drawn on AutoCAD based on these dimensions and the following assumptions:

1. Root radius = 0.361mm, the nominal value for 6AZ6g, because this dimension was difficult to measure from the scanned images,

2. Flank angles = 60˚ because any difference between nut and bolt flank angles would cause contact issues in the FEM.

This allowed the thread clearance, perpendicular to the bolt neutral axis, to be measured between adjacent thread flanks (Figure 5.1-4). These dimensions include the zinc coating thickness, and therefore do not represent those prescribed for a 6AZ6g thread tolerance class combination, which applies to the pre-coated condition.

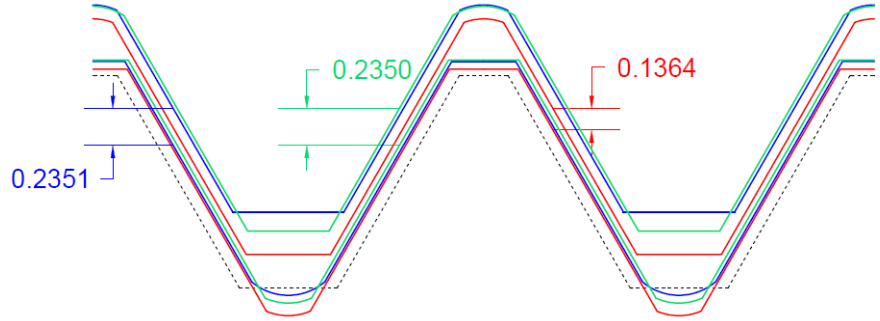

Figure 5.1-4 Thread profiles and associated values of thread clearance based on the measured dimensions in Table 5.1-1 where the black dotted line represents the basic thread profile ISO 68-1 and red = A, blue = B, green = C

In order to determine the thickness of the zinc layer on nut threads in the batch, clearance was measured in the same way as for bolt-assemblies prior to tensile testing (Figure 4.1-2), and before and after zinc removal from three further bolts from the same batch. Molten zinc was removed from the surface of the threads using a wire brush after heating the nuts for 15 min at 550˚C. Clearance measurements; prior to zinc removal were 0.00, 0.09 and 0.16 mm, and after zinc removal these were 0.06, 0.14 and 0.23 mm respectively. The differences in clearance, and therefore approximate zinc coating thicknesses, were 0.03, 0.025 and 0.035 mm respectively. These values fall below the maximum coating thickness of 98 µm specified in ISO 10684 [62]. However, at 550˚C only the eta and zeta layers will have melted completely. In some areas the clearance may be much larger than these measured values. The remaining delta and gamma phase

layers will obviously not have been taken into account in the measurement of coating thickness in this way. Their melting points and hardness values are higher than those of the eta and zeta phases and will, therefore, be closer to the properties of the steel substrate. Since the thicknesses of these layers are relatively small compared to the thicknesses of the eta and zeta phases they will be considered as part of the thread profile. The thickness of the zinc coating was further verified using SEM on an Inspect F FEG SEM which shows the eta and broken-up zeta layers to be approximately 70 µm in thickness (Figure 5.1-5).

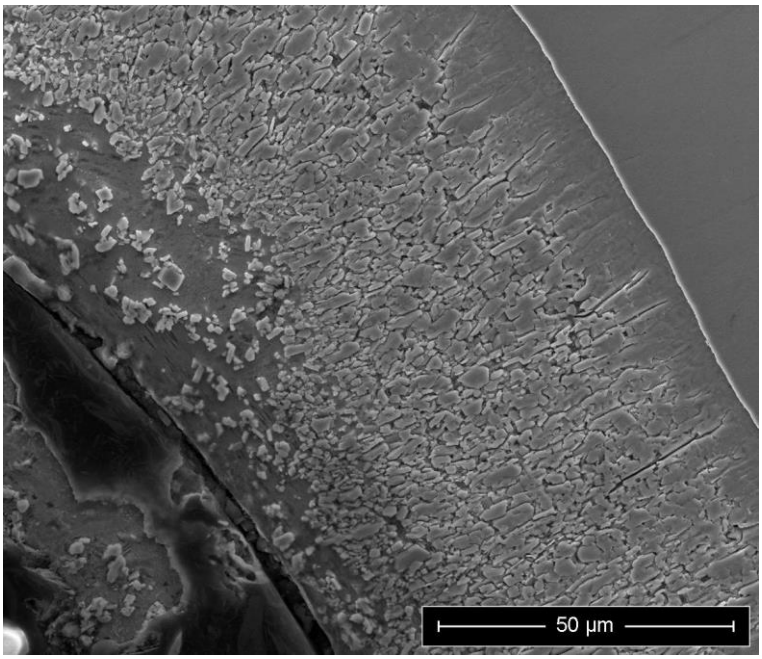

Figure 5.1-5 SEM image of the zinc coating at a bolt thread root

In order to exclude the zinc coating thicknesses from the measured thread clearances in Figure 5.1-4, 0.06 mm has been added to each measured clearance value. The estimated clearances, neglecting zinc thickness, are therefore 0.196, 0.295 and 0.295 for sections A, B and C respectively; an average of 0.262 mm. The minimum specified clearance for tolerance Class 6AZ6g is 0.196 mm to allow adequate room for the zinc coating thickness.

Since the thread profile geometries of sections A-C vary significantly, it was decided that the nominal geometry of the 6AZ6g thread profile (Figure 5.1-1) would be used in the FEM with a nominal clearance of 0.196 mm. ***Clearance in this chapter will be referred to in the form 6AZ6g + x mm, where x is an additional clearance to the 0.196 mm already included in the 6AZ6g profile.*** Since the average clearance of the three thread profiles measured was 0.262 mm, this is equivalent to a thread profile of ***6AZ6g + 0.066 mm***.

5.1.1.2 External Geometry

An axisymmetric model has been chosen, neglecting the helical angle and bolt head, and assuming a cylindrical nut in order to reduce computational time. The 2D geometry used has been based on the thread profile geometry discussed in the previous section and the limiting geometries given in ISO 4017 [72] and ISO 4032 [73] (Table 2.3-6).

A regular hexagon with a nominal 30 mm distance between flats has a 34.641 mm distance between corners. This distance was chosen as the diameter of the cylindrical nut, and equates to a radius of 17.3205 mm, with a nominal nut height of 18 mm. A 45˚ countersink was applied to both faces of the nut and the bottom of the bolt shank. At the head end of the bolt shank a 5 mm flat shank of pitch diameter, including a 0.8 mm radius at the underside of the bolt head was used in accordance with ISO 4032 (Figure 5.1-6).

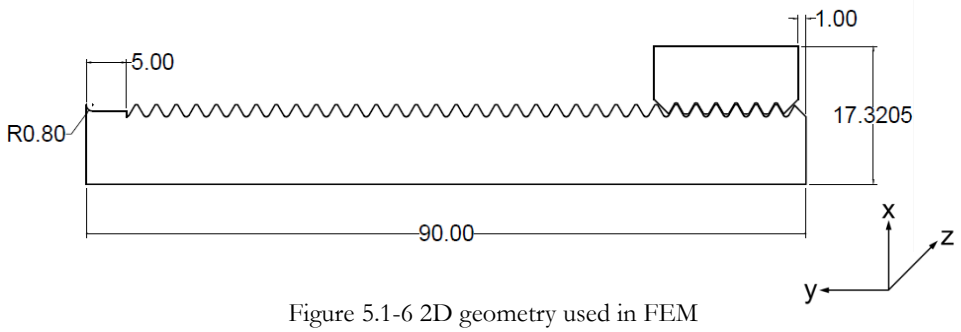

Figure 5.1-6 2D geometry used in FEM

An analytically rigid plate was used to apply a displacement force to the top surface of the nut to allow for nut dilation. This was 10 x 10 mm, and positioned 10 mm from the bolt axis, just beyond the bolt threads, and 19 mm from the bottom of the bolt shank.

5.1.2 Material Properties

The plastic properties of the bolt were based on the results of uniaxial tensile testing of the turned-down bolts, while those of the nut were based on the nominal yield and ultimate tensile strengths of a Property Class 10 nut, strength reduction factors and the shape of the flow curve described in EN 1993-1-2 for the mechanical properties of carbon steels. Non-plastic material properties were the same for both the nut and bolt, and were based on the properties described in EN 1993-1-2.

The units used throughout the model were N, g, mm, MPa, tonne/mm^3, K unless specified otherwise.

5.1.2.1 Non-Plastic Properties

Density

Density is considered to be independent of temperature with a value of 7850 kg/m^3 [8] = 7.85 x10^{-9} tonne/mm^3.

Elastic

Elastic modulus has been calculated using the modulus reduction factor, $k_{E,\theta}$, from Table 3.1, EN 1993-1-2 and the ambient-temperature Young's modulus of 210,000 MPa as specified in EN 1993-1-1 [94] (Table 5.1-2). Poisson's ratio = 0.3, and was assumed to be independent of temperature [94].

Table 5.1-2 Elastic properties input to Abaqus

$k_{E,\theta}$ [8]	Young's Modulus (N/mm^2)	Poisson's Ratio	Temp (K)
1.00	210000	0.3	294
1.00	210000	0.3	374
0.90	189000	0.3	474
0.80	168000	0.3	574
0.70	147000	0.3	674
0.60	126000	0.3	774
0.31	65100	0.3	874
0.13	27300	0.3	974

Thermal Elongation

Thermal expansion has been calculated using the following equation (Table 5.1-3) [8] (where θ_a = steel temperature and 20< θ_a <750°C):

$$\frac{\Delta l}{l} = 1.2x10^{-5}\theta_a + 0.4x10^{-8}{\theta_a}^2 - 2.416x10^{-4}$$

Table 5.1-3 Expansion properties input to Abaqus

Elongation ($\frac{\Delta l}{l}$)	Temp (K)
0.000	294
0.001	374
0.002	474
0.004	574
0.005	674
0.007	774
0.008	874
0.010	974

Specific heat and Conductivity

Specific heat and conductivity have been omitted, because uniform temperature has been assumed in the model.

5.1.2.2 Plastic Properties

Nut

The nut material properties were based on a nominal stress at 0.2% non-proportional elongation (proof stress at 0.2 % strain) of 900 MPa and tensile strength of 1000 MPa [11]. The shape of the flow curves followed that described for the mechanical properties of carbon steels in EN 1993-1-2 (Figure 5.1-7).

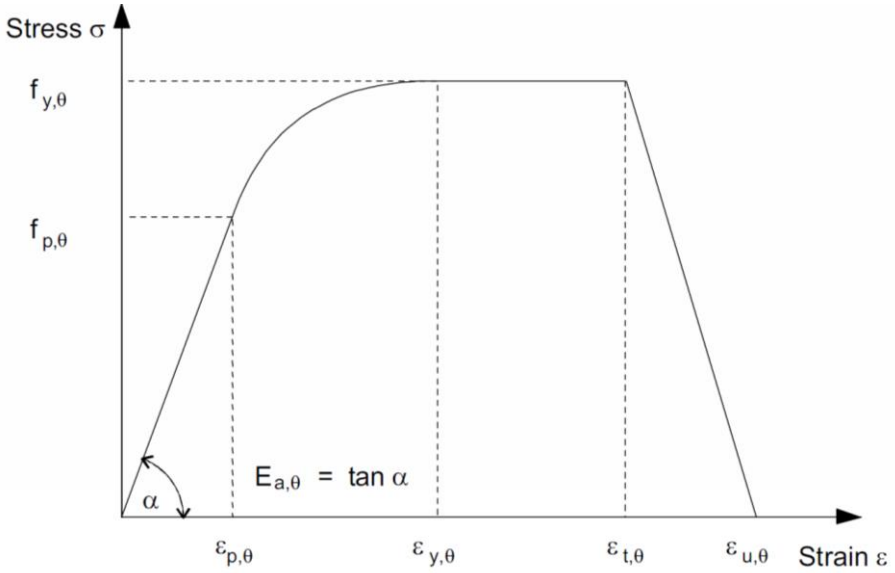

Figure 5.1-7 Stress-strain relationship for carbon steel at elevated temperatures (Copied from EN 1993-1-2) [95]

Using this information, and a Young's modulus, E_a, of 210,000 MPa [8] the following equations were used to calculate stress within certain ranges of strain (Table 5.1-4).

Table 5.1-4 Stress calculations at different strain ranges [8]

Strain range	Stress
$\varepsilon \leq \varepsilon_{p,\theta}$	$\sigma = \varepsilon . E_{a,\theta}$
$\varepsilon_{p,\theta} < \varepsilon < \varepsilon_{y,\theta}$	$\sigma = f_{p,\theta} - c + \left(\frac{b}{a}\right)\left[a^2 - \left(\varepsilon_{y,\theta} - \varepsilon\right)^2\right]^{0.5}$
$\varepsilon_{y,\theta} < \varepsilon \leq \varepsilon_{t,\theta}$	$\sigma = f_{y,\theta}$
$\varepsilon = \varepsilon_{u,\theta}$	$\sigma = 0$

Where: $\varepsilon_{p,\theta} = \frac{f_{p,\theta}}{E_{a,\theta}}$, $\varepsilon_{y,\theta} = 0.02$, $\varepsilon_{t,\theta} = 0.15$ and $\varepsilon_{u,\theta} = 0.20$

and:

$$a^2 = \left(\varepsilon_{y,\theta} - \varepsilon_{p,\theta}\right)\left(\varepsilon_{y,\theta} - \varepsilon_{p,\theta} + \frac{c}{E_{a,\theta}}\right)$$

$$b^2 = c\left(\varepsilon_{y,\theta} - \varepsilon_{p,\theta}\right)E_{a,\theta} + c^2$$

$$c = \frac{\left(f_{y,\theta} - f_{p,\theta}\right)^2}{\left(\varepsilon_{y,\theta} - \varepsilon_{p,\theta}\right)E_{a,\theta} - 2\left(f_{y,\theta} - f_{p,\theta}\right)}$$

Reduction factors $k_{y,\theta}$ and $k_{p,\theta}$ are given in Table 3.1 of EN 1993-1-2, and multiply f_y and f_p to give the elevated-temperature properties $f_{y,\theta}$ and $f_{p,\theta}$. A different strength reduction factor $k_{b,\theta}$, is given for bolts in Table D1, EN 1993-1-2. Comparing these strength reduction factors (Figure 5.1-8) it is clear that $k_{b,\theta}$ gives lower elevated-temperature tensile strength values than using $k_{y,\theta}$. It was decided, therefore, that $k_{b,\theta}$ would be used for all plastic strength values for consistency and to produce conservative values. Because a separate modulus reduction factor for bolts is not given for the elastic range, Young's modulus at elevated temperatures was still calculated using $k_{E,\theta}$ rather than $k_{b,\theta}$.

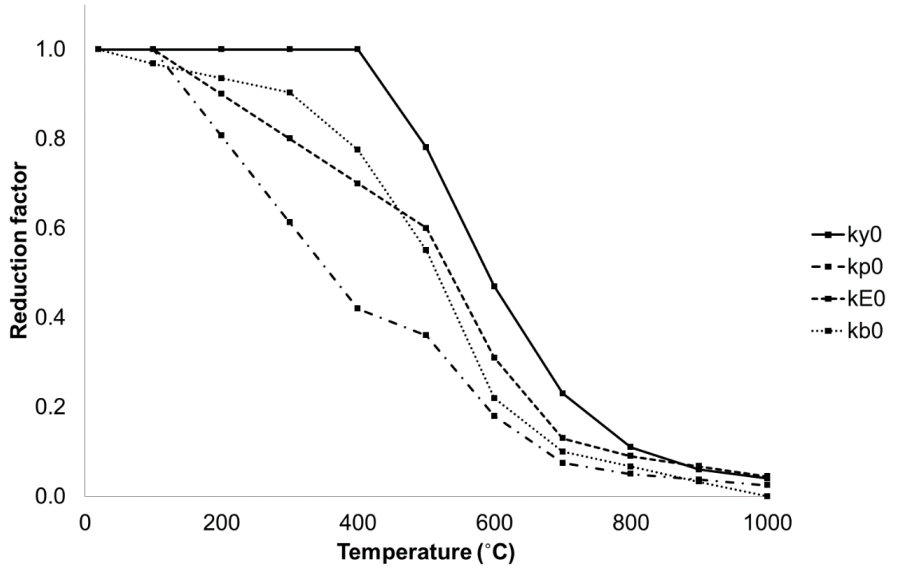

Figure 5.1-8 Strength reduction factors prescribed in EN 1993-1-2 for carbon steel ($k_{y,\theta}$, $k_{p,\theta}$ and $k_{E,\theta}$) and bolts ($k_{b,\theta}$)

Values of stress have been plotted at ε=0, $\varepsilon_{p,\theta}$, 0.005, 0.01, 0.015, $\varepsilon_{y,\theta}$, $\varepsilon_{t,\theta}$ and $\varepsilon_{u,\theta}$ in order to include a number of points within the work-hardening curve at $\varepsilon_{p,\theta} < \varepsilon < \varepsilon_{y,\theta}$. The calculated curves can be seen in Figure 5.1-9. Since the calculations provided in EN 1993-1-2 do not include a strain-rate parameter the material properties of the nut part are temperature-dependent but not strain-rate-dependent.

The calculated plastic properties are given in Table 5.1-5 for property Class 10 nuts using reduction factor $k_{b,\theta}$. Plastic strain (ε_{pl}) is equal to (total mechanical strain - strain at the proportional limit). Since Abaqus will not accept a stress value of zero, a value of 1.0 has been input at total strain.

Table 5.1-5 Plastic nut properties input to Abaqus using Eurocode 3 stress calculations and strength reduction factors $k_{b,\theta}$ and $k_{E,\theta}$

294K		374K		474K		574K	
σ (MPa)	εpl	σ (MPa)	εpl	σ (MPa)	εpl	σ (MPa)	εpl
900	0.000	871	0.000	842	0.000	813	0.000
928	0.001	901	0.001	864	0.001	823	0.000
976	0.006	946	0.006	912	0.006	880	0.005
995	0.011	963	0.011	930	0.011	898	0.010
1000	0.016	968	0.016	935	0.016	903	0.015
1000	0.146	968	0.146	935	0.146	903	0.145
1	0.196	1	0.196	1	0.196	1	0.195

674K		774K		874K		974K	
σ (MPa)	εpl	σ (MPa)	εpl	σ (MPa)	εpl	σ (MPa)	εpl
698	0.000	495	0.000	198	0.000	90	0.000
710	0.000	514	0.001	208	0.002	94	0.002
755	0.005	538	0.006	216	0.007	98	0.007
771	0.010	547	0.011	219	0.012	100	0.012
775	0.015	550	0.016	220	0.017	100	0.017
775	0.145	550	0.146	220	0.147	100	0.147
1	0.195	1	0.196	1	0.197	1	0.197

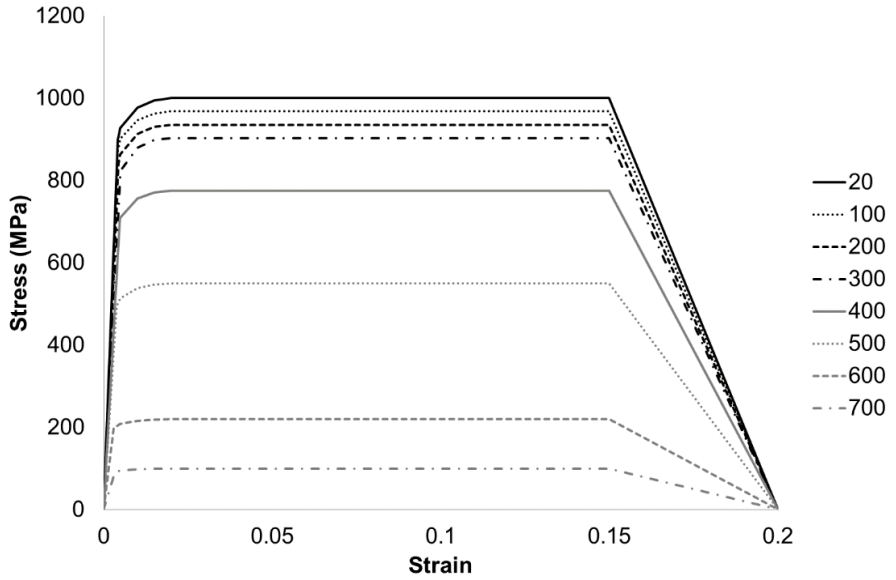

Figure 5.1-9 Calculated stress-strain curves over a range of temperatures using strength reduction factors $k_{b,\theta}$ and $k_{E,\theta}$

Bolt

The plastic behaviour of the bolt part was determined from the results of uniaxial tensile testing carried out on turned-down bolts. The elastic portions of each graph prior to the 0.2% proof stresses provided in Table 3.7-3 were removed, and plastic stress plotted. The yield plateaux observed at ambient temperature were removed, and the average of all three strain-rates was used to describe the strain-rate-independent behaviour at ambient temperature. These averages and the elevated-temperature curves for each strain-rate were then simplified so that approximately 8-10 points were plotted per curve and input to Abaqus as tabular data. The temperature-dependent plastic material properties input to Abaqus are shown in Table 5.1-6 to Table 5.1-8.

Table 5.1-6 Plastic bolt properties input to Abaqus for 0.02 min^{-1} strain-rate

294K		824K		894K		974K	
σ (MPa)	ε pl	σ (MPa)	ε pl	σ (MPa)	ε pl	σ (MPa)	ε pl
638	0.000	219	0.000	126	0.000	66	0.000
638	0.006	235	0.004	137	0.010	72	0.014
790	0.026	240	0.010	142	0.028	73	0.049
874	0.050	244	0.019	139	0.072	73	0.129
910	0.073	240	0.040	124	0.180	61	0.294
930	0.098	217	0.087	98	0.250	49	0.372
917	0.136	169	0.149	71	0.306	31	0.422
840	0.181	128	0.184	44	0.343		
720	0.220	72	0.227				

Table 5.1-7 Plastic bolt properties input to Abaqus for 0.01 min^{-1} strain-rate

294K		824K		894K		974K	
σ (MPa)	ε pl	σ (MPa)	ε pl	σ (MPa)	ε pl	σ (MPa)	ε pl
638	0.000	183	0.000	98	0.000	48	0.000
638	0.006	203	0.008	112	0.013	56	0.023
790	0.026	212	0.027	118	0.040	59	0.056
874	0.050	213	0.043	117	0.094	58	0.098
910	0.073	187	0.157	100	0.257	51	0.300
930	0.098	132	0.246	79	0.358	44	0.448
917	0.136	72	0.311	57	0.414	34	0.547
840	0.181						
720	0.220						

Table 5.1-8 Plastic bolt properties input to Abaqus for 0.002 min^{-1} strain-rate

294K		824K		894K		974K	
σ (MPa)	ε pl	σ (MPa)	ε pl	σ (MPa)	ε pl	σ (MPa)	ε pl
638	0.000	143	0.000	83	0.000	36	0.000
638	0.006	156	0.019	92	0.010	40	0.014
790	0.026	157	0.042	95	0.027	40	0.046
874	0.050	147	0.197	94	0.066	38	0.168
910	0.073	124	0.312	89	0.191	36	0.307
930	0.098	90	0.400	80	0.326	31	0.398
917	0.136			63	0.434		
840	0.181						
720	0.220						

Although the flow behaviour of bolt material is both temperature- and strain-rate-dependent it was decided that each strain-rate would be treated independently. Using temperature- but not strain-rate-dependent material properties avoids overcomplicating the model by allowing force to be applied to the plate via a displacement rather than a velocity. Since the strain-rate dependence of the material had already been investigated in mechanical testing it was decided that three strain-rates would be sufficient for this study.

5.1.3 Interactions

Interactions between nut and bolt threads and the plate and top surface of the nut were specified. The interaction properties were the same for both interactions and included a 0.2 friction coefficient, “Hard” contact over-closure, and separation was allowed after contact.

5.1.4 Constraints

A reference point was placed on the top surface of the analytically rigid plate. This was constrained to the plate using a rigid-body constraint, allowing both temperature and displacement to be applied. “History output requests” were assigned to a set created for this reference point and the forces and displacements generated were used to create force-displacement curves.

5.1.5 Boundary Conditions

The boundary conditions differed, depending on whether the model was 3D or axisymmetric due to the different global co-ordinate systems used.

5.1.5.1 3D model

- X-symmetry was applied to all surfaces in the Z-plane,

- Z-symmetry applied to all surfaces in the X-plane,
- All degrees of freedom on the top surface of the bolt were restrained,
- Displacement was applied to the reference point assigned to the rigid plate.
    - In Step 1 all degrees of freedom are restrained except for U2 which was left unchecked,
    - In Step 2, at which displacement was applied, tabular amplitude was applied to U2. Since plastic data exists for each strain-rate separately this was applied as a displacement rather than a velocity, and remained the same for each simulation. The table simply stated that at step 0, displacement = 0 (mm) and at step 2000, amplitude = 15 (mm)

5.1.5.2 Axisymmetric Model

- X-symmetry was applied to the bolt axis
    - In Step 1 all degrees of freedom were restrained, except for U2 which was left unchecked,
- All degrees of freedom on the top surface of the bolt were restrained,
- In Step 2, at which displacement was applied, tabular amplitude was applied to U2. This tabular data was the same as for the 3D model.

5.1.6 Predefined fields

Constant temperatures were applied to the parts as predefined temperature fields. The temperature field for the plate was applied to the reference point.

5.1.7 Verification of whether axisymmetric model accurately represents 3D behaviour

Computing times can be significantly reduced by using an axisymmetric model rather than a full 3D model. It was decided that a simple comparison between the results of a 3D and an axisymmetric model, using the same mesh size and type and material properties, would be carried out. The chosen temperature was 550˚C and the material properties for the 0.02 min^{-1} strain-rate were used. A relatively coarse global mesh size of 2 was used with a hex-dominated mesh for the 3D model and quad-dominated mesh type for the axisymmetric model. Both of these had identical mesh arrangements when the 3D model was viewed in the Y-Z plane.

Since the axisymmetric model represents a very thin slice of a 3D shape, the forces calculated should represent those experienced by the full 3D shape. The 3D model, however, is one quarter of the whole 3D shape and the resultant forces were therefore multiplied by four. Plotting the force-displacement curves for the two model types shows that both models give very similar values up to UTS (Figure 5.1-10). Beyond this point the two curves begin to diverge. However, without damage or failure criteria included in the FEM, this portion of the graph does not accurately reflect the flow behaviour of a bolt assembly during heavy plastic deformation. Due to the close correlation of results from the axisymmetric and 3D models it was decided that axisymmetric models would therefore be used for all subsequent FEM work.

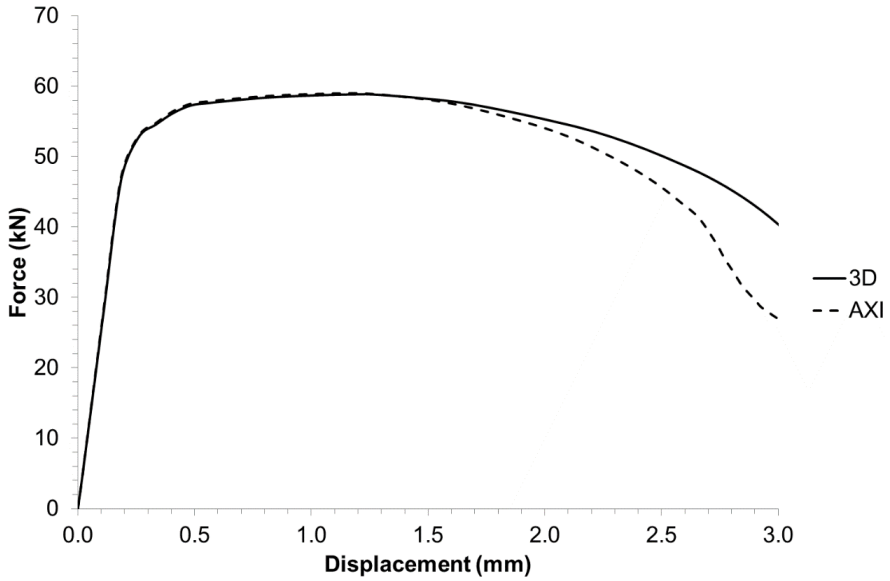

Figure 5.1-10 A comparison between the force-displacement results of an axisymmetric and 3D model

5.1.8 Mesh

A suitable mesh type and size was determined via a mesh sensitivity study carried out on an axisymmetric model with 6AZ6g thread profile and 6AZ6g + 0.5 mm clearance. This was to ensure that both necking and thread-stripping failures should happen. The same material properties were used as for the axisymmetric-3D model comparison.

For the 6AZ6g + 0.5 mm thread profile it was found that a quad-dominant element shape caused necking failure for a uniform global mesh size of 2, but for a global mesh size of 2 and a local mesh size of 0.3 at the interacting threads thread-stripping was observed. Both simulations aborted with errors when using the same two mesh sizes with a tri (triangular) element shape. It was decided that the rest of the study into the most suitable mesh would centre on a quad-dominated (square) element type.

The following global mesh sizes were considered; 0.1, 0.2, 0.3, 0.4, 0.5, 0.6, 0.7, 0.8 for both the 6AZ6g and 6AZ6g + 0.5 mm thread profiles.

For the 6AZ6g + 0.5 mm thread profile, both the 0.1 and 0.2 global sizes aborted just after the onset of thread-stripping, 0.3-0.6 all completed and failed due to thread-stripping, however, the failure mode transformed from thread-stripping to necking at 0.7 and 0.8 global sizes at very similar values of ultimate load capacity. The correlation between mesh size and ultimate load capacity shows a general trend for larger mesh sizes to produce a higher force (Figure 5.1-11).

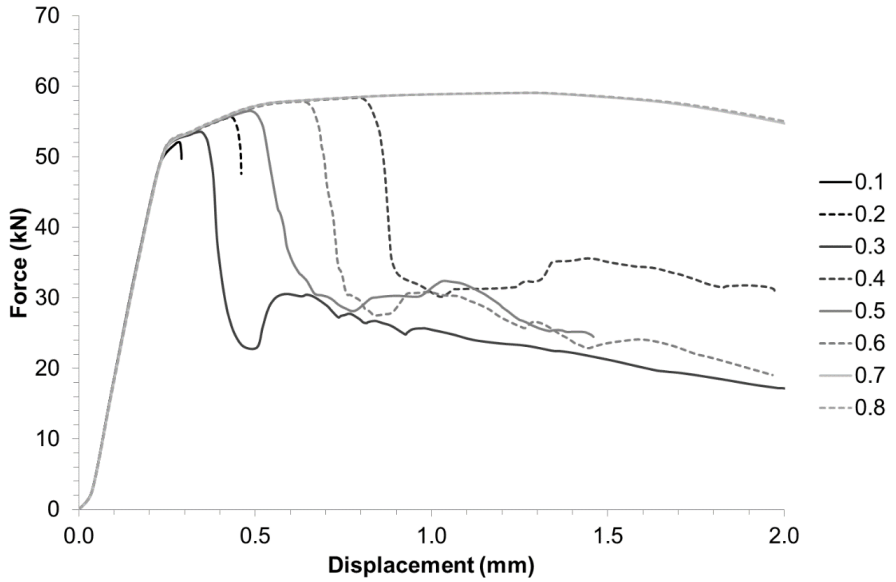

Figure 5.1-11 Force-displacement curves for different global mesh sizes using a quad-dominated element type for thread profile 6AZ6g + 0.5 mm

For the 6AZ6g thread profile all simulations completed with necking failures. Although the simulations using a mesh size of 0.1 and 0.2 completed, they did produce a slight drop in ultimate load capacity. For mesh sizes greater than 0.3, the ultimate tensile force began to converge (Figure 5.1-12).

Since 0.3 was the finest possible mesh size which produced thread-stripping failure without causing the simulation to abort, when using a 6AZ6g + 0.5 mm combination, it was decided that this should produce the most accurate results. At this mesh size von Mises stress contours were smooth-shaped and transferred

smoothly from one thread set to the next (Figure 5.1-13 (a)) rather than following the mesh edges, as was the case for coarser meshes.

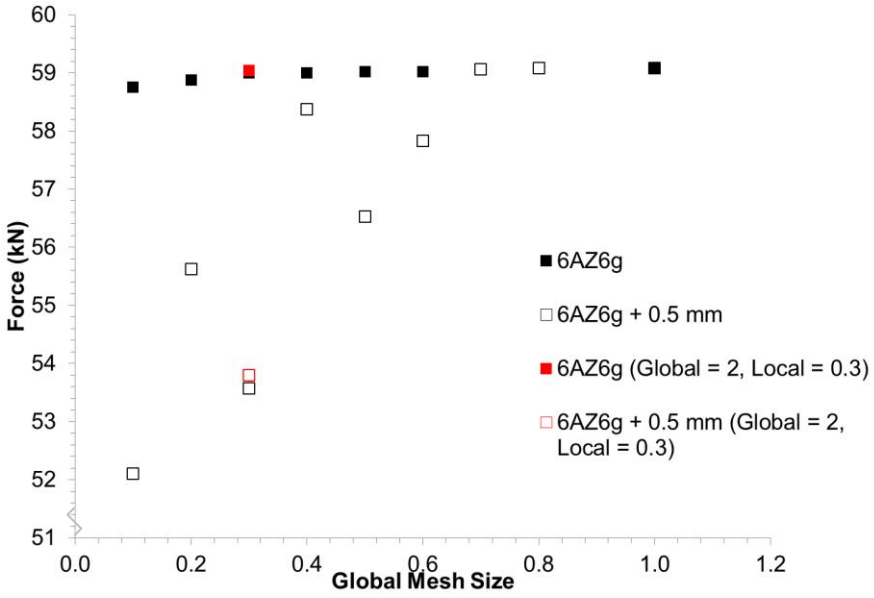

Figure 5.1-12 A comparison between global mesh size and ultimate load capacity for 6AZ6g and 6AZ6g + 0.5 mm thread profiles

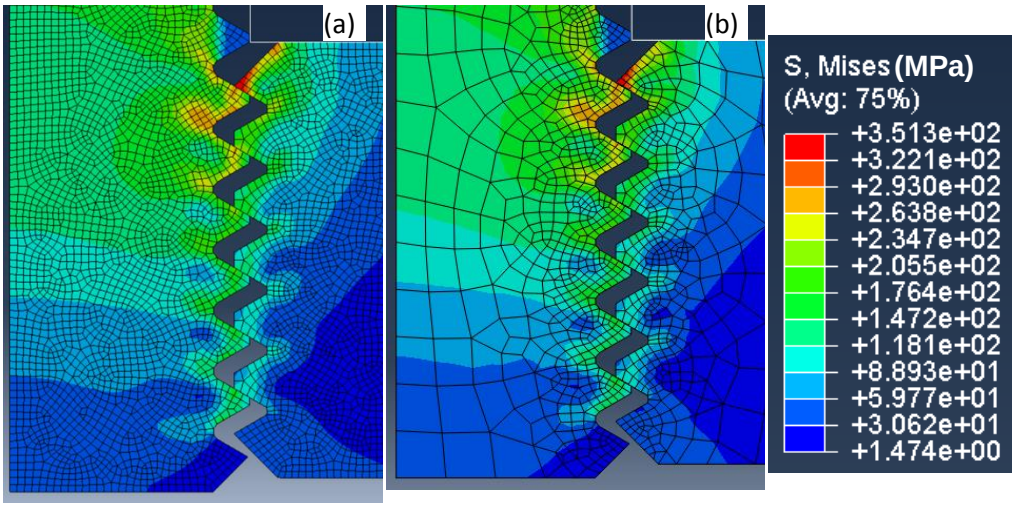

Figure 5.1-13 The smooth von Mises contours observed for (a) a global mesh size of 0.3 and (b) global mesh size of 2 and local mesh of size 0.3 at interacting threads, with a thread profile of 6AZ6g + 0.5 mm at step 25

Since a mesh size of 0.3 is quite fine and leads to a relatively long computational time, one additional mesh size was considered which used a global mesh size of 2 together with local edge seeds at the interacting threads of 0.3 mm, the area of highest deformation during thread-stripping failures. The results can be seen in

Figure 5.1-12 to be similar to those from the global mesh size of 0.3, and similar smooth von Mises contours were observed (Figure 5.1-13(b)). This mesh was therefore chosen for this study.

5.2 Validation of the model

Before carrying out a study into the effect of various variables on failure mode and ultimate tensile capacity, the model was firstly validated against the results of uniaxial tensile tests carried out on bolt assemblies. Although an average clearance value has been calculated for three assemblies to be 6AZ6g + 0.066 mm, clearance is one of the variables that has been investigated further in FEM, and therefore the generic geometry of 6AZ6g + 0.5 mm has been chosen for this study, as it is known from the mesh size investigation to produce the correct failure mode.

Using a thread clearance of 6AZ6g + 0.5 mm produced thread-stripping failures with very similar ultimate load capacities to those obtained in uniaxial testing (Figure 5.2-1). The unrealistically large clearance, however, caused premature failure at small values of displacement.

At 20˚C the FEM failed through thread-stripping, due to the large thread clearance However, the shape of the force-displacement curve closely follows those obtained for bolt assemblies containing a pearlite microstructure (on which the input material properties at this temperature are based) (Figure 5.2-1(a)). The results of simulations carried out using material data obtained at 0.02 min^{-1} have also been plotted for simulations carried out at 550˚C and 700˚C and the shapes of the curves can be seen to follow closely the results obtained through mechanical testing (Figure 5.2-1(b-c)).

The failure modes (Table 5.2-1) and resultant load capacities (Table 5.2-2) show that the simulation carried out at 700˚C using material data obtained at 0.002 min^{-1} produced a necking failure mode and a higher ultimate load capacity than expected.

For tighter tolerances it is likely that further elongation of the bolt shank would occur prior to thread-stripping. Therefore the ultimate load capacities are likely to be lower than would be expected from tighter thread tolerances. A comparison of the maximum loads obtained from FEM and mechanical testing shows that results obtained through FEM, which produced the correct mode of failure are within +/- 15% of the values obtained through mechanical testing, despite the large clearance used in the FEM.

Table 5.2-1 Failure modes of FEM simulations carried out at a range of temperatures and strain-rates using a thread profile of 6AZ6g + 0.5 mm

	Failure mode		
	0.02	0.01	0.002
20	strip	strip	strip
550	strip	strip	strip
700	strip	strip	neck

Table 5.2-2 Ultimate load capacities obtained through FEM using a thread profile of 6AZ6g + 0.5 mm and mechanical testing at a range of temperatures and strain-rates

T (˚C)	Ultimate Tensile Force (kN)					
	FEM			Experimental Avg.		
	0.02	0.01	0.002	0.02	0.01	0.002
20	192.26	192.26	192.26	209.52	209.52	209.52
550	53.79	47.81	36.45	63.05	53.39	37.55
700	17.43	13.72	9.68	18.55	14.24	8.07

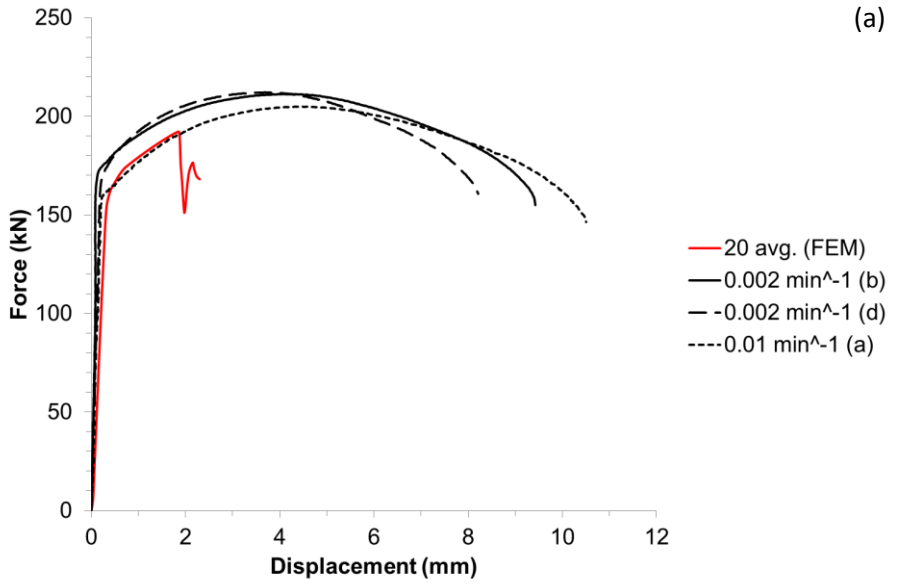
(a)
250
200
150
100
50
0
Force (kN)
0
2
4
6
8
10
12
Displacement (mm)
20 avg. (FEM)
0.002 min^-1 (b)
-0.002 min^-1 (d)
0.01 min^-1 (a)

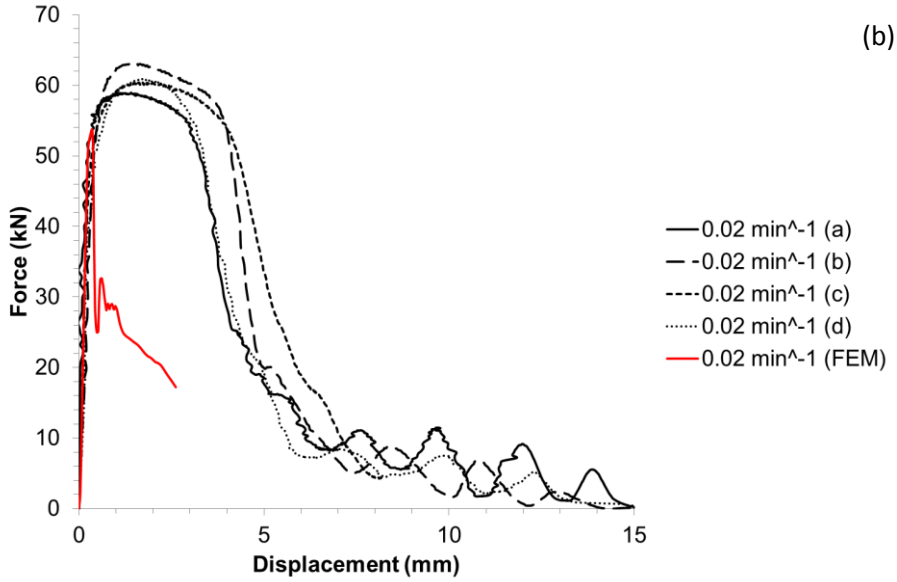
(b)
70
60
50
40
30
20
10
0
Force (kN)
0
5
10
15
Displacement (mm)
0.02 min^-1 (a)
-0.02 min^-1 (b)
0.02 min^-1 (c)
0.02 min^-1 (d)
0.02 min^-1 (FEM)

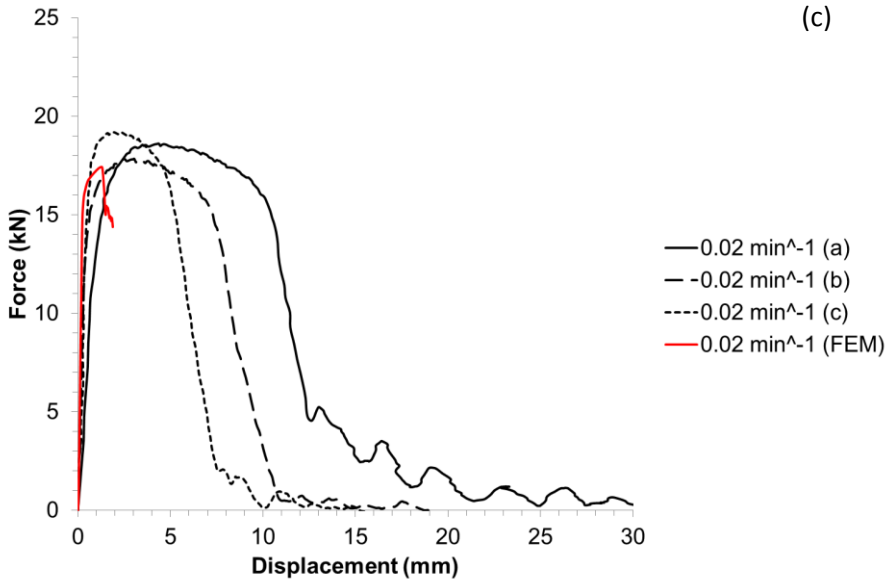

Figure 5.2-1 Results of FEM for (a) 20, and at 0.02 min^{-1} for (b) 550 and (c) 700°C with a thread profile of 6AZ6g + 0.5 mm

This study has shown that the force-displacement curves obtained through FEM closely match those obtained in mechanical testing, validating the model and showing it to be suitable to be carried forward to study variables which cannot be validated against mechanical test data.

5.3 Study of the effects of different variables on failure mode and strength

Three variables formed the basis of this study;

1. The number of bolt threads exposed beyond the bottom face of the nut:

   The British Standard for suitability testing of non-preloaded structural bolting assemblies, EN 15048-2 [7], states that *"The end of the bolt shall protrude not more than one pitch (1 P) beyond the unloaded face of the nut"*, however, no explanation is given as to why this is recommended. If the number of bolt threads protruding beyond the bottom face of the nut is significant, many different shank lengths must be specified, dependent on the thicknesses of the

members being connected. Difficulties may arise on site if contractors are asked to use many bolts of the same diameter but differing shank lengths.

2. Nut height:

   Nut height is a factor in the calculation of thread engagement length in Alexander's analytical model, and contributes to bolt and nut thread-stripping strength [44].

3. Thread clearance:

   Kirby concluded that "...a practical solution to improving the integrity of threads. This may be achieved by specifying the nut and bolt dimensional properties to the tighter tolerance classes of BS3692 (i.e. 6H6g)". This is the thread tolerance class combination equivalent to 6AZ6g for uncoated bolt assemblies. Alexander's analytical model also includes the internal and external major and minor diameters, in order to take into account the influence of clearance on the tensile stress area and the shear areas of the internal and external threads [44].

5.3.1 Influence of number of threads below nut

The original geometry assumed that one thread was partially visible below the face of the nut (Figure 5.1-6). Keeping the bolt length constant at 90 mm and moving the nut part in the y-direction by one pitch (2.5 mm) meant that two, and for 5 mm three, threads were partially visible. These analyses were again run with; a quad-dominated mesh of global size 2 and local size 0.3 at the intersecting threads, a temperature of 550˚C˚C, and using the material properties associated with a strain-rate of 0.02 min^{-1} and a thread clearance of 6AZ6g + 0.5 mm. The resultant force-displacement behaviour show that the number of threads exposed below the unloaded nut face has negligible effect on thread-stripping behaviour (Figure 5.3-1). The effect of the position of the nut on the bolt shank is therefore negligible.

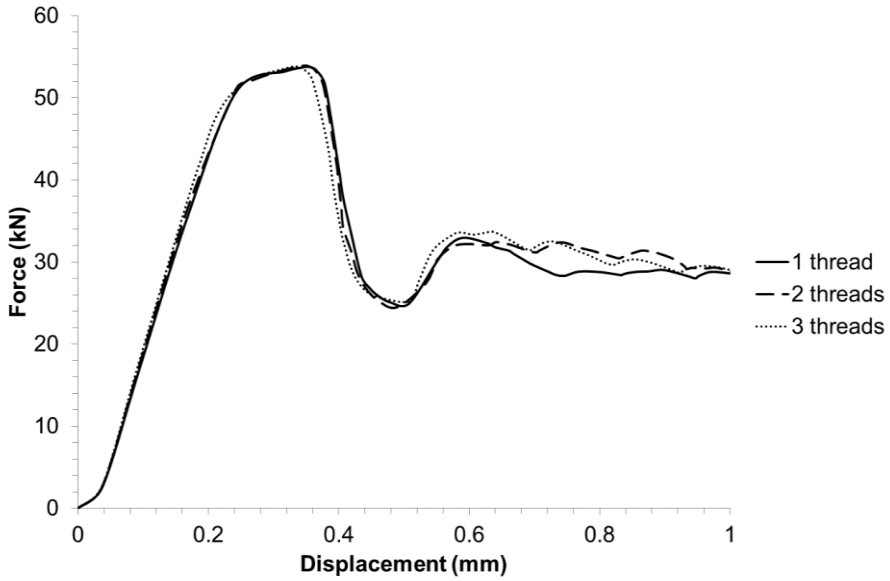

Figure 5.3-1 Force-displacement curves for bolt assemblies with one, two and three threads visible underneath the unloaded nut face, keeping bolt length 90 mm using a 6AZ6g + 0.5 mm clearance at 550˚C and using material data obtained at 0.02 min^{-1}

5.3.2 Influence of nut height

Using the same material properties and a clearance combination of 6AZ6g + 0.5 mm, three different nut heights were considered at three temperatures; 20˚C, 550˚C and 700˚C˚C. These nut heights consisted of; a nominal nut height of 18 mm, containing five full threads, 18 mm + 1P (Where P = thread pitch = 2.5 mm), and 18 mm – 1P. Increasing the nut height from 18mm to 20.5 mm caused the failure mode to change from thread-stripping to necking failure, which occurred at a higher ultimate tensile force (Figure 5.3-2 (a-c)). Nut heights of 18 mm and 15.5 mm both caused thread-stripping failures at all temperatures, and the minimum nut height investigated caused failure at a lower tensile force and displacement.

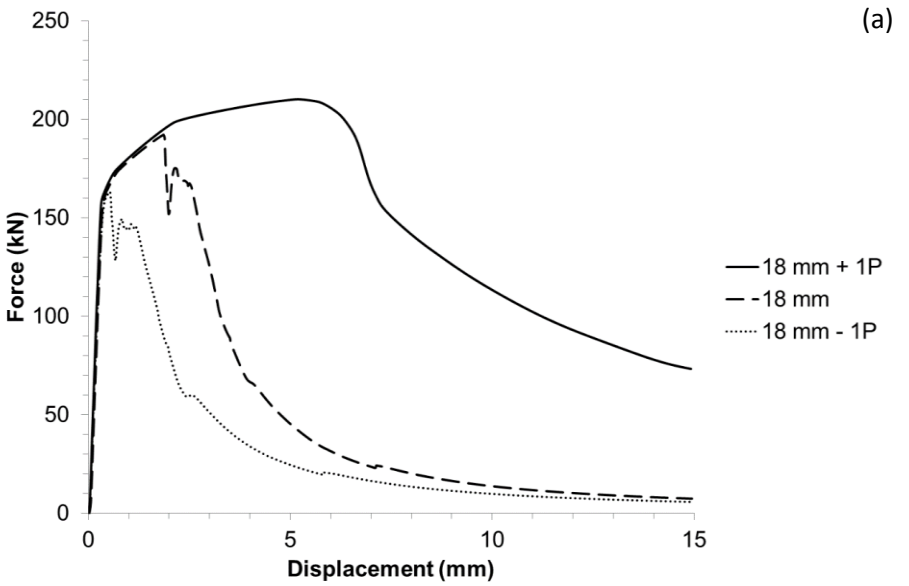
(a)
250
200
150
100
50
0
Force (kN)
0
5
10
15
Displacement (mm)
18 mm + 1P
18 mm
18 mm - 1P

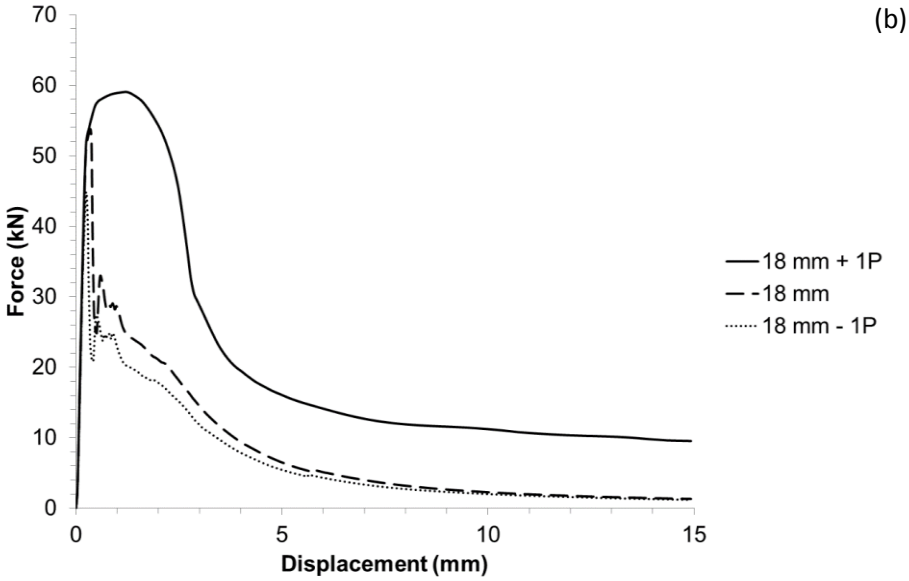
(b)
70
60
50
40
30
20
10
0
Force (kN)
0
5
10
15
Displacement (mm)
18 mm + 1P
18 mm
18 mm - 1P

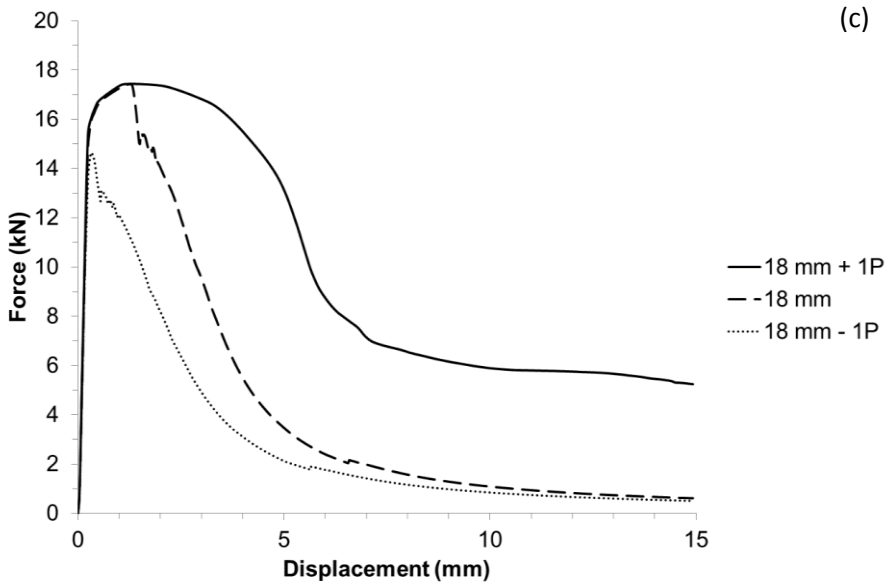

Figure 5.3-2 Force-displacement curves obtained (a) 20˚C, (b) 550˚C and (c) 700 ˚C using a clearance of 6AZ6g + 0.5 mm and nut heights of 18 mm - 1P, 18 mm, and 18 mm + 1P

The von Mises contour plots for the three different nut heights at a temperature of 700˚C˚C (Figure 5.3-3 (a-c)) show localised stresses in the nut and bolt threads during thread-stripping and in the bolt shank during necking. Despite thread-stripping failure occurring for a nut height of 18 mm, it can be seen, by comparing Figure 5.3-3(a) and (b), that higher stresses were able to build up in the bolt shank prior to thread failure than in the nut of 15.5 mm height. The deformed geometries also show that extension of the bolt shank increases with nut height, and therefore improved ductility is achieved.

The height of an M20 nut prescribed in ISO 4033 for “high nuts” recommends a maximum nut height of 20.3 mm, very similar to the maximum nut height of 20.5 mm used in this study. Specifying nuts to ISO 4033 [96] rather than ISO 4032 [73] would mean that, at elevated temperatures beyond the melting point of the thickest zinc coating layers, necking failures could be ensured despite an increased relative clearance compared with ambient temperature. For improved ductility and to

ensure necking failure, even for unrealistically large thread clearances, a taller nut specified to ISO 4033 should be used.

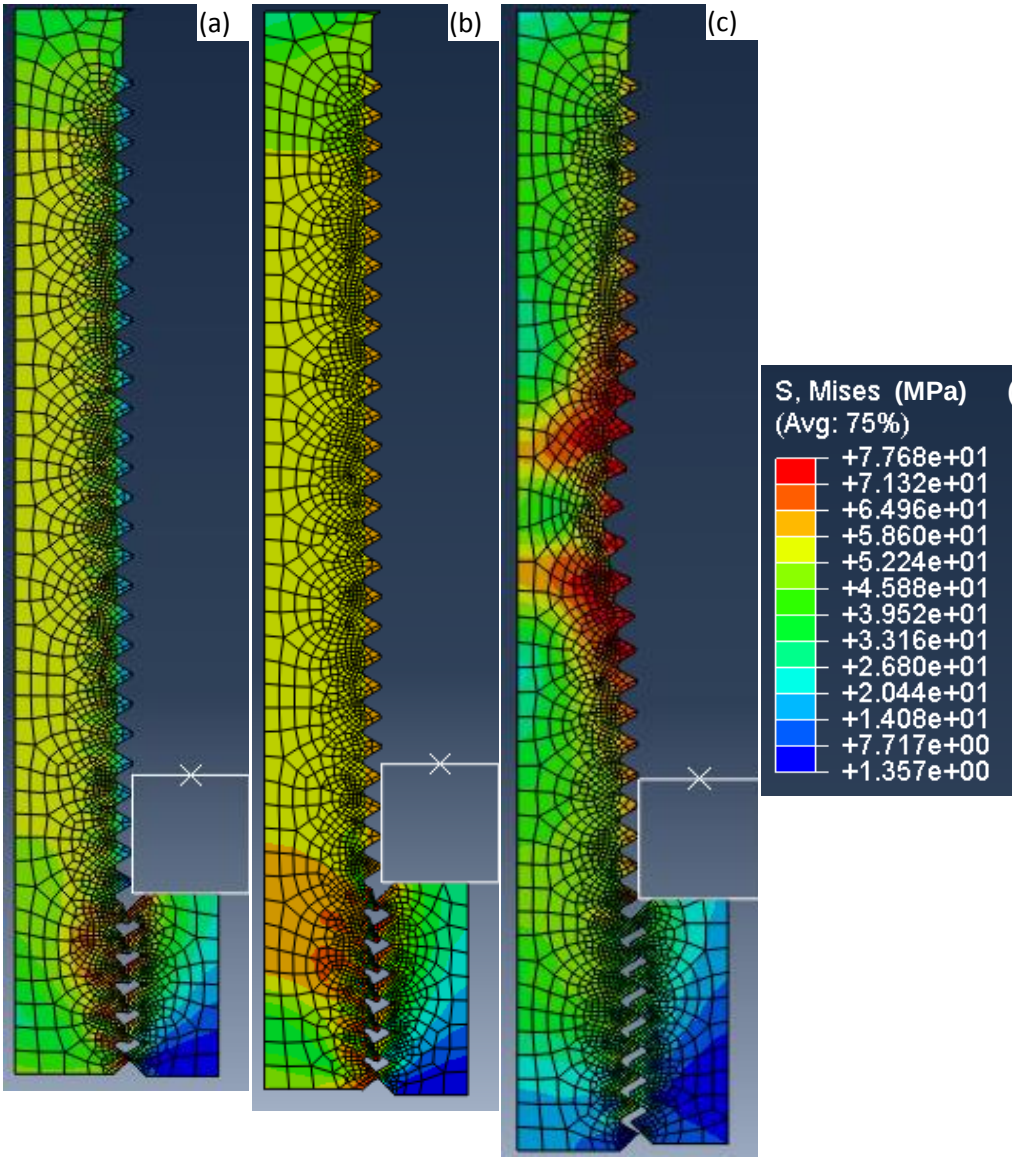

Figure 5.3-3 Von Mises contour plots obtained at 700˚C at 0.02min^{-1} using nut heights of (a) 18 mm – 1P, (b) 18 mm, (c) 18 mm + 1P

5.3.3 Influence of Thread Clearance

A nut height of 18 mm was used for this study, and every temperature and strain-rate combination used for bolt assembly testing was considered. After a process of trial and error it was found that the transition from necking to thread-stripping

failures always occurred between clearances of 6AZ6g + 0.4 mm and 6AZ6g + 0.6 mm. Increments of 0.025 and 0.05 mm were used to identify the clearance at which the failure mode changes for each temperature and strain-rate combination. The resulting critical clearances can be seen in Table 5.3-1. It appears that the transition from the ductile (necking) to brittle (thread-stripping) failure mode occurs at increasing thread clearances for decreasing strain-rates.

Table 5.3-1 Critical clearances at which failure mode transitioned from necking to thread-stripping at a range of temperatures and strain-rates

	Critical clearance (6AZ6g + x mm)		
	20°C	550°C	700°C
0.02 min^{-1}	0.425	0.45	0.5
0.01 min^{-1}	0.425	0.475	0.5
0.002 min^{-1}	0.425	0.5	0.55

Constant failure loads were observed for increasing clearance, before the onset of thread-stripping. As the clearance was increased beyond this point, the failure mode fluctuated between necking and thread-stripping failures at elevated temperatures and a strain-rate of 0.02 min^{-1} (Figure 5.3-4(b-c)) before thread-stripping occurred at gradually decreasing failure loads. With increasing clearance, the failure load begins to flatten-out at a minimum ultimate load capacity. This behaviour is most visible in the results obtained at ambient temperature (Figure 5.3-4(a)) for which strength drops from 210 kN at a thread clearance of 6AZ6g + 0.4 mm by around 20 kN before a minimum ultimate tensile force of 192 kN at a thread clearance of 6AZ6g + 0.5 mm was obtained. The ultimate tensile forces obtained in tensile testing are comparable to those obtained at 0.4 mm clearance using FEM in most cases; however, the failure mode at elevated temperatures during tensile testing was thread-stripping for all strain-rates, whereas FEM produced a combination of failure modes.

The dotted lines on the charts in Figure 5.3-4 represent the average failure loads obtained in tensile tests carried out on bolt assemblies (Figure 4.2-1). The average

values obtained in tensile testing have been represented as a line, because accurate thread clearance information is not known, and 0.066 mm is far from the clearances identified as determining the onset of thread-stripping failure in this study.

FEM has predicted necking failures, or combinations of necking and thread-stripping, at 0.4 mm clearance for all strain-rate and temperature combinations. The ductile-brittle transition clearance predicted by FEM therefore occurs at significantly larger clearances than expected on the basis of the results of mechanical testing, which identified thread-stripping failure at every temperature and strain-rate combination with a thread clearance calculated to be 0.066 mm. This clearance was measured at ambient temperature with no applied load and would increase with localised reduction in area of the bolt shank and during nut dilation under tension which explains the difference observed between measured clearance and the critical thread clearance modelled.

(a)

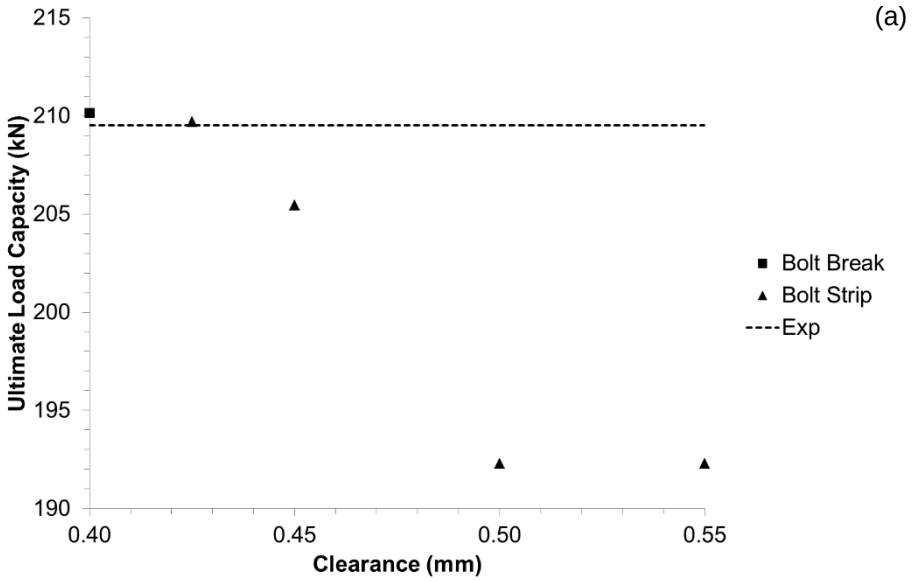

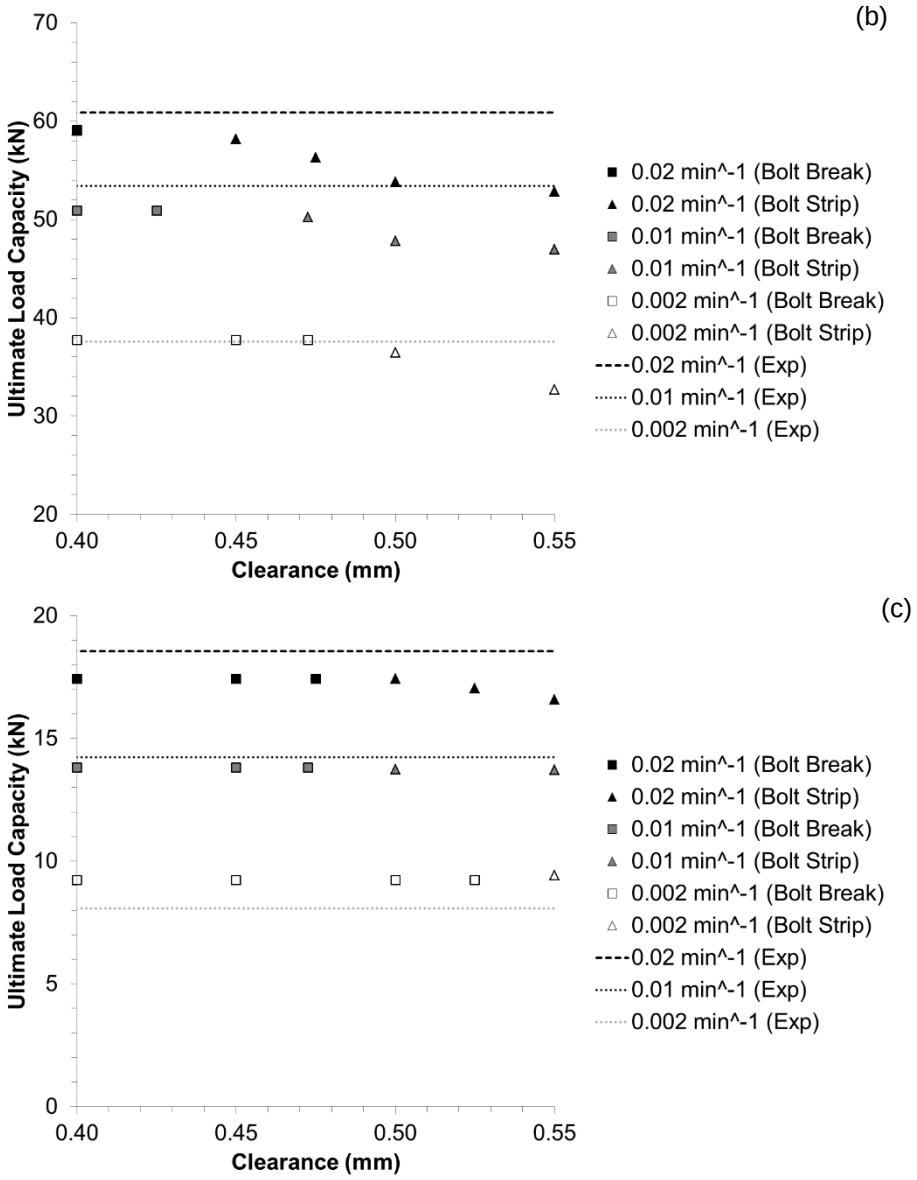

Figure 5.3-4 Ultimate load capacities obtained by FEM for a range of thread clearance values at (a) 20°C, (b) 550°C and (c) 700°C compared to the average values obtained by tensile testing of bolt assemblies.

Since the decrease in strength associated with increasing thread clearance appears to be most significant at lower temperatures it was decided that strength reduction factors would be calculated for each temperature. Each ultimate tensile force was normalised with respect to the maximum necking force obtained *at each temperature*, rather than with respect to ambient temperature in this case. At every temperature the maximum force obtained was at 0.4 mm clearance and 0.02 min^{-1}

strain-rate. The largest reduction in strength was observed at the slowest strain-rate of 0.002 min^{-1} and the highest temperature of 700°C, which produced a strength reduction factor of 0.54 for necking failures with respect to the maximum force of 17.4 kN, obtained with a clearance of 0.4 mm and strain-rate of 0.02 min^{-1} (Figure 5.3-5(c)).

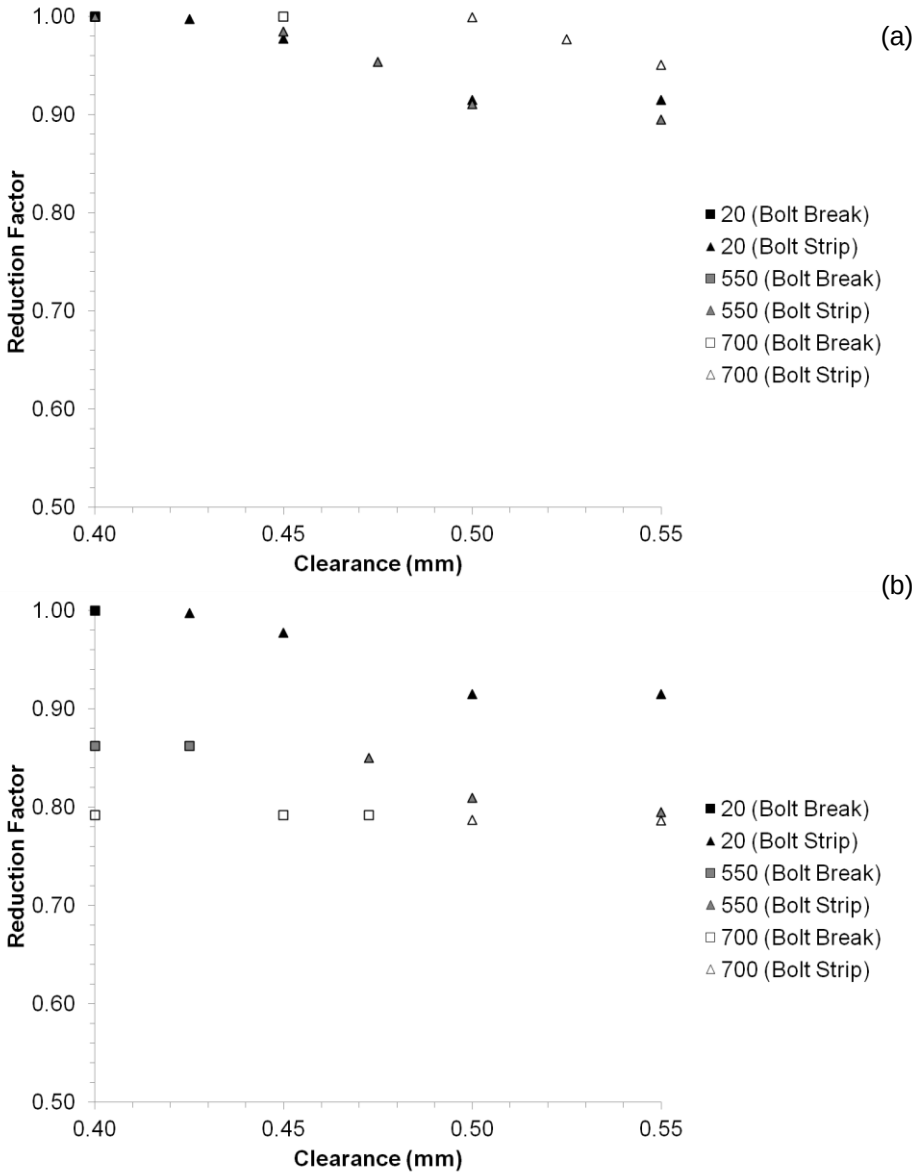

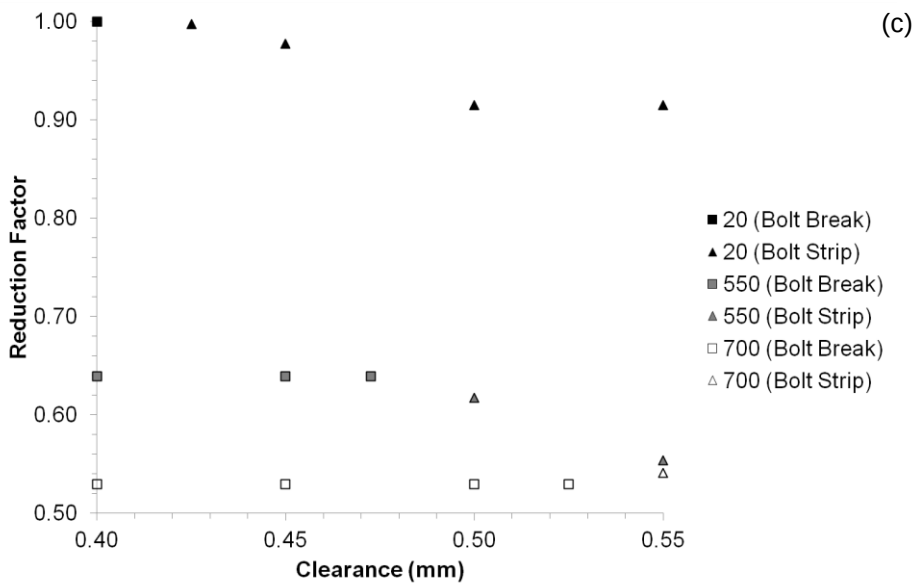

Figure 5.3-5 Strength reduction factors with respect to maximum failure load obtained at each temperature at strain-rates of (a) 0.02 min^{-1}, (b) 0.01 min^{-1} and (c) 0.002 min^{-1}.

5.3.4 Influence of Nut Height and Thread Clearance

E. M. Alexander's model [44] was used to calculate bolt breakage, nut stripping and bolt stripping loads for the FEM input properties at ambient temperature for the three nut heights considered previously in this chapter. Details of the input variables and the calculations carried out can be found in Appendix A3. One of the input variables is the geometry (length and mean diameter) of the bell-mouthed section of the nut. No bell-mouthed section has been assumed, and therefore the mean diameter, Dm, is equal to D1i, the basic minor internal diameter. The countersink height and diameter were measured from an AutoCAD drawing input to the FEM model geometry. Bolt fracture, and bolt and nut fracture, loads were calculated for thread clearances of 0-0.6 in 0.1 mm increments, for the three nut heights of 15.5, 18, and 20.5 mm. These are plotted against FEM results at 0.2 mm increments, ranging from 0-0.6 mm clearance (Figure 5.3-6). The average ultimate tensile forces of assemblies which failed via necking and thread-stripping failures were plotted at the calculated clearance of 0.066mm in red, for a nut height

of 18 mm, so that Alexander's analytical model was compared to the results of FEM and mechanical testing (Figure 5.3-6(b)).

(a)

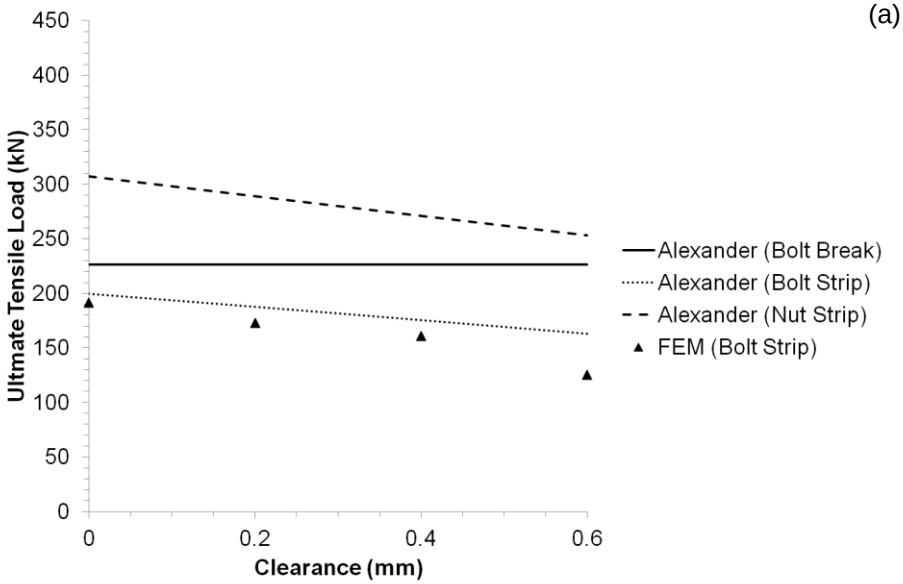

(b)

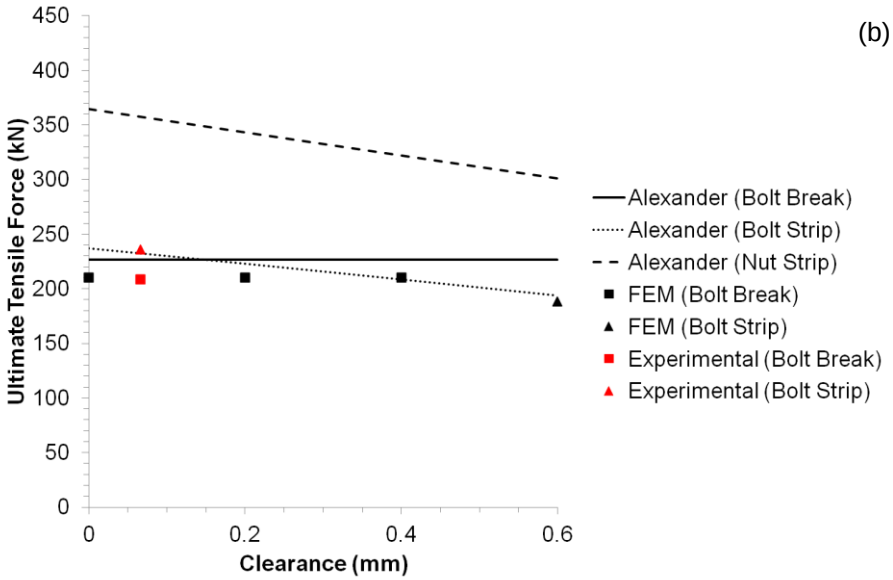

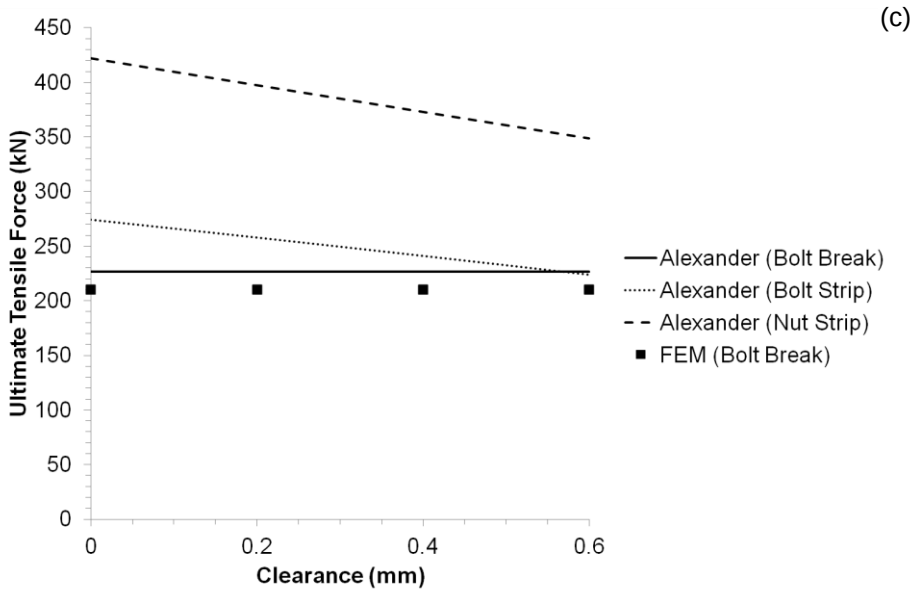

Figure 5.3-6 Calculated failure loads using Alexander's model and FEM using nut heights of (a) 15.5 mm, (b) 18mm and (c) 20.5 mm. Necking failures are shown by squares and thread-stripping failures by triangles.

It is obvious from the plotted results that Alexander's analytical model produces ultimate tensile forces and failure modes very similar to those predicted by FEM. The bolt fracture load was predicted to be 226.6 kN in the analytical model, which is slightly higher than the 210.17 kN predicted by FEM.

In order to determine whether the analytical model was also accurate for elevated temperatures and a range of strain-rates, bolt fracture, and bolt and nut thread-stripping strengths were calculated using the ultimate tensile strengths input to the FEM, at 700°C for the three strain-rates; 0.02, 0.01 and 0.002 min^{-1}. These were all calculated for a nut height of 18 mm so that the results could again be compared to the results of mechanical testing (Figure 5.3-7). The analytical model produced results very similar to FEM. However, the experimental results which showed failure due to thread-stripping did so at significantly lower clearances than were predicted by either the FEM or analytical models. Failure loads were very similar for all three methods.

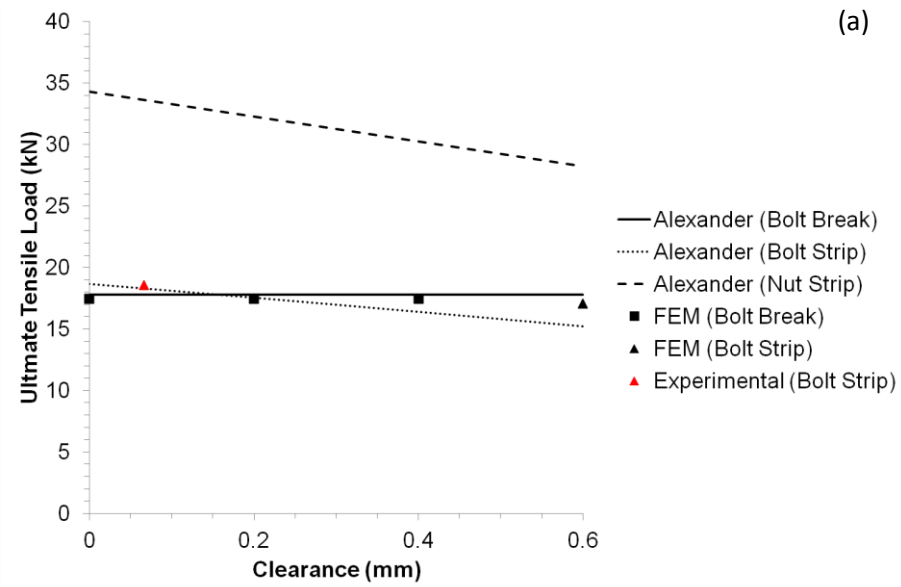
(a)
Ultmate Tensile Load (kN)
40
35
30
25
20
15
10
5
0
0
0.2
0.4
0.6
Clearance (mm)
Alexander (Bolt Break)
Alexander (Bolt Strip)
Alexander (Nut Strip)
FEM (Bolt Break)
FEM (Bolt Strip)
Experimental (Bolt Strip)

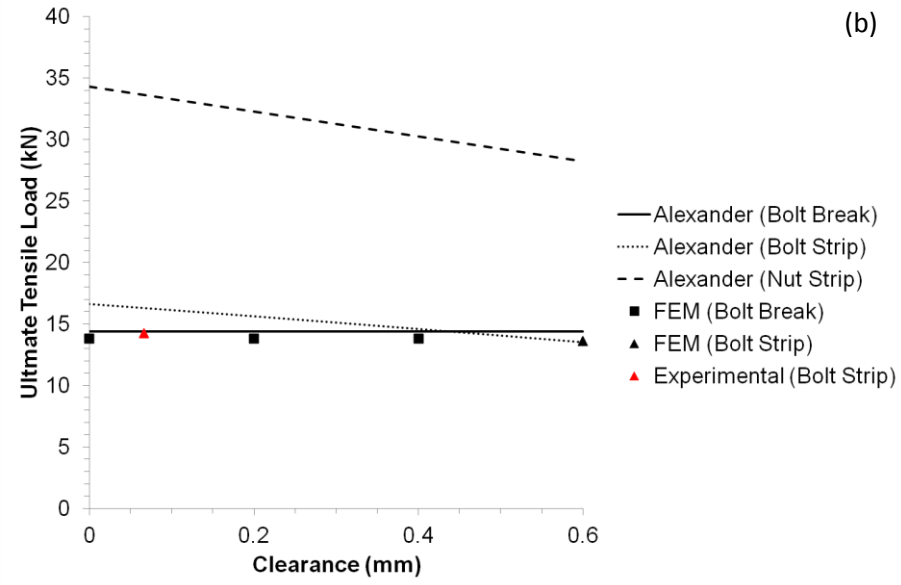
(b)
Ultmate Tensile Load (kN)
40
35
30
25
20
15
10
5
0
0
0.2
0.4
0.6
Clearance (mm)
Alexander (Bolt Break)
Alexander (Bolt Strip)
Alexander (Nut Strip)
FEM (Bolt Break)
FEM (Bolt Strip)
Experimental (Bolt Strip)

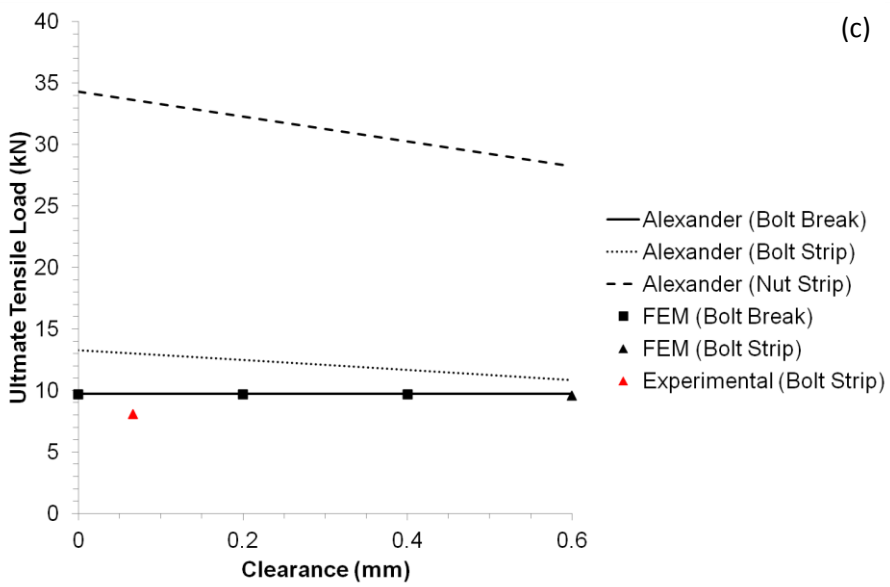

Figure 5.3-7 Calculated failure loads using Alexander's model and FEM using a nut height of 18 mm at 700°C and strain-rates of (a) 0.02 min^{-1} (b) 0.01 min^{-1} and (c) 0.002 min^{-1}.

5.4 Summary

From the current analysis it can be concluded that FEM can be used to effectively model bolt assemblies, which significantly reduces time and cost, and it can therefore be used to optimise the design and production processes for nut and bolt assemblies. Based on the study which has been performed, the following conclusions can be drawn:

- Approximating high-temperature nut strength using the nominal nut strength and strength reduction factors $k_{b,\theta}$ and $k_{E,\theta}$ was adequate for modelling bolt assemblies in this case, where nut strength was 70 MPa greater than bolt strength.
- An axisymmetric model using a cylindrical nut and no helix angle gave accurate results for significantly shorter computation times than an equivalent 3D model.
- Results of FEM were very sensitive to mesh type and density. A quad-dominated mesh type with global mesh size of 2 and local mesh size of 0.3

at the interacting threads was found to give the most accurate readings in this case.

- The number of threads protruding beyond the unloaded face of the nut has negligible effect on thread-stripping behaviour for a clearance of 6AZ6g + 0.5 mm.
- The FEM has been validated using a clearance of 6AZ6g + 0.5 mm against force-displacement curves obtained in tensile testing and with Alexander's analytical model.
- Failure mode, ductility and ultimate load capacity are dependent on nut height. Even though nut heights of 15.5 and 18 mm both cause thread-stripping failures, those using an 18 mm tall nut failed at significantly higher force and displacement at all temperatures.
- Specifying a nut height of 20.3 mm in accordance with ISO 4033 will ensure bolt necking failure, even for unrealistically large values of clearance at all temperatures.
- Plotting failure load against clearance produces an inverse S-shaped curve with plateaux at low and high values of clearance.
- The critical clearance at which the failure mode transitions from ductile to brittle is between 6AZ6g + 0.4 mm to 6AZ6g + 0.6 mm for all the temperatures and strain-rates considered in this study.
- The critical clearance at which the failure mode changes is larger for higher temperatures, for slower strain-rates and taller nuts.
- All assemblies failed due to thread-stripping at elevated temperatures during mechanical testing. However, for values of clearance less than 6AZ6g + 0.4 mm necking failures occurred in FEM and Alexander's analytical model. Either these models predict failure at larger clearances

than in mechanical testing, or the measured clearance is not representative of the actual clearance at elevated temperatures.

The calculated thread clearance of 0.066 mm was based on measured thread geometries at ambient temperature. It is assumed that clearance remains constant at all temperatures and that strain-rates do not take into account reduction in area or nut dilation during elongation. At slow strain-rates and high temperatures, such as 0.002 min^{-1} and 700°C, the steel considered in this study exhibited high ductility in turned-down bolt tests. Total strain varied from around 25% at ambient temperature (Figure 3.7-8(a)) to 60% at 700°C when tested at a strain-rate of 0.002 min^{-1} (Figure 3.7-8(c)). During bolt assembly tests, thread-stripping occurred prior to these strains being reached. Despite premature failure, there was significant elongation of the bolt shank prior to thread-stripping, particularly at elevated temperatures at which a certain amount of necking occurred prior to the onset of thread-stripping (Figure 4.2-1). An extension of 5-10 mm will be accompanied by a reduction of area. During elastic deformation this would be controlled by the Poisson's ratio of the material. However, the cross-sectional area continues to decrease during plastic deformation. Much of this reduction in area is localised in the necking area; however, there will be some reduction of area of the bolt shank along its whole shank length.

Nut dilation is caused by the wedging action of the threads, and results in an increase in the nut's minor diameter and a reduction in effective shear areas [44]. Dilation of the loaded face under loading therefore results in radial movement, a reduction in thread engagement length and an increase in thread clearance.

All of these factors caused a relative increase in thread clearance compared to the 0.066 mm measured at ambient temperature on three unloaded bolt assemblies.

Page Intentionally Left Blank

6 Discussion

Microstructural characterisation, mechanical testing and finite element modelling carried out in this project have led to a number of key findings:

1. Significant microstructural variations exist between bolts from different manufacturers, even within a single batch.
2. The strength reduction factors provided in Eurocode 3 for the elevated-temperature design of bolt assemblies were found to be unconservative compared to the results of bolt material and bolt assembly tensile tests.
3. Nut height and thread clearance had a significant effect on failure mode.

6.1 Microstructural Variations

Results of microstructural characterisation carried out on six bolts from five different manufacturers highlighted that some bolts may pass inspection despite containing a non-tempered martensitic microstructure. Optical and electron microscopy are not required quality assurance checks, and the suitability of heat treatment is verified by mechanical testing, including; tensile, impact and hardness testing. The rate of carbon diffusion during transformation to pearlite and bainite is dependent on the transformation temperature and rate of cooling. At low transformation temperatures and rapid rates of cooling, as suggested by SEM images taken at the centres of bolts with lower hardness, the rate of carbon

diffusion is slow. This results in fine lamellae pearlite and/or fine carbides within the bainitic ferrite laths, and therefore relatively high hardness and strength.

The hardness values measured at the centre of one bolt containing a non-martensite microstructure were close to the limit specified in ISO 898-1, and the same bolt may therefore have passed inspection in industry. One explanation for the range in hardness values obtained was attributed to the batch cooling process used during the quench. Bolts near the centre of the batch will be insulated by surrounding bolts, and may not, therefore, experience an adequate cooling rate unless the quench medium is heavily agitated. If the rate of cooling varies depending on a bolt's location within the batch being quenched, a small proportion of bolts within that batch may have been cooled at an insufficient rate.

In order to ensure that every bolt in a batch has had an adequate quench for martensitic transformation the following measures could be taken:

- Increase sample size at inspection;
- Increase minimum specified hardness;
- Decrease maximum hardness range within the half radius.

The number of bolts containing a pearlitic and/or bainitic microstructure may be significant, since 30% of those characterised did not contain tempered martensite. Although the bolts which were characterised from the batch used for mechanical testing produced consistent hardness from surface to centre, other bolts from the same batch were also found to have poor hardness at their centres.

These microstructural variations not only caused significant differences in the flow behaviour of the bolt material, but also determined the failure mode in ambient temperature nut-bolt assembly tests. Those bolts containing steel exhibiting a non-

martensitic microstructure failed by bolt fracture at significantly lower loads than those containing tempered martensite, which failed due to thread-stripping. Despite containing steel with an average hardness at the centre of the cross section lower than the specified minimum, all assemblies had an ultimate load capacity greater than the specified minimum. At elevated temperatures the failure mode was consistent, despite differences in the as-received microstructures.

The failure mode is more critical at elevated temperatures, at which ductility is essential to allow the continued transfer of forces from beams to columns during thermal expansion and subsequent sagging of members during the heating phase of a fire. Since all failures were due to thread-stripping at elevated temperature, despite the existence of a range of microstructures within the batch, the as-received microstructure is clearly not a significant factor in determining the failure mode.

In the literature, Kirby [1] used optical microscopy to investigate microstructural changes on heating of three bolts from one bolt set to different temperatures; however, optical microscopy was not carried out on bolts from every set. The degree of scatter in load capacities observed at a range of temperatures was small for assemblies which failed due to a single failure mode. One assembly failed by a combination of thread-stripping and bolt breakage. However, the degree of scatter was small, and both failure modes existed at all temperatures, suggesting that there were no significant variations in microstructure in the assemblies used in this research. At the time of Kirby's study, however, bolt assemblies tended to be manufactured in the UK, as opposed to being manufactured overseas and quality-checked and stamped by a UK distributor.

If the as-received microstructure only affects the failure mode at ambient temperature, at which strength is more significant than ductility, the question must

be raised as to whether a tempered martensite microstructure is necessary or whether a pearlite/ bainite microstructure of sufficient hardness and strength is suitable for M20 Grade 8.8 bolt applications.

6.2 Strength Reduction Factors

Elevated-temperature strengths, calculated using the nominal ambient-temperature strength and the bolt strength reduction factors prescribed in EN 1993-1-2, were found to be significantly higher than those produced by tensile testing of both turned-down bolts and bolt assemblies, particularly at low strain-rates. The strength reduction factors in Eurocode 3 are based on the research carried out by Kirby [1] on bolts of similar composition and at similar strain-rates, in the rate 0.001-0.003 min^{-1}, to those investigated in this study. Research carried out by Hu [3] and Gonzalez [5] also produced strength reduction factors lower than those prescribed in Eurocode 3. One explanation for the larger reduction in strength for bolts tested in this study is that the ambient-temperature strength was higher than those tested by Kirby, even for assemblies which contained pearlite and bainite If the failure loads at elevated temperature were similar in this and Kirby's studies, the reduction factors would be lower when calculated with respect to higher ambient-temperature strength. Neglecting ambient-temperature strength and comparing the results obtained at elevated temperature, however, it is seen that the strengths obtained by bolt assemblies in this study at 550°C and 700°C were significantly lower than the strengths obtained by either Kirby or Gonzalez, even at the highest strain-rate of 0.02 min^{-1}.

Normalising the strengths obtained by Gonzalez and Hu at elevated temperatures with respect to ambient-temperature strengths also produced significantly lower strength reduction factors than those in Eurocode 3. The bolts tested by Gonzalez

[5] were Grade 10.9, and therefore also had higher ambient-temperature strength than those tested by Kirby [1].

The heating rates used for tensile testing may explain these differences, since the rate of heating in this study was very slow in a large wrap around furnace. The heating rates used by Kirby and Gonzalez [5] were 5-10 and 2-2.5 °C/min respectively, however, the furnace used in this study produced an average heating rate of 2.5-3.5 °C/min for the turned-down bolt specimens. The holding times used in this study and by Kirby were longer than those used by Gonzalez, who increased strain-rate beyond the 2% proof strength. Increasing the strain-rate may have led to misleadingly high values of ultimate tensile strength. Kirby [1], however, maintained a consistent strain-rate until failure, and therefore the bolts tested in this study should have produced results consistent with those produced by Kirby [1].

Despite Kirby's research having been carried out prior to the introduction of "structural" bolt assemblies and having used a thread tolerance class combination of 8g7H, the mechanical properties of bolts specified to BS 4190 by Kirby, and ISO 15048 in this study, are very similar. The strength reduction factors calculated for turned-down bolts were also very similar to those calculated for bolt assemblies, and therefore, the differences between strength reduction factors obtained in this study and those prescribed in Eurocode 3 cannot be attributed to thread geometry.

6.3 Nut Height and Thread Clearance

Mechanical testing has shown that both temperature and strain-rate effect the total strain and strength of turned-down bolt specimens. However, at elevated temperatures, all bolt assemblies failed due to thread-stripping with similar values of total strain. Temperature and strain-rate therefore appear to affect the macroscopic flow behaviour but not the failure mode. The finite element model

allowed variables which could not easily be tested by mechanical testing to be investigated. The two factors which affected the failure mode most significantly were clearance and nut height. The transition from bolt fracture ("necking") to bolt thread-stripping was predicted to be between 6AZ6g + 0.4 and 6AZ6g + 0.6 mm at all temperatures and strain-rates, using both FEM and Alexander's analytical model [44]. The critical clearance at which the failure mode changes from bolt fracture to thread-stripping increased with increasing temperature and decreasing strain-rate.

Non-destructive thread clearance measurement is difficult to achieve in practice, however, making it difficult to calculate whether thread-stripping or bolt breakage are more likely, particularly at elevated temperatures, due to nut dilation and stretching of the bolt shank. The thread clearance of uncoated bolt assemblies at elevated temperatures is likely to be smaller than for galvanised bolt assemblies. This is due to not only to the low melting point of zinc, reducing the effective thread clearance, but also to the smaller cross section of the nut which is tapped over-size to accommodate the galvanised zinc layer on the bolt threads. The bolt assemblies tested in literature which produced strength reduction factors most comparable to the results in this study were also galvanised [44].

One factor which is much easier to quantify is nut height. This study has found that increasing the nut height by just one thread pitch changes the failure mode from thread-stripping to bolt fracture, even for a large thread clearance such as 6AZ6g + 0.5 mm. This nut height is similar to the "tall" nut height of 20.3 mm specified in ISO 4033. Nuts should, therefore, be specified to ISO 4033 rather than ISO 4032 to ensure that bolt necking is the more likely failure mode.

The effects of thread clearance and nut height compared well with the results predicted by Alexander's analytical model [44], and with the failure loads measured in mechanical testing, however, plotting the failure loads against the measured

ambient-temperature clearance of 6AZ6g + 0.066 mm did not reflect the failure modes predicted by either FEM or the analytical model.

Page Intentionally Left Blank

7 Conclusions and Future Work

The first main conclusion that should be drawn from this research is that large microstructural variations exist both between different batches and within a single batch of bolts. These microstructural differences affect flow behaviour and, at ambient temperature, failure mode. Tempered martensite microstructures led to thread-stripping failure, while pearlite and/or bainite microstructures led to bolt necking failures at lower loads. This behaviour has not been identified in previous research, which presumably used batches containing bolts of consistent material properties. At elevated temperatures all bolt assemblies failed via thread-stripping, despite microstructural differences at ambient temperature. Thread-stripping failures at elevated temperature occurred at values of load significantly lower than those predicted by the strength reduction factors prescribed in Eurocode 3, in accordance with literature published since the research carried out by Kirby.

At elevated temperatures the effective clearance between threads is thought to have increased due to nut dilation and melting of the galvanised zinc layers on the bolt threads. Thread clearance is known from previous research to affect the failure mode; however this is a difficult variable to quantify. In order to ensure bolt fracture

failure, even for a clearance of 6AZ6g + 0.5 mm, a taller nut should be specified to ISO 4033.

The FEM has been validated against mechanical testing and an analytical model. However, future work to include a damage criterion in the FEM would allow more accurate deformation behaviour to be investigated beyond ultimate tensile strength. It would also allow investigations into the heavy thread deformation observed at thread tips, which cannot be represented in the current model due to all elements being fixed to their adjacent nodes.

Nut dilation is taken into account in Alexander's analytical model [44]. However, further investigations should be carried out to determine whether nut dilation is temperature-dependent. Currently the analytical model predicts necking failure for the measured ambient temperature thread clearance despite thread-stripping occurring in mechanical testing.

References

1. Kirby, B.R., *The behaviour of high-strength grade 8.8 bolts in fire.* Journal of Constructional Steel Research, 1995. **33**(1-2): p. 3-38.
2. Kirby, B.R., *The Behaviour of High Strength 8.8 Bolts in Fire*, in *British Steel Technical Lab report, Swinden Laboratories*. 1992.
3. Hu, Y., et al. *Comparative study of the behaviour of BS 4190 and BS EN ISO 4014 bolts in fire*. 2007.
4. Gonzalez, F., *Untersuchungen zum Material- und Tragverhalten von Schrauben der Festigkeitsklasse 10.9 wahrend und nach einem Brand*, in *Veroffentlichung des Institutes fur Stahlbau und Werkstoffmechanik*. 2011, Technischen Universitat Darmstadt: Darmstadt.
5. Gonzalez, F. and J. Lange, *Behaviour of Galvanized High Strength Grade 10.9 Bolts under Fire Conditions.* 2009: p. 908-915.
6. Huang, S.S., J.B. Davison, and I.W. Burgess, *High-temperature tests on joints to steel and partially-encased H-section columns.* Journal of Constructional Steel Research, 2013. **80**: p. 243-251.
7. BSEN15048-2, *Non-preloaded structural bolting assemblies - Part 2: Suitability test.* British Standards Institution, 2007.
8. BSEN1993-1-2, *Design of steel structures, Part 1-2: General rules - Structural fire design.* British Standards Institution, 2005.
9. BSEN15048-1, *Non-preloaded structural bolting assemblies - Part 1: General requirements.* British Standards Institution, 2007.
10. Moore, D., *Private Communication, BCSA*. 2010: Sheffield.
11. BSENISO898-1, *Mechanical properties of fasteners made of carbon steel and alloy steel - Part 1: Bolts, screws and studs with specified property classes - Coarse thread and fine pitch thread (ISO 898-1: 2013).* British Standards Institution, 2013.
12. Eames, A. *The history of the bolt*. Nord-Lock; Bolt securing systems 2012 [cited 2013 Accessed 06 September]; http://www.nord-lock.com/bolted/the-history-of-the-bolt/].
13. Krauss, G., *Microstructures, Processing, and Properties of Steels*, in *ASM Handbook*. 1990. p. 289-301.
14. Tata. *http://www.tatasteeleurope.com/file_source/StaticFiles/Spectra/ImportedDocs/Intro_and_hot_rolled.pdf*. Product Catalogue - Tata Steel [Cited 2013 Accessed 10 February].
15. Kirby, B.R. and R.R. Preston, *High temperature properties of hot-rolled, structural steels for use in fire engineering design studies.* Fire Safety Journal, 1988. **13**(1): p. 27-37.
16. BS5950-8, *Structural use of steelwork in building - Part 8: Code of practice for fire resistant design.* British Standards Institution, 1990.
17. Kodur, V., M. Dwaikat, and R. Fike, *High-Temperature Properties of Steel for Fire Resistance Modeling of Structures.* Journal of Materials in Civil Engineering, 2010. **22**: p. 423-434.

18. Lange, J. and N. Wohlfeil, *Examination of the Mechanical Properties of Steel S460 for Fire.* Journal of Structural Fire Engineering, 2010. **1**(3): p. 189-204.
19. Schneider, R. and J. Lange, *Constitutive Equations and Empirical Creep Law of Structural Steel S460 at High Temperatures.* Journal of Structural Fire Engineering, 2011. **2**(3): p. 217-229.
20. Toric, N., et al. *Modelling of the Influence of Creep Strains on the Fire Response of Steel Elements*. in *Application of Structural Fire Engineering*. 2013. Prague, Czech-Republic.
21. Regulations, B., *Approved Document B: Fire Safety*. 2006.
22. BSEN1991-1-2, *Eurocode 1: Actions on structures - Part 1-2: General actions - Actions on structures exposed to fire.* British Standards Institution, 2002.
23. Stern-Gottfried, J., G. Rein, and J. Torer, *Travel guide.* Fire Risk Management, 2009: p. 12-16.
24. Steel, B., *The behaviour of multi-storey steel framed buildings in fire.* Swinden Technology Centre, Rotherham, UK, 1999.
25. steelconstruction.info. *http://www.steelconstruction.info/Structural_fire_engineering*. [cited 2013.
26. Bailey, C.G., *Membrane action of slab/beam composite floor systems in fire.* Engineering Structures, 2004. **26**(12): p. 1691-1703.
27. Bailey, C.G., T. Lennon, and D.B. Moore, *The behaviour of full-scale steel-framed buildings subjected to compartment fires.* Structural Engineer, 1999. **77**: p. 15-21.
28. NIST, *Final Report on the Collapse of World Trade Centre Building 7.* U.S. Department of Comerce and National Institute of Standards and Technology, USA., 2008.
29. BSEN1993-1-8, *Eurocode 3: Design of steel structures - Part 1-8: Design of joints.* British Standards Institution, 2005.
30. Simoes da Silva, L., A. Santiago, and P. Vila Real, *A componenet model for the behaviour of steel joints at elevated temperatures.* Journal of Constructional Steel Research, 2001. **57**: p. 1169-1195.
31. Spyrou, S., et al., *Experimental and analytical investigation of the 'compression zone' component within a steel joint at elevated temperatures.* Journal of Constructional Steel Research, 2004. **60**: p. 841-865.
32. Spyrou, S., et al., *Experimental and analytical investigation of the 'tension zone' components within a steel joint at elevated temperatures.* Journal of Constructional Steel Research, 2004. **60**: p. 867-896.
33. Block, F., in *Development of a Component-Based Finite Element for Steel Beam-to-Column Connections at Elevated Temperatures*. 2006, PhD Thesis, Department of Civil and Structural Engineering: University of Sheffield.
34. Yu, H., et al., *Experimental investigation of the behaviour of fin plate connections in fire.* Journal of Constructional Steel Research, 2009. **65**(3): p. 723-736.
35. Yu, H., et al., *Experimental and Numerical Investgations of the Behavior of Flush End Plate Connections at Elevated Temperatures.* Journal of Structural Engineering, 2011: p. 80-87.
36. Zhao, B., et al., *Appendix A - Experimental and Analytical Investigation of Joint Components under Natural Fire Conditions*, in *Conenctions of Steel and Composite Structures under Natural Fire Conditions (COSSFIRE)*. 2009, Technical Report, Research Programme of the Research Fund for Coal and Steel. p. 45-60.

37. DIN931-1:1982-07, *Hexagon head bolts with shank; M 1,6 to M 39 screw threads; Product grades A and B, ISO 4014 modified.* German Institute for Standardization, 1982.
38. Buehler, *BUEHLER Hardness Conversion Charts*.
39. Riaux, H., *Comportement à l'incendie des assemblages simples boulonnés*, in *INSA de Rennes*. 1980, INSA de Rennes.
40. Dieter, G.E., *Mechanical Metallurgy*. SI Metric Edition ed. 1988: McGraw-Hill.
41. ASM.International, *Annealing of Steel*, in *ASM Handbook Volume. 4*. 1991. p. 102-135.
42. Munoz-Garcia, E., J.B. Davison, and A. Tyas. *Analysis of the Response of Structural Bolts Subjected to Rapid Rates of Loading*. in *4th European Conference on Steel and Composite Structures*. 2005. Maastricht: Eurosteel 2005.
43. Fransplass, H., M. Langseth, and O.S. Hopperstad, *Tensile behaviour of threaded steel fasteners at elevated rates of strain.* International Journal of Mechanical Sciences, 2011. **53**(11): p. 946-957.
44. Alexander, E.M., *Analysis and Design of Threaded Assemblies*, in *International Automotive Engineering Congress and Exposition*. 1977, Ref. No 770420: Detroit.
45. Mouritz, A.P., *Failure mechanisms of mild steel bolts under different tensile loading rates.* International Journal of Impact Engineering, 1994. **15**(3): p. 311-324.
46. Sopwith, D.G., *The distribution of load in screw threads.* Proceedings of the Institute of Mechanical Engineers, 1948. **159**: p. 378-383.
47. Kenny, B. and E.A. Patterson, *Load and stress distribution in screw threads.* Experimental Mechanics, 1985. **25**(3): p. 208-213.
48. Maruyama, K., *Stress Analysis of a Bolt-Nut Joint by the Finite Element Method and the Copper-Electroplating Method.* Bulletin of the JSME, 1974. **17**(106): p. 442-450.
49. Bretl, J.L. and R.D. Cook, *Modelling the Load Transfer in Threaded Connections by the Finite Element Method.* International Journal for Numerical Methods in Engineering, 1979. **14**(9): p. 1359-1377.
50. Tanaka, M., et al., *Application of the Finite Element Method to Bolt-Nut Joints.* Bulletin of the JSME, 1981. **24**(192): p. 1064-1071.
51. Tanaka, M., K. Hongo, and E. Asaba, *Finite Element Analysis of Threaded Connections Subjected to External Loads.* Bulletin of the JSME, 1982. **25**(200): p. 291-298.
52. Kenny, B. and E.A. Patterson, *Figure 3*, in *Load and Stress Distribution in Screw Threads*. 1985. p. 210.
53. Zhao, H., *Analysis of the load distribution in a bolt-nut connector.* Computers & Structures, 1994. **53**(6): p. 1465-1472.
54. BSEN14399-4, *High-strength structural bolting assemblies for preloading - Part 4: System HV - Hexagon bolt and nut assemblies.* British Standards Institution, 2005.
55. Kirby, B.R., *Figure 3: Capacity of high strength grade 8.8 bolts in tension at elevated temperatures (bolt set A)*, in *The Behaviour of High-strength Grade 8.8 Bolts in Fire*. 1995, Journal of Constructional Steel Research. p. 12.
56. Speich, G.R. and W.C. Leslie, *Tempering of steel.* Metallurgical and Materials Transactions B, 1972. **3**(5): p. 1043-1054.

57. Bhadeshia, H. and R. Honeycombe, *Steels: Microstructure and Properties, Third Edition*. 2006: Butterworth-Heinemann.
58. Martinez, M.M., A. Ferrand, and J. Guillot, *Finite Element Analysis of Thread Stripping of a Threaded Assembly.* Transactions on Engineering Sciences, 2001. **32**: p. 263-272.
59. Martinez, M.M. and D.Z. Rios, *An Empirical Model to Calculate the Threads Stripping of a Bolt Installed in a Tapped Part.* World Academy of Science, Engineering and Technology, 2008. **46**: p. 418-421.
60. Davison, J.B. and G.W. Owens, *Steel Designer's Manual (DRAFT)*. 7 ed. Steel Construction Institute, ed. B. Science.
61. SCI and BCSA, *Joints in Steel Construction - Simple Connections.* 2002.
62. BSENISO10684, *Fasteners - Hot dip galvanized coatings.* British Standards Institution, 2004.
63. *Bolts - the vital components*, in *New Steel Construction Magazine*. , March 2011. p. 26-29.
64. BSEN10045-1, *Charpy impact test on metallic materials - Part 1: Test method (V- and U- notches).* British Standards Institution, 1990.
65. BSENISO898-2, *Mechanical properties of fasteners - Part 2: Nuts with specified proof load values - Coarse thread.* British Standards Institution, 1992.
66. BSENISO6507-1, *Metallic materials - Vickers hardness test - Part 1: Test method.* British Standards Institution, 2005.
67. BS3643-1, *ISO metric screw threads - Part 1: Principles and basic data.* British Standards Institution, 2007.
68. BS3643-2, *ISO metric screw threads - Part 2: Specification for selected limits of size.* British Standards Institution, 2007.
69. BSISO68-1, *ISO general purpose screw threads - Basic profile - Part 1: Metric screw threads.* British Standards Institution, 1998.
70. BSISO965-1, *ISO general purpose metric screw threads - Tolerances - Part 1: Principles and basic data.* British Standards Institution, 1988.
71. BSISO965-5, *ISO general purpose metric screw threads - Tolerances - Part 5: Limits of sizes for internal screw threads to mate with hot-dip galvanized external screw threads with maximum size of tolerance position h before galvanizing.* British Standards Institution, 1998.
72. BSENISO4017, *Hexagon head screws - Product grades A and B.* British Standards Institution, 2001.
73. BSENISO4032, *Hexagon nuts, style 1 - Product grades A and B.* British Standards Institution, 2012.
74. BSENISO4018, *Hexagon head screws - Product grade C.* British Standards Institution, 2011.
75. BSENISO4034, *Hexagon regular nuts (style 1) - Product grade C.* British Standards Institution, 2012.
76. *Screw threads*, in *Manual of British Standards in Engineering Metrology*, B.S. Institution, Editor. 1984. p. 140-153.
77. BSENISO898-1, *Mechanical properties of fasteners made of carbon steel and alloy steel, Part 1: Bolts, screws and studs with specified property classes — Coarse thread and fine pitch thread.* British Standards Institution, 2009.

78. Callister, W.D., *Materials Science and Engineering: An Introduction*. 7th ed. 2007: John Wiley & Sons.
79. Pickering, F.B., *The Structure and Properties of Bainite in Steels*, in *Transformation and Hardenability in Steels*, A.J. Herzig, Editor. 1968, American Metal Climax Inc: Michigan.
80. Reed-Hill, R.E., *Physical Metallurgy Principles*. 3 ed. 1992, Boston: PWS Publishing Company.
81. Marder, A.R., *Figure 8*, in *The metallurgy of zinc-coated steel*. 2000, Progress in Materials Science. p. 203.
82. Langill, T.J., *Batch Process Hot Dip Galvanizing*, in *ASM Handbook Volume 13A, Corrosion: Fundamentals, Testing, and Protection*. 2003, ASM Handbook. p. 794-802.
83. BS4190, *Specification for ISO metric black hexagon bolts, screws and nuts.* British Standards Institution, 1967.
84. ASM.International, *Classification and Designation of Carbon and Low-Alloy Steels*, in *ASM Handbook Volume 1, Properties and Selection: Irons, Steels and High-Performance Alloys*. 1990. p. 140-194.
85. Kuch, E.R., *Hardenable Carbon and Low-Alloy Steels*, in *ASM Handbook*. 1990. p. 451-463.
86. N .Saunders, et al., *Using JMatPro to Model Materials Properties and Behaviour.* The Member Journal of The Minerals, Metals & Materials Society, 2003: p. 60-65.
87. C. Zener and J.H. Hollomon, *Effect of Strain Rate Upon Plastic Flow of Steel.* Journal of Applied Physics, 1944. **15**(1): p. 22-32.
88. ASFP, *Yellow Book: Fire Protection for Structural Steel in Buildings, 4th Edition*. 2010.
89. BS476-20, *Fire tests on building materials and structures - Part 20: Method for determination of the fire resistance of elements of construction (general principles).* British Standards Institution, 1987.
90. R. E. Bailey, R. R. Shiring, and H.L. Black, *Hot Tension Testing*, in *Workability Testing Techniques*, G.E. Dieter, Editor. 1984, American Society for Metals: Ohio.
91. DraftBSENISO6892-2, *Metallic materials - Tensile testing, Part 2: Method of test at elevated temperature.* British Standards Institution, 2009.
92. BSENISO6892-1, *Metallic materials - Tensile testing, Part 1: Method of test at ambient temperature.* British Standards Institution, 2009.
93. White, D. and A. Take, *GeoPIV: Particle Image Velocity (PIV) Software for use in Geotechnical Testing.* CUED/D-SOILS/TR322, 2002.
94. BSEN1993-1-1, *Design of steel structures - Part 1-1: General rules and rules for buildings.* British Standards Institution, 2005.
95. BSI, *Figure 3.1: Stress-strain relationship for carbon steel at elevated temperatures*, in *BSEN1993-1-2*. 2005. p. 21.
96. BSENISO4033, *Hexagon nuts (style 2) - Product grades A and B.* British Standards Institution, 2012.

Page Intentionally Left Blank

Appendix

A1: CCT Diagrams calculated for bolts 1-6 (a-f) respectively based on prior austenite grain size and chemical composition Where F = ferrite, P = pearlite, B = bainite and M = martensite, (s) = start, (f) = finish and (90%) = 90% of transformation.

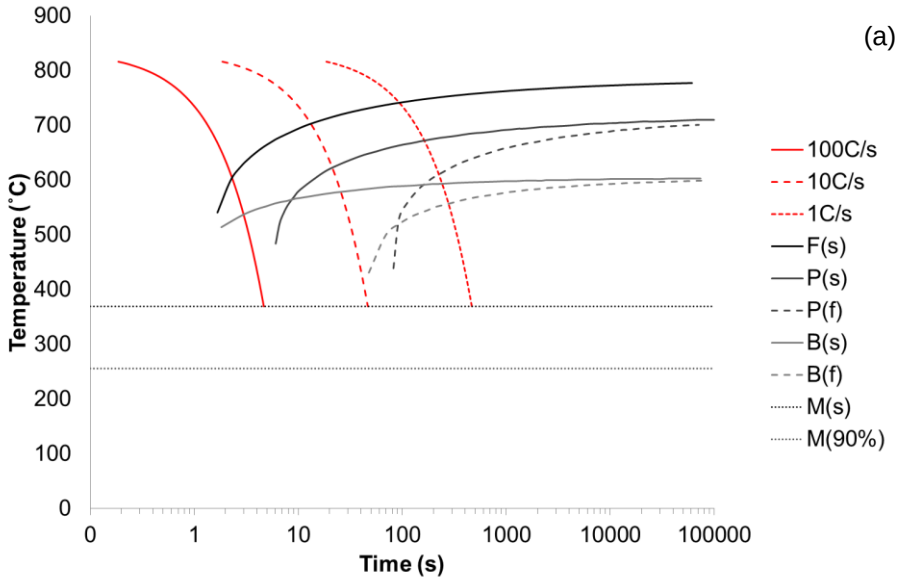

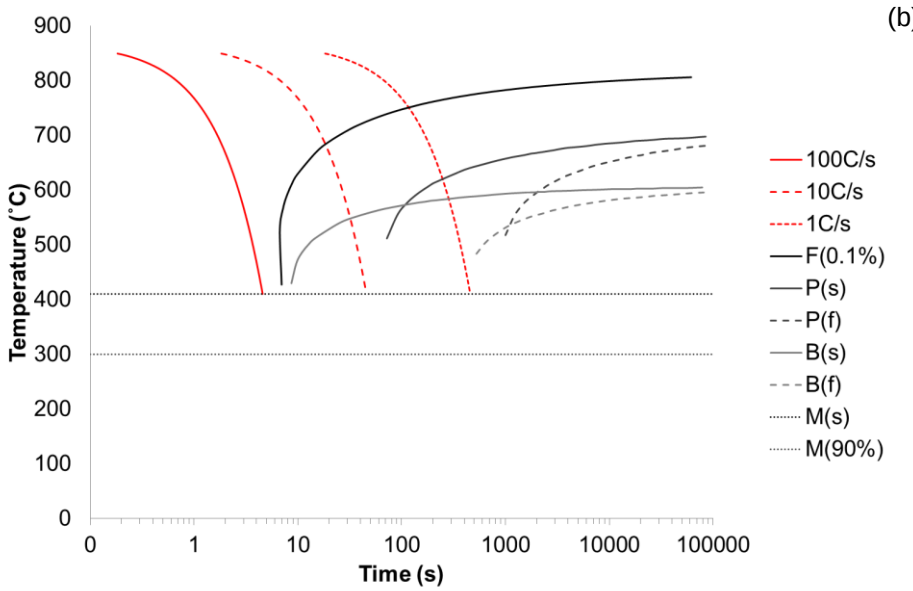

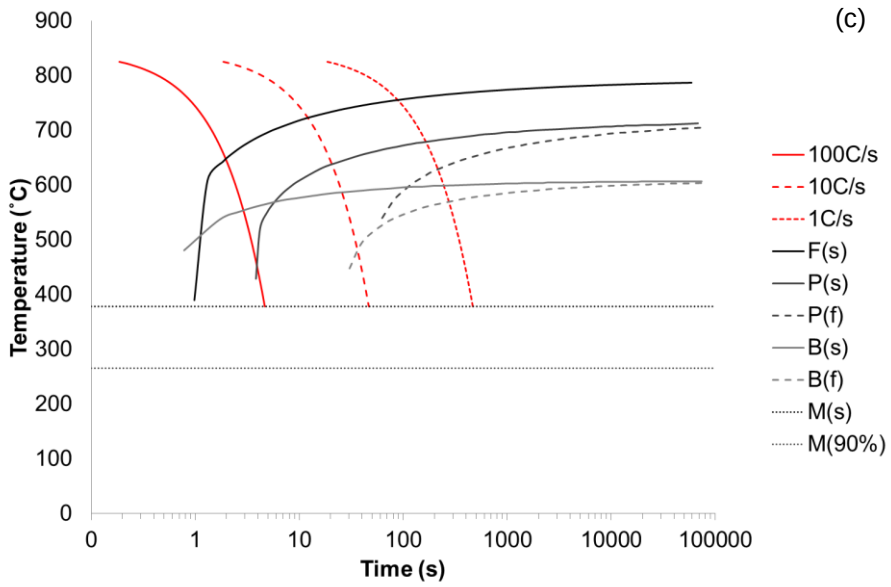
(c)
900
800
700
600
500
400
300
200
100
0
Temperature (°C)
0
1
10
100
1000
10000
100000
Time (s)
100C/s
10C/s
1C/s
F(s)
P(s)
P(f)
B(s)
B(f)
M(s)
M(90%)

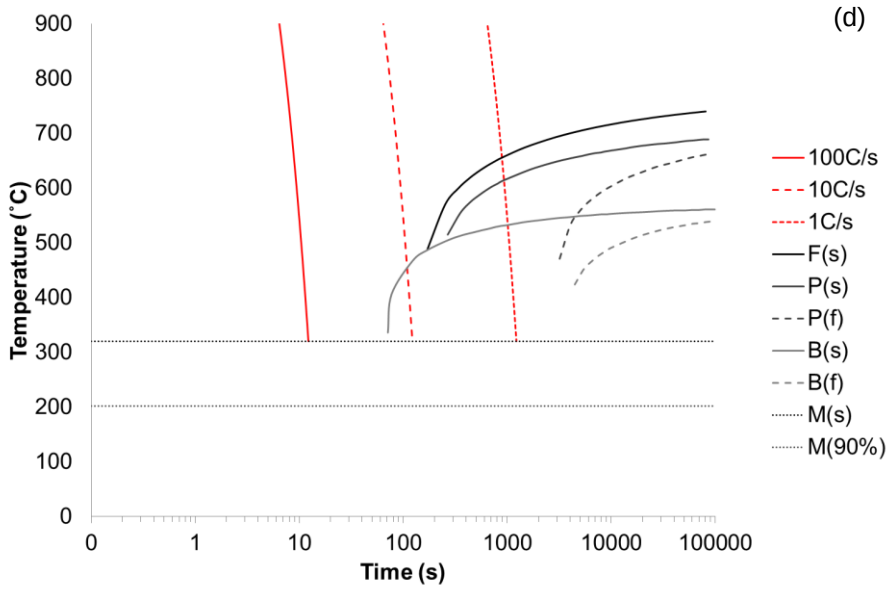
(d)
900
800
700
600
500
400
300
200
100
0
Temperature (°C)
0
1
10
100
1000
10000
100000
Time (s)
100C/s
10C/s
1C/s
F(s)
P(s)
P(f)
B(s)
B(f)
M(s)
M(90%)

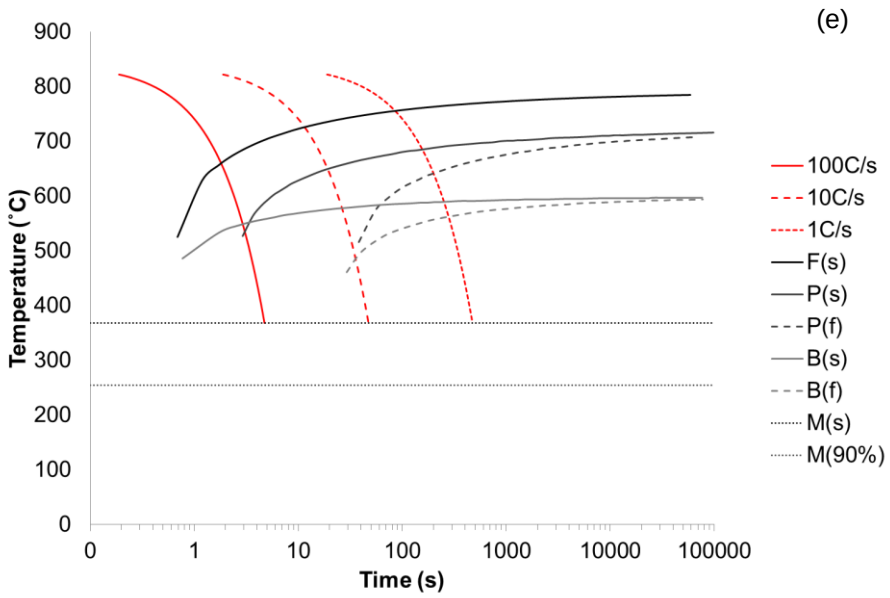
(e)
900
800
700
600
500
400
300
200
100
0
Temperature (°C)
0
1
10
100
1000
10000
100000
Time (s)
100C/s
10C/s
1C/s
F(s)
P(s)
P(f)
B(s)
B(f)
M(s)
M(90%)

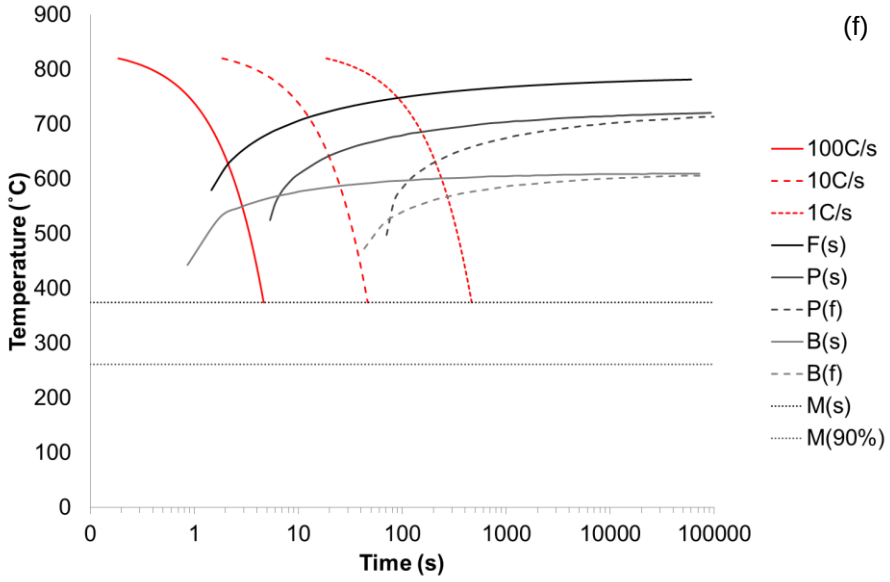
(f)
900
800
700
600
500
400
300
200
100
0
Temperature (°C)
0
1
10
100
1000
10000
100000
Time (s)
100C/s
10C/s
1C/s
F(s)
P(s)
P(f)
B(s)
B(f)
M(s)
M(90%)

A2: Derivation of limiting strain-rate based on limiting deflection rate prescribed in BS 476-20

Substitution of the following equations (7 (9)

$$y = \frac{d}{2} \tag{7}$$

$$s = E.e \tag{8}$$

$$M = \frac{w.l^2}{8} \tag{9}$$

Into the engineers bending equation (10)

$$\frac{M}{I} = \frac{s}{y} \tag{10}$$

Can be re-arranged to give equation (11):

$$\frac{w.l^2}{8.I} = \frac{2.E.e.}{d}$$

$$\therefore E.I = \frac{w.l^2.d}{16.e} \tag{11}$$

Substitution of (11) into the equation for maximum deflection at the mid-span of a simply supported beam (12) gives (7):

$$\partial = \frac{5.w.l^4}{384.E.I} \tag{12}$$

$$\partial = \frac{5.w.l^4.16.e}{384.w.l^2.d} = \frac{5.l^2.e}{24d} \tag{13}$$

Therefore (14):

$$\dot{\partial} = \frac{5.l^2.\dot{e}}{24d} \tag{14}$$

Substituting the limiting deflection in BS 476-20 (15) into (14) gives (16)

$$\dot{\partial} = \frac{l^2}{9000.d} \tag{15}$$

$$\dot{e} = \frac{l^2.24.d}{5.l^2.9000.d} = \frac{1}{1875} min^{-1} = 5.\dot{3}e^{-4} min^{-1} \tag{16}$$

A3 Excel Spreadsheet calculation of bolt breaking, bolt stripping and nut stripping loads using Alexander's analytical model. List of symbols on next page.

	A	B	C
1	s	30	
2	D	20	
3	σn	1000	
4	σs	900	
5	C1	=(-(($B$1/$B$2)^2)+3.8*($B$1/$B$2)-2.61)	
6	mi	18	
7	P	2.5	
8	PI	=PI()	
9	d2	18.334	
10	D2i	18.726	
11	d3	17.252	
12	D1i	17.644	
13	Ri	0.361	
14	root3	=SQRT(3)	
15	Dm	20.35	
16	LE	=B6-((2*1.8126)*0.6)	
17	LB1	0	
18			
19		0	0.1
20	D2i	18.726	=B21+0.1
21	D1i	17.644	=B22+0.1
22	d2i	18.334	=B23
23	di	19.958	=B24
24	Assi(1)	=(($B$16-$B$17)/$B$7)*$B$8	=(($B$16-$B$17)/$B$7)*$B$8
25	Assi(2)	=B22*(($B$7/2)+((B23-B22)*(1/$B$14)))	=C22*(($B$7/2)+((C23-C22)*(1/$B$14)))
26	Assi(3)	=($B$17/$B$7)*$B$8*$B$15*(($B$7/2)+($B$23-$B$15)*(1/$B$14))	=($B$17/$B$7)*$B$8*$B$15*(($B$7/2)+($B$23-$B$15)*(1/$B$14))
27	As	=($B$8/4)*(($B$9+$B$11)/2)^2	=($B$8/4)*(($B$9+$B$11)/2)^2
28	Asi	=($B$8/4)*(B23-0.43301*$B$7+$B$13)^2	=($B$8/4)*(C23-0.43301*$B$7+$B$13)^2
29	ASsi	=B25*B26+B27	=C25*C26+C27
30	ASni	=($B$16/$B$7)*$B$8*B24*(($B$7/2)+((B23-B21)*(1/$B$14)))	=($B$16/$B$7)*$B$8*C24*(($B$7/2)+((C23-C21)*(1/$B$14)))
31	Rs	=($B$3/B31)/($B$4/B30)	=($B$3/C31)/($B$4/C30)
32	C2	=5.594-(13.682*B32)+14.107*(B32^2)-6.057*(B32^3)+0.9353*(B32^4)	=5.594-13.682*C32+14.107*C32^2-6.057*C32^3+0.9353*C32^4
34	C3	0.897	0.897
35			
36	BOLT BREAKING LOAD	=$B$4*B29*0.001	=$B$4*C29*0.001
37	BOLT STRIPPING LOAD	=$B$4*B30*$B$5*B33*0.6*0.001	=$B$4*C30*$B$5*C33*0.6*0.001
38	NUT STRIPPING LOAD	=$B$3*B31*$B$5*B34*0.6*0.001	=$B$3*C31*$B$5*C34*0.6*0.001
39			

	Description
s	Width of nut across flats
D	Nominal diameter
σn	Nut strength
σs	Bolt Strength
C1	Nut dilation factor
mi	Nominal nut height
P	Thread pitch
PI	π
d2	Nominal pitch diameter (bolt)
D2i	Nominal pitch diameter (nut)
d3	Nominal internal diameter (bolt)
D1i	Nominal external diameter (nut)
Ri	Nominal root radius
root3	$\sqrt{3}$
Dm	Mean diameter of bell-mouthed section of nut
LE	Nominal internal diameter (nut)
LB1	Length of bell-mouthed section of nut
Assi(1)	First section of ASsi calculation
Assi(2)	Second section of ASsi calculation
Assi(3)	Third section of ASsi calculation
As	Tensile stress area
Asi	Bolt tensile stress area
ASsi	Shear area of bolt threads
ASni	Shear area of nut threads
Rs	Strength ratio between nut and bolt threads
C2	Strength reduction factors for bolt thread bending
C3	Strength reduction factors for nut thread bending